

Editor in chief

Dr.Shaker M. Al-Jobori

Deputy editor in Chief

Dr. Jabbar F. Al-Maadhidi

Editorial board

Lect. Isam Atta Ajaj

Editor

Dr. Saeed Selman Kamoon

Dr. Mousa M. Al-jobori

Dr. Sabah Abdul Latif Nassif

Dr. Usama Aladdin Ibrahim

Dr. Saad Abdolridha Makki

Dr. Abd Almonem K. Hammadi

Dr. Ali Mahdi

Dr. Hussain H. Ahmed

Dr. Farooq Abdul Azeez Mohammed

Dr. Ayaid K. Zgair

Advisaori Board

Prof. Dr. AbdolHazim Al-Rawi, Alrashed University

Prof. Dr. TawficNajim, Al-mammon University College

Prof. Dr. Ghazi Faisal, Al-Nahrin University

Prof. Dr. Nabil Hashim, Babel University

Dr. Ayad A. Al-Taweel, Ministry of Science and Technology

Assis. Prof. Ahmed Mossa, Technical University

Dr. Ammer M. Ali, MadentAlelem College

Dr.IbrahimKhammas, MadentAlelem College



INSTRUCTIONS to AUTHERS

Submitted articles to the Journal of Madinat Al-Elem University College can be published in all fields related to the Academic Departments of the College (Biology, Law, programming Engineering Sciences, Computer Techniques Engineering Law, Medical Physics, Civil Engineering, and Accounting).

Written request for publication and signing a consent form to publish must be for articles which have not been published or submitted for publication to other journals. Three copies with CD are needed. Manuscripts should be typed on: A4 white paper, double spaced, written in Times New Roman font size 14. Margins should be 3cm from top, bottom, left and right. The main title should be in: bold Times New Roman font size 14. Author names should be written in the following sequence: first name, middle name, the family name, followed by the names of departments and institutions of work. A footnote accompanies the first page stating the full address of correspondence author.

Articles need to contain the following items:

- Abstract in English and Arabic not more than 300 words.
- Article includes the following items: Introduction, Materials and Methods, Results and Discussion, Conclusion and References.
- References should be numbered in the text according to the sequence appeared in the text and listed in order.
- Tables and figures should be appropriately titled with size not exceed an A4 page.

The editor reserves the right to reject or accept any article submitted.

Publication charges: Each accepted paper is required to pay the publication charge (100,000 Iraqi dinars). Five thousands Iraqi dinar are requested for each extra page extra printed page.

Contents

	Page
Study of Parathyroid gland function in normal pregnant women in Tikrit city Prof Dr. Mossa M. Marbut, , Mena D. Mustafa, and Dr. Jawad A. Salih.	1
Suggested hybrid Transform Technique for image compression Dr.Ismael Hadi challoob , Rasha Riyadh Mahmood	15
Using Laplace Transformation Technique to solve boundary value problems Dunya Mohee Hayder	28
Hydraulic transient analysis in pumping stations due to power failure. (Al-Mazak Closed Irrigation System), Kut, Iraq. Dr. Mohammed Najm Abdullah	37
Emergency Notification System for the Detection of Falling, Car Accident and Heart Rate Failure Using Smart phone and Smart watch. Hamid M. Ali , Ali M. Muslim	54
Analytical Study using Association Rules and Mean of Confidence to Analyze The Poverty Factors in Baghdad Capital of Iraq Ali Sami, Dr. Ali Mohammed Sahan, Ghazi Johnny	73
Estimation of Daily Evaporation from Calculated Evapotranspiration in Iraq Dr. Hussain Zaydan Ali , - Saad H. Faraj	84
On Solve Fuzzy Boundary Value Problem Amani E. Kadhm	97
Spectrophotometric Determination of Chloramphenicol in Bulk and Pharmaceutical Preparation Tariq Y. Mahmoud, Sarmad B. Dikran, Alaa K. Mohammed	114

Study of Parathyroid gland function in normal pregnant women in Tikrit city

Prof Dr. Mossa M. Marbut, Mena D. Mustafa, and Dr. Jawad A. Salih.

Dept. of Physiology, College of Medicine, Tikrit University.

Mosaa1955p@yahoo.com

Abstract:

Background: During pregnancy, there an increase in calcium demands to helps building of fetus's skeleton, to met this demands the parathyroid gland secretes parathyroid hormone to maintain calcium homeostasis. **Aim of study:** is determine the function of parathyroid gland and calcium turnover during pregnancy in normal healthy pregnant women in Tikrit city. **Subjects and methods:** A longitudinal follow up study was conducted in Ibn-Rushed health care center at Tikrit city. The study was done from the 15th of November 2016 to the end of March 2017. Thirty healthy pregnant women was participated in the present study, aged from 18 to 40 years in their 15–18th week of pregnancy. All pregnant women were followed up every month, about 5 ml of venous blood was drawn from the pregnant women every four weeks till the end of the 2nd trimester or the beginning of 3rd trimester. The blood lifted to clotted then centrifuged to separate the serum. The separated serum kept in deep freezing, until collection of all samples to be used in hormone and biochemical analysis. **Results:** PCV and Hb shows a highly-significant difference ($P \leq 0.01$) among these three followed-up months. There is a highly-significant difference ($P \leq 0.01$) in serum PTH in the three followed-up months. Prolactin concentrations were significantly higher during the second trimester, in other hand there is no-significant difference in serum osteocalcin concentration between the first trimester as compare with the second trimester ($P > 0.05$). Serum calcium and phosphors shows a no-significant difference ($P > 0.05$) in the three followed-up month of 30 pregnant women. Magnesium shows a significant difference ($P \leq 0.05$) in the results of the three-follow-up month, while in ALP there is a highly-significant difference ($P \leq 0.01$) in the results, the highest value in the 5th month.

Key word: Pregnancy, First and second trimester, Parathyroid hormone, Calcium, Alkaline phosphates.

دراسة وظيفة الغدة جنب الدرقية في النساء الحوامل في مدينة تكريت

ا.د موسى محمود مربوط , مينا داود مصطفى , د. جواد علي صالح

*كلية الطب – جامعة تكريت ** كلية الصيدلة – جامعة تكريت

الخلاصة:

خلال فترة الحمل، وهناك زيادة في احتياج الكالسيوم للمساعدة في بناء الهيكل العظمي للجنين، لتلبية هذا الاحتياج الغدة جنب الدرقية تفرز هرمون الغدة جنب الدرقية للحفاظ على التوازن الكالسيوم. الهدف من الدراسة: هو تحديد وظيفة الغدة الدرقية ودوران الكالسيوم أثناء الحمل في النساء الحوامل الأصحاء الطبيعيات في مدينة تكريت. الأشخاص والطرائق العمل: أجريت دراسة متابعة طولية في مركز ابن رشد للرعاية الصحية بمدينة تكريت. أجريت الدراسة من 15 نوفمبر 2016 حتى نهاية مارس 2017. وقد شاركت ثلاثين امرأة حامل صحية في هذه الدراسة، اللاتي تتراوح أعمارهن بين 18 و40 عاما في الأسبوع 15- 18 من الحمل. تمت متابعة جميع النساء الحوامل كل شهر، حيث تم سحب حوالي 5 مل من الدم الوريدي من النساء الحوامل كل أربعة أسابيع حتى نهاية الثلث الثاني من الحمل أو بداية الثلث الثالث من الحمل. الدم يوضع في جهاز الطرد المركزي لفصل المصل. المصل فصل وتم الاحتفاظ به في تجميد عميق، حتى جمع جميع العينات لاستخدامها في التحليل الهرموني والكيمياء الحيوية. **النتائج:** حجم كريات الدم المضغوطة والهيموكلوبين يظهر فرق كبير جدا ($P \leq 0.01$) بين هذه الأشهر الثلاثة المتابعة. هناك فرق كبير جدا ($P \leq 0.01$) في هرمون الغدة جنب الدرقية في المصل في الأشهر الثلاثة. كانت تراكيز البرولاكتين أعلى بكثير خلال الثلث الثاني من الحمل، ومن ناحية أخرى لا يوجد فرق معنوي في تركيز أوستيوكلاسين المصل بين الثلث الأول من الحمل مقارنة مع الثلث الثاني ($P < 0.05$)

يظهر الكالسيوم والفسفور في مصل الدم فرقا غير معنوي ($P < 0.05$) في الشهر الثالث من المتابعة. يظهر المغنيسيوم فرقا معنويا ($P \leq 0.05$) في نتائج الشهر الثالث للمتابعة، بينما في ALP هناك فرق كبير جدا ($P \leq 0.01$) في النتائج، وهي أعلى قيمة في الشهر الخامس.

الكلمات المفتاحية: الحمل، الثلث الأول و الثاني، هرمون جنب الدرقية و الكالسيوم

The requirement of calcium for the growing fetus is about 30 gm of calcium to complete mineralization of

Introduction:

its skeleton system and insure proper physiological process. This requirement generally induces alterations in maternal homeostasis of calcium to allow active transport throughout placenta. ⁽¹⁾

There are several factors that known to be involved in balanced relationship between the large pool of calcium in skeleton and the much smaller pool of extra cellular fluid, one of the important factors that maintain the calcium and other related minerals balance such as magnesium and phosphate are hormones such as parathyroid hormone (PTH). ⁽²⁾

PTH acts mainly on three tissues which are bone, kidney and intestine, this hormone raises blood calcium level (hyper calcium effect). PTH stimulate calcium reabsorbtion in kidney and also enhance hydroxylation of 25-Hydroxy vitamin D3 which responsible for increasing calcium uptake by small intestine.

Finally in bone, PTH stimulates bone resorption of serum calcium, this process increase in pregnancy to met the large demand for calcium. ⁽³⁾

So PTH levels are inversely related to calcium concentration in blood, increasing PTH when there is an increasing in calcium level, acting through PTH receptor which is highly in bone and kidney. The increases are evident by early to mid pregnancy for calcium by growing skeleton of the fetus. In addition releasing of PTH controlled by plasma phosphorus and magnesium levels, any elevation in plasma phosphorus levels increase PTH secretion. ^(4,5)

Aim of study:

Is to determine the function of parathyroid gland and calcium turnover during pregnancy in normal healthy pregnant women in Tikrit city.

Subjects and methods:

A longitudinal follow up study was conducted in Ibn-Rushed health care center at Tikrit city. The study was done from the 15th of November 2016 to the end of March 2017. Thirty healthy pregnant women was participated in the present study, aged from 18 to 40 years in their 15–18th week of pregnancy. All pregnant women were followed up every month, about 5 ml of venous blood was drawn from the pregnant women every four weeks till the end of the 2nd trimester or the beginning of 3rd trimester. The blood lifted to clotted then centrifuged to separate the serum. The separated serum kept in deep freezing, until collection of all samples to be used in hormone and biochemical analysis. All data were presented as Mean and Stander deviation (SD). F test (One way, ANOVA) was used to compare between means of variables. P value less than 0.05 or 0.01 was used as significant value.

Results:

Regarding PCV there is a highly-significant difference ($P \leq 0.01$) among these three followed-up months, the 3rd month of pregnancy **36.200 ± 2.295 %** as compare with the 4th month **34.733 ± 2.212** and the 5th month **33.333 ± 2.294**. As the same as in Hb, there is a highly-significant difference ($P \leq 0.01$) among these three followed-up months, the 3rd month of pregnancy shows the highest value **11.777 ± 0.910 gm/dl** as compare with the 4th month **11.050 ± 0.785 gm/dl** and the 5th month **10.643 ± 0.849 gm/dl**, as shown in table (1).

There is a highly-significant difference ($P \leq 0.01$) in serum PTH in the three followed-up months, the 5th month shows the highest value **40.73 ± 2.78 pg/mL** as compare with the 4th month **25.88 ± 1.73 pg/mL** and the 3rd month **19.41 ± 2.16 pg/mL**, as shown in table2. Prolactin concentrations

were significantly higher during the second trimester 6464 ± 439 pg/mL as compared with first trimester 1920 ± 389 pg/mL ($P \leq 0.01$). There is no-significant difference in serum osteocalcin concentration between the first trimester 15.63 ± 6.54 ng/ml as compare with the second trimester 16.229 ± 4.7 ng/ml ($P > 0.05$), as shown in table (3).

Serum calcium and phosphors shows a no-significant difference ($P > 0.05$) in the three followed-up month of 30 pregnant women. Magnesium shows a significant difference ($P \leq 0.05$) in the results of the three-follow-up month. The 4th month shows the lowest value 1.9000 ± 0.1287 as compare with 5th month 1.9733 ± 0.1230 and 6th month 1.9833 ± 0.1234 , while in ALP there is a highly-significant difference ($P \leq 0.01$) in the results, the highest value in the 5th month 170.97 ± 44.03 μ kat/L as compare with 4th month 134.23 ± 28.14 μ kat/L and 3rd month

116.37 ± 31.21 μ kat/L, as shown in table (4).

Discussion:

In this study there was an anemia in pregnancy due to iron and vitamin B₁₂ deficiency which is most cause of anemia in pregnant women, because iron supplementation programs are ineffective programs. Other nutritional deficiencies and inflammatory or infectious disease also cause anemia. ⁽⁶⁾

In the present study, there is a highly significant increase ($P \leq 0.01$) in the concentration in Parathyroid hormone due to significant changes that combine pregnancy changes in all chemical parameters and hormones, including the sex steroids, prolactin, placental lactogen, and insulin-like growth factor type 1, all of these could have direct or indirect effects on calcium and bone metabolism during pregnancy. ⁽⁷⁾

Decreasing in total serum calcium and rising in parathyroid hormone may cause secondary hyperparathyroidism in pregnancy, this is a rare condition. ⁽⁸⁾

There was a profound increasing in Parathyroid hormone during 2nd trimester of pregnancy, which is indicate the elevated calcium demined by maternal and fetus. This demined may stimulates PTH release due to changes in calcium-sensing receptor (CaR) sensitivity of the parathyroid gland during pregnancy. ⁽⁹⁾

Maternal calcium absorption mediated through increases in PTH synthesis rises during pregnancy to meet these demands. Paralleling a decline in serum albumin, total serum calcium concentrations decline during gestation, with little change in ionized calcium. In response to placental calcium transfer as well as an expanding extracellular volume and increased urinary calcium loss,

maternal PTH concentrations rise during pregnancy. ⁽¹⁰⁾

Prolactin increase during pregnancy and activate prolactin receptors. Prolactin concentrations may increase throughout the course of pregnancy, reaching a maximum at the end of pregnancy, due to changes in serum PTHrP during the course of pregnancy, the pregnancy stimulate increase in calcitropic hormone concentration, which may lead to primary mediator of the changes in maternal calcium metabolism, but the involvement of other factors cannot be excluded. ⁽¹¹⁾

Osteocalcin consider as a bone-specific protein which released into circulation due to increasing in the rate of new bone formation. We founded that serum osteocalcin concentrations were moderately increased at the second trimester. Such changes are consistent with the expected changes in maternal bone

turnover during the course of pregnancy: bone turnover is in limited levels during early pregnancy, in the second trimester bone turnover started to elevated until it reaches the highest level in third trimester. Other study disagrees with our results. ⁽¹²⁾

Calcium fractional absorption ratio may lead to normal levels of calcium concentration from GI which is duplicates in the second trimester and remains at the same level until the end of pregnancy. The main reason for this alteration of absorption is increase of calcitriol due to the maternal renal hydroxylase or extrarenal sources of hydroxylase like fetus kidney or placenta. ⁽¹¹⁾

The expanded intravascular space during pregnancy may cause serum total calcium, phosphate and magnesium tend to be low. In addition, calcium concentrations may also have affected by the reduced albumin concentration. However,

results all remain within the reference range. ⁽¹³⁾

In pregnancy there are high alteration in ca homeostasis due to the increasing demands of calcium during pregnancy and lactation. In late of gestation 2–3% of maternal Ca is transferred to the fetus to meet the high demands of calcium, also during pregnancy there are an increase in absorption of intestine and bone turnover. ⁽¹⁴⁾

The P and Mg levels conceder as an additional regulatory control of PTH releasing, decrease in the formation of arachidonic acid and activity of phospholipase are the ways to increase PTH secretion in case of plasma phosphorus levels is elevated so the inhibition effect of PTH secretion is removed. Elevations in P levels can also affect PTH release indirectly by decreasing plasma Ca^{+2} levels and vitamin D activation. ⁽¹⁵⁾

The concentration of magnesium in the serum plays consider as a key role in PTH regulation, a moderate decrease in magnesium levels may stimulates a paradoxical block in PTH release. In addition, any decrease in magnesium levels may cause hypertension in pregnancy. ⁽¹⁶⁾

Magnesium plays an important role during pregnancy, pregnant women tend to have low blood magnesium level than non pregnant because of increase demand for mother due to growing fetus and increase renal excretion, the loss of magnesium in pregnant women 25% higher than non-pregnant women due to increase in GFR and haemodilution in 2nd and 3rd trimester. ⁽¹⁷⁾

In the present study, serum ALP level had a highly significant increased in second trimester compared to the first trimesters, which may show an increase in the metabolism of bones, in other studies

the researchers had described this status as loss in bone density. ⁽¹⁸⁾

In pregnancy the most important parameters are ALP and calcium, which undergo a high alteration in homeostasis hormones that may have effect on these parameters in pregnant women, as well as calcium related to the building of fetus body. ⁽¹⁹⁾ This increase in serum ALP levels in progressing of pregnancy may indicate bone problems due to an increase in calcium demands as a results of new bone formation (fetus growing). ⁽²⁰⁾

The physiological alterations of pregnancy considered as adaptation that occur normally in maternal body to insure better accommodation of embryo or fetus during pregnancy. Calcium, the most abundant mineral in the human body, has several important functions. The significant increasing of total alkaline phosphatase (TAP) suppose there is a

mainly stimulation caused by bone origin.⁽²¹⁾

This study concludes there was profound increase in PTH secretion during the second trimester as compare with first trimester.

References:

1. Kovacs CS. Calcium and bone metabolism disorders during pregnancy and lactation. *Endocrinology and metabolism clinics of North America*. 2011;40(4):795-826.
2. Wysolmerski JJ. Conversations between breast and bone: physiological bone loss during lactation as evolutionary template for osteolysis in breast cancer and pathological bone loss after menopause. *Bone Key- Osteovision*. 2007 Aug 1;4(8):209-25.
3. Partridge NC, Li X, Qin L. Understanding parathyroid hormone action. *Annals of the New York Academy of Sciences*. 2006;1068(1):187-93.
4. Slatopolsky E, Brown A, Dusso A. Role of phosphorus in the pathogenesis of secondary hyperparathyroidism. *Am. J. of kidney diseases*. 2001 Jan 31;37(1): S54-7.
5. Prentice, A. Calcium in pregnancy and lactation. *Annu. Rev. Nutr.* 2000. **20**:249-272.
6. Stoltzfus RJ. Defining iron-deficiency anemia in public health terms: a time for reflection. *J Nutr* 2001;131 (2S-2):565S-7S
7. Woodrow JP, Noseworthy CS, Fudge NJ, *et al*. Calcitonin /calcitonin gene-related peptide protect the maternal skeleton from excessive resorption during lactation [abstract]. *J Bone Miner Res* 2003;18 (Suppl 2): S37.

8. Horjus C, Groot I, Telting D, van Setten P, van Sorge A, Kovacs CS, Hermus AR, de Boer H. Cinacalcet for hyperparathyroidism in pregnancy and puerperium. *J Pediatr Endocrinol Metab.* 2009; 22(8):741-9.
9. Black AJ, Topping J, Durham B, Farquharson RG, Fraser WD. A detailed assessment of alterations in bone turnover, calcium homeostasis, and bone density in normal pregnancy. *J. of Bone and Mineral Research.* 2000;15(3):557-63.
10. Kovacs CS, Fuleihan GE. Calcium and bone disorders during pregnancy and lactation. *Endocrinology and metabolism clinics of North America.* 2006 Mar 31;35(1):21-51.
11. Gharedaghi M, Ghomian N, Rahimi H, Bahari M, Ariamanesh AS. Serum Calcium, Phosphorous and Alkaline Phosphatase levels in Different Trimesters of pregnancy. *Iranian J. of Obstetrics, Gynecology and infertility.* 2008;10(2):101-6.
12. Naylor KE, Iqbal P, Fledelius C, Fraser RB, Eastell R. The effect of pregnancy on bone density and bone turnover. *J. of bone and mineral research.* 2000 Jan 1;15(1):129-37.
13. Tran HA. Biochemical tests in pregnancy. *Australian prescriber.* 2005 Aug;28(4):98-101.
14. Ramasamy I. Recent advances in physiological calcium homeostasis. *Clinical Chemical Laboratory Medicine.* 2006; 44(3): 237-73.
15. Radanovic T, Wagner CA, Murer H, Biber J. Regulation of Intestinal Phosphate Transport I. Segmental expression and adaptation to low-Pi diet of the type IIb Na⁺-Pi cotransporter in

- mouse small intestine. *Am. J. of Physiology-Gastrointestinal and Liver Physiology*. 2005; 288(3): G496-500.
16. Lindheimer MD, Taler SJ, Cunningham FG. ASH position paper: hypertension in pregnancy. *The Journal of Clinical Hypertension*. 2009;11(4):214-25.
17. Takaya J, Yamato F, Kaneko K. Possible relationship between low birth weight and magnesium status: from the standpoint of “fetal origin” hypothesis. *Magnesium research*. 2006 ;19(1):63-9.
18. Manten GT, Franx A, Van der Hoek YY, Hameeteman TM, Voorbij HA, Smolders HC, Westers P, Visser GH. Changes of plasma lipoprotein (a) during and after normal pregnancy in Caucasians. *J. Maternal-Fetal & Neonatal Medicine*. 2003 ;14(2):91-5.
19. Choi JW, Pai SH. Serum lipid concentrations change with serum alkaline phosphatase activity during pregnancy. *Annals of Clinical & Laboratory Science*. 2000;30(4):422-8.
20. Zeni SN, Soler CR, Lazzari A, López L, Suarez M, Di Gregorio S, Somoza JI, de Portela ML. Interrelationship between bone turnover markers and dietary calcium intake in pregnant women: a longitudinal study. *Bone*. 2003; 33(4): 606-13.
21. Beckett G, Walker SW, Rae P, Ashby P. *Lecture Notes: Clinical Biochemistry*. John Wiley & Sons; 2010 Feb 8.55-80.

Table (1) PCV and Hb differences during the three follow-up months of pregnancy:

Parameters	PCV %	Hb gm/dl
Subjects		
3rd month	36.200 ±2.295 a	11.777 ±0.910 a
4th month	34.733 ±2.212 b	11.050 ±0.785 b
5th month	33.333 ±2.294 c	10.643 ±0.849 c
P-Value	0.0002	0.0003

Table (2) PTH differences during the three follow-up months of pregnancy:

Parameters	PTH(pg/mL)
Subjects	
3rd month	19.41 ±2.16
4th month	25.88 ±1.73
5th month	40.73 ±2.78
P-value	0.0001

Table (3) Prolactin and osteoclastin differences during first and second trimester:

Parameters	Prolactin (pg/mL)	Osteoclastin (ng/ml)
Subjects		
First trimester	1920 ± 389	15.630 ± 6.54
Second trimester	6464 ± 439	16.229 ± 4.70
P-value	P ≤ 0.01	P ≤ 0.05

Table (4) Biochemical parameters differences during the three follow-up months of pregnancy:

Parameters	Calcium levels (mg/dL)	Phosphors levels (mg/dL)	Magnesium levels (mg/dl)	Alkaline Phosphates (μkat/L)
Subjects				
3rd month	8.7600 ±0.4256	3.8703 ±0.2136	1.9000 ± 0.1287	116.37 ±31.21
4th month	8.5670 ±0.6950	3.8741 ±0.2118	1.9733 ± 0.1230	134.23 ±28.14
5th month	8.6733 ±0.5139	3.8221 ± 0.2025	1.9833 ± 0.1234	170.97 ±44.03
P-Value	0.407	0.575	0.05	0.001

Suggested hybrid Transform Technique for image compression

Dr. Ismael Hadi challoob

ismaelhadi73@yahoo.com

Head of IT department \ Middle Technical University \ Technical College of Management - Baghdad

Rasha Riyadh Mahmood

rashara9292@gmail.com

Middle Technical University \ Technical College of Management – Baghdad \ Information

Abstract

Digital images are used in several domains. Large amount of data is necessary to represent the digital images such data needs large transmission bandwidth for the transmission over the network and also require storage capacity. Hence the data in the images should be compressed by extracting only the visible elements. The image compression technique can reduce the storage and transmission costs. Image compression techniques should also maintain the quality of images. This paper proposes a hybrid image compression technique which combines Discrete Cosine Transform (DCT) with Slantlet Transform (SLT). Several methods such as Discrete Cosine Transform (DCT), is used for compressing the images. But, these methods contain some artifacts. In order to overcome this difficulty and compress the image efficiently, a combination of DCT and SLT is proposed. Firstly Transform the image to frequency domain by applying SLT and decompose it into three levels, then DCT is applied on LL3. The results indicate that hybrid (SLT-DCT) technique offers superior compression performance compared to hybrid (DWT-DCT) based approaches. Their performance is evaluated in terms of Peak Signal to Noise Ratio (PSNR), Mean Square Error (MSE), UQI, SSIM and Compression Ratio (CR).

Keywords: Image compression, Discrete Cosine Transform, Discrete wavelet Transform

الخلاصة

تستخدم الصور الرقمية في مجالات عديدة. وتتطلب كم كبير من البيانات الضرورية لتمثيلها، وهذه البيانات تتطلب مساحة تخزينية كبيرة وأيضاً نطاق ترددي عالي عند إرسالها عبر الأنترنت. لذلك يجب توفير تقنيات تقوم بضغط الصور لتقليل حجمها وكلفتها. وأيضاً يجب أن تحافظ هذه التقنيات على جودة الصورة المضغوطة. في هذا البحث تم اقتراح تقنية هجينة لضغط الصور باستخدام التحويل الجيبي المتقطع (DCT) وتحويل الأنداد المائل (SLT). العديد من التقنيات السابقة استخدمت التحويل الجيبي المتقطع في ضغط الصور ولكن هذه التقنيات كانت تحتوي على تشوهات مربعة في الصورة المضغوطة الناتجة من تقسيم الصورة إلى مصفوفات مربعة. ومن أجل تجاوز هذه العقبة وضغط الصور بصورة كفوءة تم اقتراح تحويل هجين يجمع بين كل من التحويلين السابقين حيث أن تحويل الأنداد المائل له القدرة على تحويل الصورة بأكملها دون الحاجة إلى تقسيمها. يتم أولاً تحويل الصورة إلى المجال الترددي بتطبيق ثلاث مستويات SLT بعد ذلك اختيار النطاق الفرعي LL3 وتطبيق DCT عليه. تمت مقارنة نتائج البحث مع تحويل هجين آخر هو التحويل الجيبي المتقطع-تحويل المويجي المتقطع (DWT-DCT) حيث أظهرت النتائج كفاءة تحويل SLT-DCT المقترح الهجين من حيث نسبة الضغط العالية وجودة الصور المضغوطة. باستخدام مقاييس التشوه PSNR، MSE، QUI، SSIM ونسبة الضغط CR للمقارنة بين الطرائق المختلفة.

1. Introduction

Common characteristics of most images are that the neighboring pixels are correlated. Therefore the most important task is to find a less correlated representation of image. The fundamental components of compression are reduction of redundancy and irrelevancy. Redundancy reduction aims at removing duplication from the image. Irrelevancy reduction omits parts of the signal that will not be noticed by the signal receiver namely the human visual system (HVS). Three types of redundancies can be identified: spatial redundancy, spectral redundancy and temporal redundancy. In still image, the compression is achieved by removing spatial redundancy and spectral redundancy [1]. Image compression involves reducing the size of image data files, but retaining necessary information. Two types of image compression technique lossy and lossless, lossless compression is used with the applications that don't accept any difference between the original and compressed data such as medical images [2]. Lossy methods are suitable for natural images such as photographs in applications where minor loss of fidelity is acceptable to achieve reduction in bit rate [3]. Transform coding is the most successful and pervasive technique for lossy compression, transformed from the spatial domain to the frequency domain. The idea of using transform coding is to transform the image into a new domain, where the image coefficients are less correlated [4]. An effective transform will concentrate useful information into a few low-frequency transform coefficients; the HVS is more sensitive to energy with low spatial frequency than with high spatial frequency. Therefore, compression can be achieved by quantizing the coefficients, so that important coefficients (low-frequency coefficients) are transmitted and the remaining coefficients are discarded [5].

2. Related Works

Numerous researches have been proposed by researchers for the image compression process. In this section, a brief review of some important

contributions from the existing literature is presented.

Panrong, X. 2001[6] studied image compression with wavelet transform. As a necessary background, the basic concepts of graphical image storage and currently used compression algorithms are discussed. The mathematical properties of several types of wavelets are covered and the Embedded Zero tree Wavelet (EZW) coding algorithm was introduced.

Wasan, K. S. 2004 [7], This thesis was concerned with a certain type of compression that uses hybrid technique which combines differential pulse code modulation (DPCM) with wavelet transform. The wavelet transform is applied to the difference frame instead of direct application to the original images because the different signal is almost nearly stationary.

Husen, H. H. 2006, [8] studied image compression with multiwavelets transform based image encoder. A compression example verified with wavelet-based transform once, then with a multiwavelets-based transform on the same image. Both wavelet and multiwavelets are applied to each block of the image. Such an implementation shows that Multiwavelets method is better to the wavelet method in terms of image quality. After testing several methods of multiwavelet transforms computation for image compression the mixed method was chosen.

Mohammed Hussien Miry, 2008 [9], studied new transform "improved Ridgelet Transform, he used SLT instead of DWT in the Ridgelet. A comparison was made with compression using Ridgelet transform for different images. A high quality image has been achieved for natural images. Simulation results indicate that the improvement Ridgelet transform offers superior and faster compression performance compared to the Ridgelet transform based approaches.

Ali Hussien mary, 2010 [10], used Differential pulse code modulation (DPCM) in slantlet transform and Run Length Code for image compression. Apply SLT on each component in the color image (after applying color space conversion from RGB to YCbCr) and encoding Y component by DPCM and encoding Cb and Cr with RLC. The compression ratio and Peak Signal to Noise Ratio (PSNR) are used as measurement tools. When comparing the proposed approach with other compression methods Good result is obtained.

Nushwan Y. Baithoon 2011 [11], proposed a hybrid transform based on (DWT) and (DCT) with a new enhancement method, which is the sliding run length encoding (SRLE) technique, to improve the compression. First step involves transforming the color components of the image from RGB to YUV planes to acquire the advantage of the existing spectral correlation and consequently gaining more compression. DWT is then applied to the Y, C_b and C_r color space information giving the approximate and the detail coefficients. The detail coefficients are quantized, coded using run length encoding (RLE) and SRLE. The approximate coefficients were coded using DCT, since DCT has superior compression performance when image information has poor power concentration in high frequency areas. This output is also quantized, coded using RLE and SRLE. Test results showed that the proposed DWT DCT SRLE system proved to have encouraging results in terms of (PSNR), Compression Factor (CF) and execution time when compared with some DWT based image compressions.

Moh'dAli Moustafa Alsayyh, Dzulkipli Mohamad, Waheeb abu-ulbaa 2013 [12], proposed hybrid technique between DCT & DWT. The first step is segment the image into background and foreground based, then divide the image into 8x8 blocks, implement the DCT coefficients for each block. & quantize the DCT coefficients based on quantization table, and transform the output image using DWT and apply another quantization table. PSNR and MSE is better than the old algorithms and due to. Hence overall result of hybrid compression technique is good.

Deepak Kumar Jain, Devansh Gaur, Kavya Gaur, Neha Jain [13] 2014, presents medical image compression technique using DCT and Huffman encoding. First divide the image into blocks and apply DCT to each block, quantize the DCT coefficients and encode it using Huffman encoding. This technique is better performance compared with many others compression techniques.

Zhou, Xiao, Yunhao Bai, and Chengyou Wang [14] 2015, they proposed image compression scheme, based on (DCT). It's a hybrid method, which combines vector quantization (VQ) and differential pulse code modulation (DPCM). This scheme begins with transforming image from spatial domain to frequency

domain using DCT. Then the block data is transformed into a vector according to zigzag order, and then truncated. After that, the vector is split into DC coefficient and AC coefficients. After scale quantization, DC coefficient is coded using DPCM. AC coefficients are coded using multistage vector quantization (MSVQ). Then, entropy encoding is performed on index-tables and DC part, separately. The experimental results show that, compared to conventional VQ and DCTVQ schemes, proposed scheme has a better performance.

Karthikeyan T, Thirumoorthi C. [15] 2016, they compared five image compression techniques to compress medical images. They used Fourier transform, DCT, WHT, KLT, and the proposed Sparse Fast Fourier Transform. The experimental results show that.

$$D_{DCT}(i, j) = \frac{1}{\sqrt{2N}} B(i) B(j) \sum_{x=0}^{N-1} \sum_{y=0}^{N-1} M(x, y) \cos\left[\frac{2x+1}{2N} i\pi\right] \cos\left[\frac{2y+1}{2N} j\pi\right] \dots (1)$$

where

$$B(u) = \begin{cases} \frac{1}{\sqrt{2}} & \text{if } u = 0 \\ 1 & \text{if } u > 0 \end{cases}$$

M (x,y) is the input data of size x×y. The input DCT on the blocks, DCT coefficients are then quantized using an 8×8 quantization table where parts of compression actually occur, the less important frequencies are discarded, hence the use of the lossy. Then the most important frequencies that remain are used retrieve the image in decomposition process [18].Figure.1 illustrate the whole procedure.

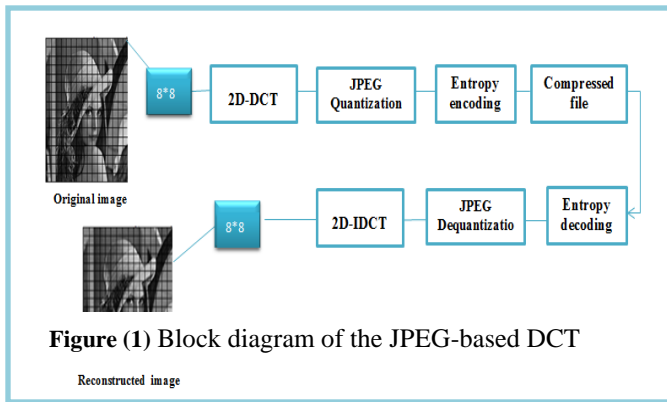


Figure (1) Block diagram of the JPEG-based DCT

compression .wavelet analysis use multiresolution analysis (MRA) technique of signals [19] that divide information of image into approximation and detail parts, were set of high pass filter & low pass filter applied to image. if the signal is put through high pass filter and low pass filter then the signal is decomposed into two parts a detail part (high frequency) and the approximation part (low frequency), the sub-signals produced from low

3. Theoretical side:

In this section, DCT, DWT, SLT and Hybrid DCT-SLT techniques are discussed.

3.1 Discrete Cosine Transform(DCT):

It’s the basis for many image and video compression algorithms, especially the baseline JPEG and MPEG standards for compression of still and video images respectively .The DCT has the property of compaction the most visually significant information of the image into few low frequency coefficients in the upper left side and requires less computational resources [16].there is mainly two type of DCT: 1D DCT and 2D DCT for N x N input signal defined as follow: [17]

image is divide into 8X8 blocks then applying the 2D-

filters will have highest frequency equal to half of the original according to Nyquist sampling this change in frequency range means that only half of original samples need to kept in order to perfectly reconstruct the signal. At every level, four sub-images are got: one approximation and three detail (LL, LH, HL, and HH) as illustrated in figure (2) [20]. Then all the coefficients are discarded, except the LL coefficients that are transformed into the second level. These coefficients are then passed through a constant scaling factor to achieve the desired compression ratio. The DWT is usually implemented in form of an iterated filter bank, where a tree structure is utilized. Hence, the component filter branches rely on product form of implementation [15]. Following figure 3 is an illustration of Two-scale Filter bank and an Equivalent of DWT. Here, F[z] is the high frequency component, and H[z] is the low frequency component. For data reconstruction, the coefficients are rescaled and padded with zeros, and passed through the wavelet filters.

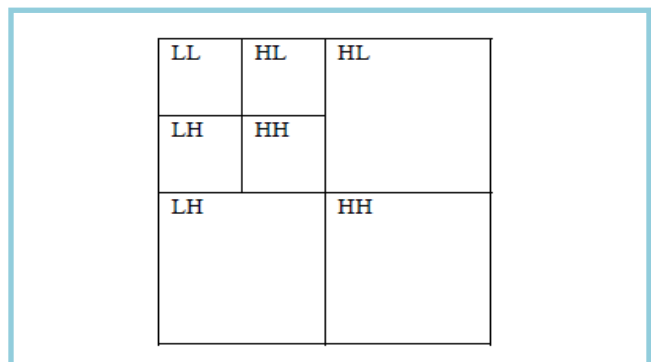


Figure (2) two level decomposition wavelet transform

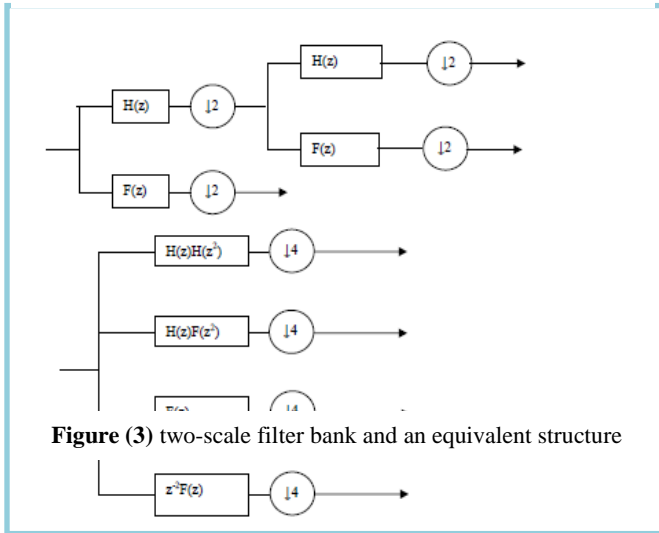
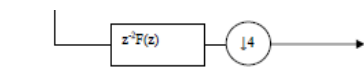


Figure (3) two-scale filter bank and an equivalent structure

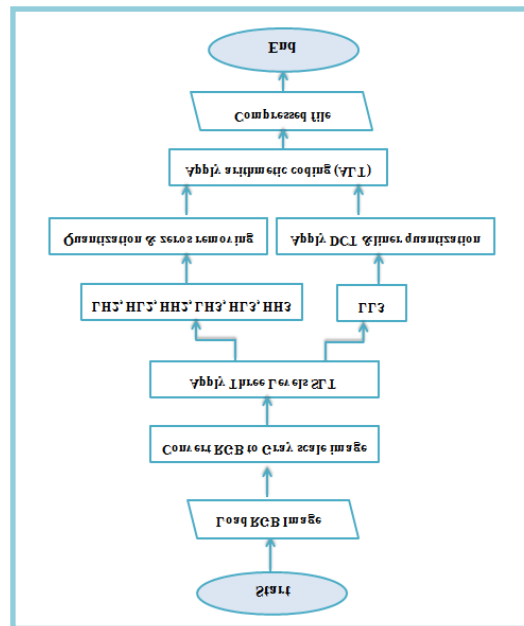


two zero moments and it provides better time localization than DWT [19].DWT requires a large number of iterations to achieve a discrete time basis for an optimal result [18]. Therefore Slantlet transform (SLT) is adopted in this paper because it is not based on iterated filter bank; instead, it is based on a filter bank structure where different filters are used for each scale; hence, the component filter branches do not rely on any product form of implementation and it possesses extra degrees of freedom. For a two-channel case the Daubechies filter is the shortest filter which makes the filter bank orthogonal and has K zero moments. For K=2 zero moments the iterated filters lengths equal 10 and 4 but the Slantlet filter bank with K=2 zero moments has filter length 8 and 4. Thus the two-scale Slantlet filter bank has a filter length which is two samples less than that of a two-scale iterated Daubechies-2 filter bank. This difference grows with the increased number of stages. Each filter bank has a scale dilation factor of two and provides a multi-resolution decomposition. The Slantlet filters are piecewise linear. Even though there is no tree structure for Slantlet it can be efficiently implemented like an iterated DWT filter bank. Therefore, computational complexity of SLT is of the same order as of DWT, but SLT gives better performance in de-noising and compression of the input signals [21].

4. The proposed hybrid technique:

The purpose of the hybrid SLT-DCT technique is to exploit the properties of both SLT and DCT. The technique begins with selecting original image of size 512x512 or any resolution and converted into the transform domain using three level of SLT, in each of these three levels low frequency coefficients (LL) are passed to the next stage where the high frequency coefficients (HL, LH, and HH) are quantized and remove zeros from it. Then DCT is applied to LL3 of the third level to achieve a higher compression liner quantization (uniform) is performed. In this

stage, many of the higher frequency components are rounded to zero. The quantized coefficients are then encoded using Arithmetic coding (ALT).Then the image is reconstructed by following the inverse procedure. During inverse SLT, zero values are padded in place of detailed coefficients [22]. The block diagrams are given in Fig. 4 & 5 below that represents the flow of the abovementioned methodology. The high frequency component is reduced using quantization factor its default range between [0.01 - 0.1] the reconstructed image will be degraded (blurred) if Factor greater than or equal to 0.1, then eliminating zeros form each sub-band, and compress each sub-band by Arithmetic Coding. DCT is applied on LL3 sub-band its component is reduced using liner quantization factor with range [0.005-0.01] its default value "0.01" is divided by low frequency LL3 component, and then compress it by Arithmetic Coding



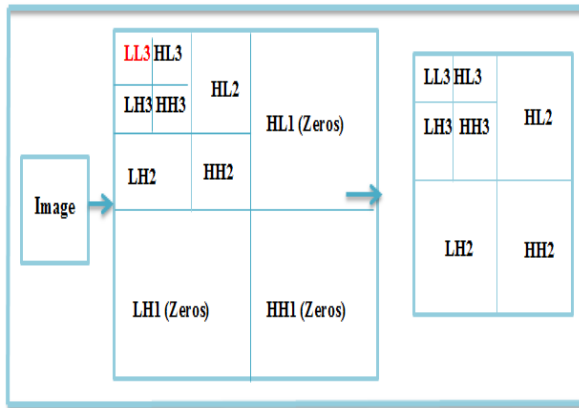


Figure (4) A flowchart of the proposed hybrid technique

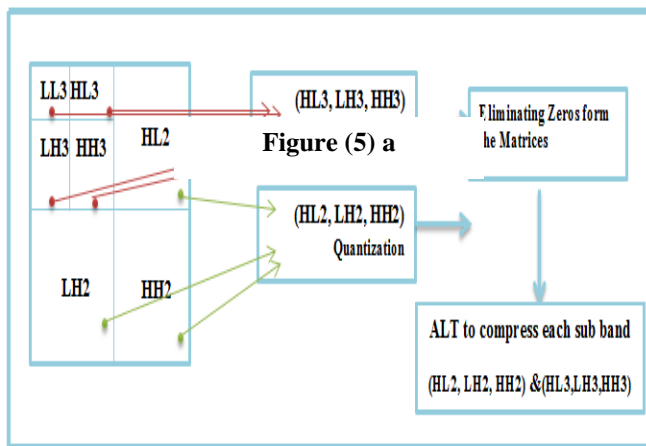


Figure (5) b

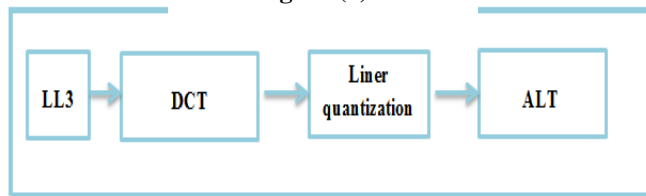


Figure (5) c – Compression technique

5. Performance evaluation parameters

1. Image quality assessment based on error sensitivity

A natural way to determine the fidelity of a recovered image is to find the difference between the original and reconstructed values. Two popular measures of distortion are:

$$MSE = \frac{1}{m \cdot n} \sum_{i=0}^{m-1} \sum_{j=0}^{n-1} [I(i, j) - K(i, j)]^2 \quad \dots (2)$$

Where I (i,j) is the original image of size i×j, K(i,j) is the reconstructed image of size i×j.

1.2 PSNR: It is the most popular tool for the measurement of the compressed image and video. It is simple to compute. The PSNR in decibel is evaluated as follows [23]:

1.1 MSE: mean squared error it is another performance evaluation parameter of Image Compression Algorithms. It is an important evaluation parameter for measuring the quality of compressed image. It compares the original data with reconstructed data and then results the level of distortion. The MSE between the original data and reconstructed data is:

$$PSNR = 10 \cdot \log_{10} \left(\frac{MAX_I^2}{MSE} \right) \dots (3)$$

2. Compression Ratio

The most popular metric of performance measure of a data compression algorithm is the compression ratio. It is defined as the ratio of the number of

$$CR = \frac{\text{uncompressed data}}{\text{compressed data}}$$

Sometimes the space savings is given instead, which is defined as the reduction in size relative to the uncompressed size:

$$\text{saving space} = \left(1 - \frac{\text{Compressed size}}{\text{uncompressed size}} \right) * 100\%$$

3.

3.1 Universal Quality Measure (UQI):

Wang and Bovik [25], developed a mathematical approach to calculate the image quality measure by having access to both the original image and distorted image as follows:

$$Q = \frac{\sigma_{xy}}{\sigma_x \sigma_y} \cdot \frac{2\bar{x}\bar{y}}{(\bar{x})^2 + (\bar{y})^2} \cdot \frac{2\sigma_x \sigma_y}{\sigma_x^2 + \sigma_y^2} \dots (5)$$

Where (x) is the base image intensity values and (y) is the distorted image intensity values with respected mean and variances:

$$\bar{x} = \frac{1}{N} \sum_{i=1}^N x_i \dots (6) \quad , \quad \bar{y} = \frac{1}{N} \sum_{i=1}^N y_i \dots (7) ,$$

$$\sigma_x^2 = \frac{1}{N-1} \sum_{i=1}^N (x_i - \bar{x})^2 \dots (8) ,$$

algorithm uses 8x8 windows and will make a map of the SSIM values. The average of the obtained SSIM map will provide the quality measure as follows:

$$MSSIM(X, Y) = \frac{1}{M} \sum_{j=1}^M SSIM(x_j, y_j) \dots (13)$$

Where M is the number of steps depending on the size of the image. The higher values of MSSIM will provide a better quality of the distorted images.

6. Experimental results

The proposed (SLT-DCT) technique and (DWT-DCT) are implemented using Matlab 2016. The techniques applied on

bits to represent the original data to the number of bits to represent the compressed data [24].

$$\sigma_y^2 = \frac{1}{N-1} \sum_{i=1}^N (y_i - \bar{y})^2 \dots (9) ,$$

$$\sigma_x^2 = \frac{1}{N-1} \sum_{i=1}^N (x_i - \bar{x})(y_i - \bar{y}) \dots (10).$$

In this algorithm there is a sliding window of size 8x8 which will slide the 8x8 portions of distorted image on the corresponding areas of the base image and calculates Q in this Equation. This will provide a map of Qs and the average value of this map will provide us the quality measure as follows:

$$Q = \frac{1}{M} \sum_{j=1}^M Q_j \dots (11)$$

where M is the number of steps depending on the size of the image. The higher values of Q may indicate a better quality for the distorted image.

3.2 Structural Similarity (SSIM):

Wang et al [25,26] developed a Structural Similarity (SSIM) quality measure method which is considered as the full original image quality measure. In this method Wang improved the (UQI) and hence calculated the image quality measure as follows:

$$SSIM(x, y) = \frac{(2\bar{x}\bar{y} + c_1)(2\sigma_{xy} + c_2)}{(\bar{x}^2 + \bar{y}^2 + c_1)(\sigma_x^2 + \sigma_y^2 + c_2)} \dots (12)$$

images), and K>1 is a small constant. Also x is the original image and y is the distorted image intensities. This gray scale images with dimension (512*512) and (256*256). Original and reconstructed images are also shown in table 5. Table No.1 shows different compression ratio and the PSNR in dB of different gray images. The proposed technique increased the CR, PSNR, SSIM and UQI over the other technique (DWT-DCT). The results revealed that average PSNR value of more than 43dB was achieved, which is considered very high, the file size reduced from (786432 byte) to (29494 bytes) in the proposed technique and reduced to (46917 byte) in the other technique. In our work the time required to compute (SLT-DCT) is 16.085sec while in (DWT-DCT) is 33.624 sec, this means that the proposed technique is better than the other technique

Table (1) CR, MSE and PSNR values obtained using hybrid (DWT-DCT) & the proposed technique (SLT-DCT) for image dimension (512*512).

Image	Transform	Uncompressed file size	Compressed file size	CR	MSE	PSNR
1	DWT-DCT	786432 bytes	46917 bytes	16.762	18.6384	35.4607
	Proposed(DCT-SLT)	786432 bytes	29494 bytes			
2	DWT-DCT	786432 bytes	358			

Table (2) SSIM ,UQI and saving space values for image dimensions

Image	Transform	SSIM
-------	-----------	------










Table (3) CR, MSE and PSNR values obtained using hybrid (DWT-DCT) & the proposed technique (SLT-DCT) for image dimension (256*256).

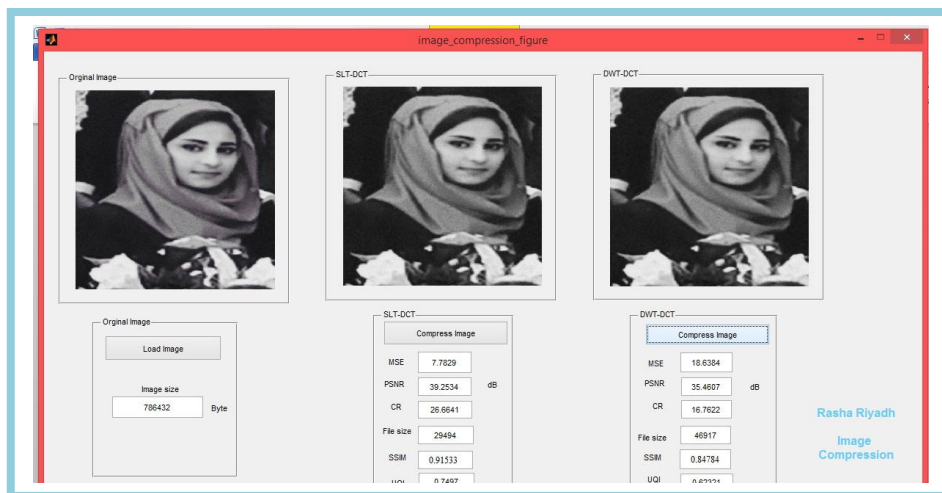
Image	Transform	Uncompressed file size	Compressed file size	CR	MSE	PSNR
1	DWT-DCT	196608 bytes	15381 bytes	12.782	28.5795	33.604
	Proposed(SLT-DCT)	196608 bytes	14036 bytes	14.007	11.5024	37.556
2	DWT-DCT	196608 bytes	14067 bytes	13.976	21.4319	34.854
	Proposed(SLT-DCT)	196608 bytes	11833 bytes	16.615	4.7238	41.421
3	DWT-DCT	196608 bytes	12923 bytes	15.213	21.483	34.843
	Proposed(SLT-DCT)	196608 bytes	12699 bytes	15.482	7.4334	39.452

Table (4) SSIM ,UQI and saving space values for image dimension (256*256).

Image	Transform	SSIM	UQI	Saving Space
1	DWT-DCT	0.81746	0.63198	92%
	Proposed(SLT-DCT)	0.93866	0.82229	92%
2	DWT-DCT	0.83945	0.70461	92%
	Proposed(SLT-DCT)	0.95597	0.90105	93%
3	DWT-DCT	0.82236	0.68424	93%
	Proposed(SLT-DCT)	0.94581	0.86725	93%

Table (5) compression of different gray image

Image	Original Image	SLT-DCT	DWT-DCT
1			
2			
3			



. Conclusion

In this work the (SLT-DCT) technique has been applied for compression of gray images. The SLT is an orthogonal DWT and provides improved time localization than DWT. It uses different filter for each scale to get different information for input signal. It is observed from the results that the hybrid SLT-DCT algorithm for image compression has better performance in quality wise and performance wise compared to DWT-DCT. The **Figure (6): Compression Program interface**

References

- [1] Kharate, Gajanan K., A. A. Ghatol, and Priti P. Rege. "Image Compression using Wavelet Packet Tree based on Threshold Entropy." *SPPRA*. 2006.
- [2] Acharya, Tinku, and Ajoy K. Ray. **Image processing: principles and applications**. John Wiley & Sons, 2005.
- [3] Elbadri, Mohammed, et al. "Hardware support of JPEG." Canadian Conference on Electrical and Computer Engineering, 2005.. IEEE, 2005.
- [4] Nick. D. P.,Ken, F. and Sukit, L.,” **Lossy Image Compression Using Wavelets Transform**”, Journal of Intelligent and Robotic Systems 28, pp.39–59, 2000.
- [5] Witten, Ian H., Radford M. Neal, and John G. Cleary. "Arithmetic coding for data compression." *Communications of the ACM* 30.6 (1987): 520-540.
- [6] Xiao, Panrong. "Image Compression by Wavelet Transform" (2001).
- [7] Wasan ,K. S., "Hybrid DPCM/Wavelet for Image Compression",Master, thesis, university of Technology ,October (2004).
- [8] Husen H. H. "Image Data Compression Using Multiwavelet Transform" ,Master thesis ,Science in Computer Science,Jan (2006).
- [9] Mohammed Hussien Miry "Image Compression Using Improved Ridgelet Transform" IRAQI JOURNAL OF COMPUTERS, COMMUNICATION AND CONTROL & SYSTEMS ENGINEERING Volume: 8 Issue: 1(2008) Pages: 58-66.
- [10] Ali Hussien mary "Hybrid Color Image Compression based DPCM and Slant Transform" Nahrain University, College of Engineering Journal (NUCEJ) Vol.13 No.1 (2010), pp.98-107.
- [11] Nushwan Y. Baithoon "Combined DWT and DCT Image Compression Using Sliding RLE Technique" Baghdad Science Journal Vol.8(3)(2011).
- [12] Moh'dAli Moustafa Alsayyh ,Dzulkifli Mohamad , Waheeb abu-ulbaa "Image Compression Using Discrete Cosine Transform and Discrete Wavelet Transform "Journal of Information Engineering and Applications www.iiste.org ISSN 2224-5782 (print) ISSN 2225-0506 (online) Vol.3, No.11, (2013).
- [13] Deepak Kumar Jain, Devansh Gaur, Kavya Gaur , Neha Jain, "Image Compression using Discrete Cosine Transform and Adaptive Huffman Coding", *Int. J. of Emerging Trends Technology in Computer Science (IJETTCS)*, Vol. 3, Issue 1, Jan. Feb. (2014).
- [14] Zhou, Xiao, Yunhao Bai, and Chengyou Wang. "Image Compression Based on Discrete Cosine Transform and Multistage Vector Quantization." *International Journal of Multimedia and Ubiquitous Engineering* 10.6 (2015): 347-356.
- [15] Karthikeyan T, Thirumoorthi C." A Novel Approach on Discrete Cosine Transform Based Image Compression Technique for Lung Cancer". *Biosci Biotech Res Asia*(2016).
- [16] R. G. Gonzalez and P. Wintz, "Digital Image Processing", Addison-Wesley, 1987.
- [17]R. K. Rao, P. Yip, "Discrete Cosine Transform: Algorithms, Advantages and Applications". NY: Academic, 1990.
- [18] Kaur, Manjinder, and Gaganpreet Kaur. "A survey of lossless and lossy image compression techniques." *International Journal of Advanced Research in Computer Science and Software Engineering* 3.2 (2013): 323-326.
- [19] Găspăresc, Gabriel. "Power Quality Data Compression". INTECH Open Access Publisher, 2013.
- [20] Rashi Agarawal " The Theory of Wavelet Transform and its implementation using Matlab" Image processing courses in YouTube,2013.
- [21] Hasan, Harith R., Ghazali Bin Sulong, and Ali Selamat,"A Novel Blind Color Image Watermarking Technique in Hybrid Domain Using LSB Approach and Discrete Slantlet Transform" *Jokull Journal* ISSN:0449.0576, Vol 63, No. 7:Jul 2013.
- [22] Said, Amir, and William A. Pearlman, "A new, fast, and efficient image codec based on set partitioning in hierarchical trees", *IEEE Transactions on Circuits and Systems for Video Technology*, vol. 6, no. 3, pp. 243–250,1996.
- [23] R.Costantini, J.Bracamonte, G.Ramponi, J.L.Nagel, M.Ansorge, and F.Pellandini, "Low complexity video coder based on discrete Walsh Hadamard transform," in *Proc. European signal processing conference*, 2002, pp. 1217–1220.
- [24] Acharya, Tinku, and Ping-Sing Tsai.,” **JPEG2000 Standard for Image Compression Concepts, Algorithms and VLSI Architectures**” A John Wiley & Sons, Inc Publication 2005.
- [25] Z. Wang, A.C. Bovik, H.R. Sheikh and E.P. Simoncelli, "Image quality assessment: from error visibility to structural similarity," *IEEE Transactions on Image Processing* , vol.13, no.4pp. 600- 612, April 2004.
- [26] Z. Wang, H. R. Sheikh, and A. C. Bovik, "Objective video quality assessment," in *The Handbook of Video Databases:Design and Applications*, B. Furht and O. Marques, Eds. CRC Press, 2003.

Using Laplace Transformation Technique to solve boundary value problems

Dunya Mohee Hayder,

Madinat Al-Elm University College

dunyamoheehaydee@gmail.com

Abstract:

In this paper, applying Laplace transform technique will be discussed and to solve partial differential equation with boundary conditions that have significant importance in engineering and physical applications, where two kinds of partial differential equations were solved using these transformations on both sides of the equations then applying the boundary equations to find the general solutions.

Keywords: Laplace transform, Partial Differential Equations, Boundary Value Problems.

الخلاصة

في هذا البحث سيتم استخدام تحويلات لابلاس في حل المسائل ذات الشروط الحدودية والتي تظهر في بعض انواع المعادلات التفاضلية الجزئية ذات الاهمية في التطبيقات الهندسية والفيزيائية، حيث تم حل نوعين من المعادلات الجزئية التفاضلية عبر استخدام تلك التحويلات على طرفي المعادلات ثم تطبيق الشروط الحدودية لايجاد الحل النهائي.

الكلمات المفتاحية: تحويل لابلاس، المعادلات التفاضلية الجزئية، مشاكل قيمة الحدود

Introduction:

In various areas of science and engineering we might use Laplace transformation technique to solve our problem because it is very powerful mathematical tool [7]. It can solve initial value problem in ordinary differential equation, initial value problem and boundary value problem in partial differential equations.

There is no general method to solve P.D.E [6], but some boundary value problem might be faced, that can be solved using differential transformation [4], and, Laplace transformation method is applied to the time domain [3]. It can solve O.D.E. and P.D.E. because it can transfer O.D.E. to algebraic equation as well as transferring P.D.E. to O.D.E., furthermore, Laplace transformation when facing an infinite domain, it can handle the boundary condition effectively [5].

1. Laplace transformation technique

The immediate Laplace transformation formula for a function $f(t)$ be a function defined for $(0 \leq t \leq \infty)$, then $f(t)$ will have the following Laplace integral:

$$\int_0^{\infty} f(t)e^{-st} dt,$$

which will be denoted $\mathcal{L}(f(t))$ [1]

1.1 Theorem 1: if $f(t)$ have an exponential order and is piecewise regular on $[0, \infty)$ and exponential order, then for any value of s which greater than the abscissa of convergence of $f(t)$, the integral $\int_0^{\infty} f(t)e^{-st} dt$ converges, (1).

1.2 Definition: The improper integral $\int_0^{\infty} F(s, t) dt$ is said to be converge uniformly over a given set S of s values of a given any $\epsilon > 0$, there exist a number B , depending on ϵ but not s , such that

$$|\int_0^{\infty} F(s, t) dt| < \epsilon \text{ for } b > B \text{ and all } s \text{ in the set } S$$

1.3 Theorem 2 if $f(t)$ is piecewise regular and of exponential order with abscissa of convergence α_0 , then for any number $s_0 > \alpha_0$,

$$\mathcal{L}\{f(t)\} = \int_0^{\infty} f(t)e^{-st} dt$$

Converges uniformly for all values of s such that $s_0 > \alpha_0$, [1].

2. Some Properties of Laplace Transformation [2]

2.1 \mathcal{L} is a linear transformation where the sum between functions will be:

$$\int_0^{\infty} e^{-st} [\alpha f(t) + \beta g(t)] dt = \alpha \int_0^{\infty} e^{-st} f(t) dt + \beta \int_0^{\infty} \beta g(t) dt$$

Whenever both integrals converge for $s > c$.

$$\begin{aligned} \mathcal{L}\{\alpha f(t) + \beta g(t)\}dt &= \\ \alpha \mathcal{L}\{f(t)\} + \beta \mathcal{L}\{g(t)\} &= \\ \alpha F(s) + \beta G(s). \end{aligned}$$

2.2 Theorem: Transform of a Derivative [2]

If $f, f', \dots, f^{(n-1)}$ are continuous on $[0, \infty)$ and are of exponential order and if $f^{(n)}$ is piecewise-continuous on $[0, \infty)$, then

$$\begin{aligned} \mathcal{L}[f^{(n)}(t)] &= s^n F(s) - \\ s^{n-1} f(0) - s^{n-2} f'(0) - \\ f^{(n-1)}(0). \end{aligned}$$

2.3 Example: consider the following problem:

$$\begin{aligned} f_{tt} - v^2 f &= 0 \\ f(0) &= 0 \\ f_t(0) &= v \end{aligned}$$

Solution: Apply theorem 2.1

$$\mathcal{L}(f_{tt} - v^2 f) = \mathcal{L}(0)$$

We know that \mathcal{L} is linear

$$\therefore \mathcal{L}f_{tt} + v^2 \mathcal{L}f = 0$$

$$\begin{aligned} s^2 F(s) - sf(0) - f_t(0) - \\ v^2 F(s) = 0 \end{aligned}$$

Substituting initial conditions

$$s^2 F(s) - v - v^2 F(s) = 0$$

$$(s^2 - v^2) F(s) = v$$

$$F(s) = \frac{v}{s^2 - v^2}$$

According to table (1)

$$\mathcal{L}^{-1}F(s) = \sinh vt$$

After solving this example, it can be noticed that the true difficulty regarding the application of Laplace transform is to obtain on inversion criteria.

Table 1: table of Laplace transforms

	$f(x)$	$F(x)$	$a(s > a)$
1		$\frac{1}{s}$	
2	e^{st}	$\frac{1}{s - a}$	a
3	$t^n (n = 1, 2, \dots)$	$\frac{n!}{s^{n+1}}$	
4	$t^n e^{at} (n = 1, 2, \dots)$	$\frac{n!}{(s - a)^{n+1}}$	a
5	$\sin kt$	$\frac{k}{s^2 + k^2}$	
6	$\cos kt$	$\frac{s}{s^2 + k^2}$	
7	$\sinh kt$	$\frac{k}{s^2 - k^2}$	$ k $
8	$\cosh kt$	$\frac{s}{s^2 - k^2}$	$ k $
9	$e^{-at} \sin kt$	$\frac{k}{(s + a)^2 + k^2}$	$-a$
10	$e^{-at} \cos kt$	$\frac{s + a}{(s + a)^2 + k^2}$	$-a$
11	\sqrt{t}	$\frac{\sqrt{\pi}}{2\sqrt{s^3}}$	
12	$\frac{1}{\sqrt{t}}$	$\frac{\sqrt{\pi}}{s}$	0

Application

Example 3.1: Let the mathematical model of the displacement $f(x, t)$ of point in a string that has a length L at rest with fixed ends, and a force $F_0 \sinh \omega t$, was applied at initial

$$\frac{\partial^2 f}{\partial t^2} = c^2 \frac{\partial^2 f}{\partial x^2} + F_0 \sinh \omega t \quad 3.1$$

$$f(0, t) = 0, \quad t > 0 \quad 3.1.1$$

$$f(L, t) = 0, \quad t > 0 \quad 3.1.2$$

$$f(x, 0) = 0, \quad 0 < x < L \quad 3.1.3$$

$$\frac{\partial f}{\partial t} = 0, \quad 0 < x < L \quad 3.1.4$$

To begin, take the Laplace transform equation to obtain

$$s^2 F(s) - sf(0) - f_t(0) = c^2 \frac{\partial^2}{\partial x^2} \mathcal{L}\{f\} + F_0 \frac{\omega}{s^2 + \omega^2}$$

By applying the boundary conditions (3.1.1) and (3.1.2), the following equations becomes:

$$s^2 F(x, s) = c^2 \frac{\partial^2 (x, s)}{\partial x^2} + F_0 \frac{\omega}{s^2 + \omega^2}, \quad 0 < x < L$$

Or

$$\frac{\partial^2 F}{\partial x^2} - \frac{s^2}{c^2} F - f_t(0) = -\frac{F_0 \omega}{c^2 (s^2 + \omega^2)} \quad 0 < x < L$$

This is now an ordinary differential equation that is subject to the transformed condition:

$$F(0, s) = 0 \quad 3.2$$

$$F(L, s) = 0 \quad 3.3$$

The homogeneous solution to this equation is

$$F(x, s) = Ae^{\frac{s}{c}x} + Be^{-\frac{s}{c}x}$$

A particular solution can be found by assuming that $F_x x = 0$,. This will give

$$F(x, s) = \frac{F_o \omega}{s^2 (s^2 - \omega^2)}$$

Therefore, the general solution will be:

$$F(x, s) = A e^{\frac{s}{c}x} + B e^{-\frac{s}{c}x} + \frac{F_o \omega}{s^2 (s^2 - \omega^2)}$$

Applying the boundary conditions (3.2) and (3.3), the following equations are obtained:

$$0 = A + \frac{F_o \omega}{s^2 (s^2 - \omega^2)}, \quad 0 = A e^{\frac{s}{c}x} + B e^{-\frac{s}{c}x} + \frac{F_o \omega}{s^2 (s^2 - \omega^2)}$$

$$A = -\frac{F_o \omega}{s^2 (s^2 - \omega^2)}$$

$$B = \frac{F_o \omega}{s^2 (s^2 - \omega^2)} e^{\frac{2sL}{c}} - \frac{F_o \omega}{s^2 (s^2 - \omega^2)}$$

Hence,

$$U(x, s) = -\frac{F_o \omega}{s^2 (s^2 - \omega^2)} e^{\frac{s}{c}x} + \frac{F_o \omega}{s^2 (s^2 - \omega^2)} e^{-\frac{s}{c}x} \\ \times \left(-1 + e^{\frac{s}{c}x} \right) e^{-\frac{s}{c}x} + \frac{F_o \omega}{s^2 (s^2 - \omega^2)}$$

Example 3.2

Now, consider what might be referred to as one dimensional wave problem:

$$\frac{\partial^2 u}{\partial t^2}(x, t) = c^2 \frac{\partial^2 u}{\partial x^2}(x, t) + \cos(\pi x), \quad 0 < x < 1, \quad t > 0$$

$$u(x, 0) = 0, \quad u_t(x, 0) = 0$$

$$u(0, t) = 0, \quad u(1, t) = 0$$

By applying the Laplace transform for the equation, and the conditions must be used, to get

$$\begin{aligned} \frac{d^2 U}{dx^2}(x, s) &= s^2 U(x, s) - su(x, 0) - u_t(x, 0) - \frac{\cos \pi x}{s} \\ &= s^2 U(x, s) - \frac{\cos \pi x}{s} \end{aligned}$$

The ordinary differential equation, which is non homogeneous with constant coefficient must be solved.

$$\frac{d^2 U}{dx^2}(x, s) - s^2 U(x, s) = \frac{\cos \pi x}{s}$$

Once again

$$U(x, s) = U_h(x, s) + U_p(x, s)$$

Where $U_h(x, s)$ is the general solution of the homogeneous problem:

$$U_h(x, s) = c_1 e^{sx} + c_2 e^{-sx}$$

Where $U_p(x, s)$ is particular solution of the non-homogeneous problem:

$$U_p(x, s) = A \cos(\pi x) + B \sin(\pi x)$$

Use the undetermined coefficient method to find A and B , where;

$$\frac{d}{dx} U_p(x, s) = -\pi A \sin(\pi x) + \pi B \cos(\pi x)$$

$$\frac{d^2}{dx^2} U_p(x, s) = -\pi^2 A \cos(\pi x) + \pi^2 B \sin(\pi x)$$

Therefore

$$\begin{aligned} \frac{d^2}{dx^2} U_p(x, s) - s^2 U_p(x, s) &= (-\pi^2 - s^2)[A \cos(\pi x) + B \sin(\pi x)] \\ &= -\frac{\cos(\pi x)}{s} \end{aligned}$$

Which will lead to the following:

$$-(s^2 + \pi^2)B = 0 \quad \text{and} \quad -(s^2 + \pi^2)A = -\frac{1}{s},$$

So that

$$B = 0, \quad A = \frac{1}{s(s^2 + \pi^2)}$$

Where;

$$U_p(x, s) = \frac{\cos(\pi x)}{s(s^2 + \pi^2)}$$

And

$$U(x, s) = c_1 e^{sx} + c_2 e^{-sx} + \frac{\cos(\pi x)}{s(s^2 + \pi^2)}$$

Next by applying the BCs to find c_1 and c_2

$$c_1 = \frac{1}{s(s^2 + \pi^2)} \quad ; \quad c_2 = 0$$

$$\therefore u(x, s) = \frac{e^{sx}}{s(s^2 + \pi^2)} + \frac{\cos(\pi x)}{s(s^2 + \pi^2)}$$

conclusions:

Laplace transformation technique is a practical tool to solve P.D.E. with initial boundary value problems, and it might give strong motivation to consider solving all kind of P.D.E. with boundary value condition like heat equation in one or two dimension.

References:

- [1] Advanced Engineering Mathematics, C.RAY WYLIE, LOUIS C. BARRETT, McGraw HILL Book Company, fifth edition 1982.
- [2] Advanced Engineering Mathematics, Dennis G. Zill, Michael R. Cullen, Sudbury, mass: Jones and Bartlett publishers, 3rd edition, 2006.
- [3] Applied Mathematical Modeling, Volume 31, Issue 4, April 2007, page 712-726
- [4] Solution of two-point boundary – value problems using the differential transformation method, Journal of optimization theorem and applications, October 1998, Volume 99 Issue1, P.P. 23-25
- [4] Solution of two-point boundary – value problems using the differential transformation method, Journal of optimization theorem and applications, October 1998, Volume 99 Issue1, P.P. 23-25
- [5] A note on solutions of wave, Laplace’s and heat equations with convolution terms by using double Laplace transform, H Eltayeb, A. Kiliçman, Applied Mathematics Letters, 21 (12) (2008), pp. 1324–1329
- [6] On Finite Product of Convolutions and classifications of hyperbolic and elliptic equations, Adem Kilicman and Hassan Eltayeb, Volume 54, Issues 9-10, November 2011, pages 2211-2219
- [7] Laplace Transforms and its Application, Sarina Adhikarc, Department of Electrical Engineering and Computer Science, University of Tennessee.

Hydraulic transient analysis in pumping stations due to power failure.
(Al-Mazak Closed Irrigation System), Kut, Iraq.

Dr. Mohammed Najm Abdullah
College of Engineering, Al-Mustansiriyah University
E-mail: dr.mohammednajim@yahoo.com

Abstract

This paper deals with the problems which may occur during transient state in pumping station in which pressure changes temporarily so much due to power failure that the network in pumping stations are damaged. A computer program was developed based on method of characteristics discussed by Chaudhry [1]. Some improvements were done in the technique used to meet the requirement of any problems may be take place in pumping stations. The developed program was applied to pumping stations in "Al-Mazak closed irrigation system" to treat the water hammering caused by power failure or sudden shutdown of the end valve. The results are presented for different assumptions and the suggested solutions to avoid any problem may be happened.

Key words: water hammer, transient state, characteristics method, power failure

التحليل الهيدروليكي العابر في محطات الضخ بسبب ف

الخلاصة

هذا البحث يتعامل مع المشاكل الناتجة عن حصول ظاهرة الحالة العابرة في محطات الضخ نتيجة للتغير الحاصل في الضغط نتيجة لانقطاع المفاجئ للتيار الكهربائي مما يسبب اضرار في شبكة الانابيب. تم بناء برنامج حاسوبي اعتمادا على طريقة الخصائص التي ناقشها [1] Chaudhry. تم تطوير البرنامج ليبيي المتطلبات لمعالجة اية مشاكل تحدث في محطات الضخ. تم تطبيق هذا البرنامج لتحليل الحالة العابرة في محطات الضخ لمشروع المزاك للري المغلق في محافظة واسط لمعالجة ظاهرة الطرق المائي نتيجة لانقطاع المفاجئ للتيار الكهربائي او نتيجة اغلاق مفاجئ للصمام عند نهاية الشبكة. نوقشت النتائج والحلول المطلوبة لتلافي اية مشاكل في تشغيل محطات الضخ.

الكلمات المفتاحية: ظاهرة الطرق المائي، الحالة العابرة، طريقة الخصائص، انقطاع التيار الكهربائي.

شمل السلطة

1- Introduction

Hydraulic transients occur when the steady state conditions change with time due to power failure or sudden shutoff of the end valve. A disturbance in steady state conditions take place at the point of disturbance, a pressure wave will travel and will be reflected back boundaries such as the valve, until a new steady state was reached, so that piping networks should be designed to withstand the

positive and negative pressure caused by transient condition.[1]

The aim of this study is to derive the equations governing the different boundary conditions in any pumping station, and then formulate a mathematical model for the project "Al-Mazak closed irrigation system", based on these equations of the transient state and the boundary conditions in which the method of characteristics was used for solving these

equations. The model is then used to account the maximum and minimum pressures occur during the transient state caused by power

failure or sudden end valve shutoff, when no control devices such as by-pass, surge tank, or control valves are available.

Table (1) Basic Design Data for Modules

Item	Description	Unit	PS#1	PS#2	PS#3
1	Design flow rate	m ³ /sec	0.352	0.652	0.652
2	Number of pumps a- Total b- Operating c- Stand-by		5 4 1	5 4 1	5 4 1
3	Pump rated capacity	m ³ /sec	0.088	0.163	0.163
4	Head	m	35	35	35
5	Natural ground level at PS	m	15.3	13.29	14.65
6	Natural ground level at suction side	m	12.6	11.99	12.51
7	Natural ground level at discharge side	m	16.08	14.49	16.15
8	Pump speed	rpm	1450	1450	1450
9	Motor speed	rpm	1450	1450	1450
10	Rated motor power	kW	36.9	69	69
11	Motor inertia WR ² Pump and motor inertia	kg.m ²	29 33	33 37	33 37

2- Non return valve

Each pump in "Al-Mazak closed irrigation system" is provided by a non return valve at its discharge pipe. The operation of this valve is such that it close whenever the head downstream the valve on the pipeline

side, is higher than the head upstream the valve on pump side, thus preventing reverse flow through pump. Closing the non return valve will isolate the effect of the pumps on the boundary condition.[2]

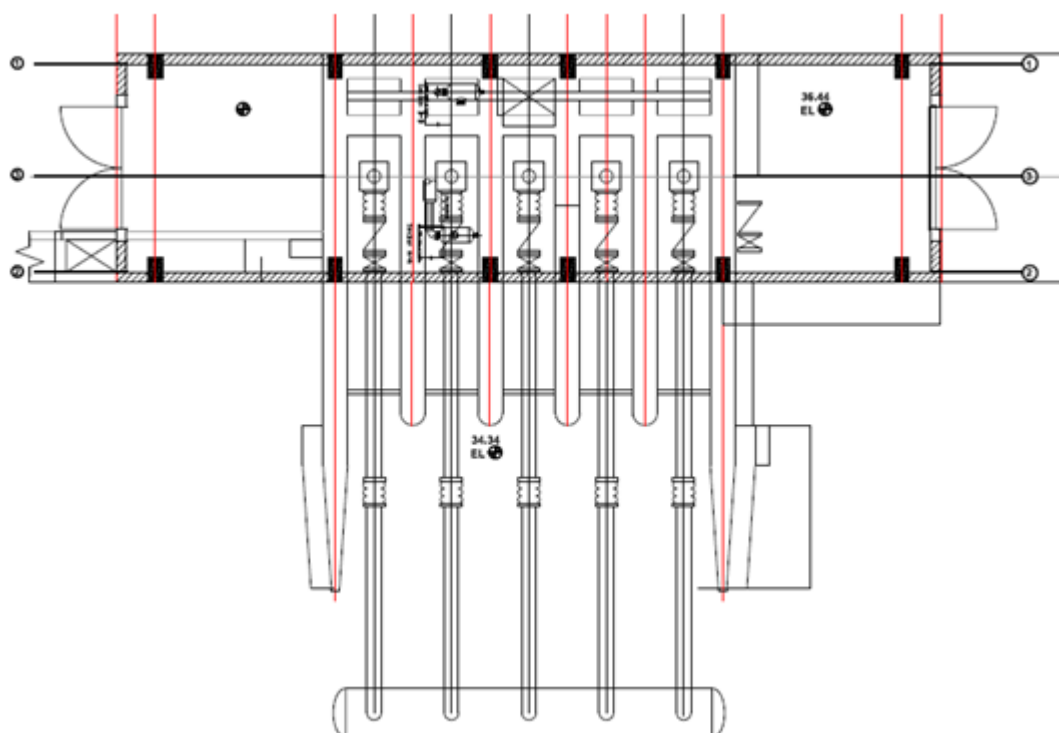


Figure (1): Schematic diagram of pumping station

3- The Mathematical Model

The pumping stations layout shown in figure 1 and pumps specifications are listed in table 1. The mathematical model based on the application of the transient state equations in elastic pipes. These equations are based on Newton's second law of motion and continuity equation. The assumptions are found in literature on fluid transient Chaudhry [1], Wylie and Streeter [2], and Paramakian [3].

The equation of motion can be written as

$$\frac{1}{\rho} \frac{\partial P}{\partial x} + v \frac{\partial v}{\partial x} + \frac{\partial v}{\partial t} + g \sin\theta + \frac{f v |v|}{2D} = 0 \quad (1)$$

And the continuity equation is

$$\rho a^2 \frac{\partial v}{\partial x} + \frac{\partial P}{\partial t} + v \frac{\partial v}{\partial x} = 0 \quad (2)$$

The two equations form a pair of hyperbolic differential equations in two independent variables, distance x and time t , and two dependent variables velocity V and pressure P .

In equations (1) and (2) the variables: wave speed (a), fluid density (ρ), pipe diameter (D) and friction factor (f) are called system parameters and do not change with time, and they may be a function of distance (x), fluid properties, flow conditions and pipe properties. It is well known that the friction factor varies with the Reynolds number and the relative roughness. Many formulas for calculating the friction factor during the steady state are available, while the variation of friction factor with the Reynolds number (Re) and the relative roughness during transient state is

unknown and no satisfactory method for calculation the friction factor during transient state available. It has become common practice that the same formulas for evaluating friction factor in steady state are assumed to be valid during transient state. In dealing with the transient problems Chaudhry [1] and Streeter & Wylie [2] considered the variation of the friction factor with Reynolds number during transient is to be small, and use constant friction factor equal to the steady state friction factor, in the transient state. The wave speed (a) in an elastic pipe is a function of the bulk

modulus of elasticity of fluid, the elastic properties of the pipe walls, pipe wall thickness, pipe diameter, density of the fluid and the pipe support conditions.[4]

Parmakian [3] shows that the convective acceleration term $v \frac{\partial v}{\partial x}$ and $v \frac{\partial v}{\partial x}$ in transient flow equations (1) & (2) are very small compared with the local acceleration terms and may be neglected. In addition when dealing with a piping system having a small angle of inclination with horizontal and the term $(g \sin \theta)$ is very small and can be neglected.

The equations (1) & (2) can be written in terms of piezometric head and discharge as dependent variables. The pressure and discharge are:

$$P = \rho g(H - z) \tag{3}$$

and

$$v = \frac{Q}{A} \tag{4}$$

Since the slope of the pipe is neglected, then $\frac{\partial z}{\partial x} = 0$. Liquid density variation with pressure is too small and can be neglected. Hence, the partial derivatives of pressure with respect to time and distance become:

$$\frac{\partial P}{\partial t} = \rho g \frac{\partial H}{\partial t} \tag{5}$$

And

$$\frac{\partial P}{\partial x} = \rho g \frac{\partial H}{\partial x} \tag{6}$$

If the pipe walls are considered slightly deformable, then the variation of pipe cross section area (A) due to the variation of pressure may be neglected, and the partial derivatives of velocity w.r.t distance and time can be written as:

$$\frac{\partial v}{\partial x} = \frac{1}{A} \frac{\partial Q}{\partial x} \tag{7}$$

And

$$\frac{\partial v}{\partial t} = \frac{1}{A} \frac{\partial Q}{\partial t} \tag{8}$$

Incorporating the above simplifications in transient flow equations (1) &(2) can be rewritten as

$$\frac{\partial Q}{\partial t} + g A \frac{\partial H}{\partial x} + \frac{fQ|Q|}{2DA} = 0 \tag{9}$$

And

$$\frac{\partial H}{\partial t} + \frac{a^2}{gA} \frac{\partial Q}{\partial x} = 0 \tag{10}$$

Equations (9) & (10) governing the transient state in elastic pipes and they are quasi-linear hyperbolic partial differential equations. These equations cannot be solved analytically. A numerical technique however made accurate methods for analyzing the transient state conditions in simple and complex piping systems possible. The method of characteristics is the one most widely used in solving transient problems.

4- The Method of Characteristics

The method of characteristics utilizes a special property of hyperbolic partial

differential equations to find their numerical solutions. For a system of hyperbolic partial differential equations there are two characteristic directions in the x-t plane in which the integration of the partial differential equations is reduced to the integration of a system of ordinary differential equations.

The advantages of this method are that it is a method of solution which allows the direct inclusion of friction losses. It affords ease in handling the boundary conditions and in programming complex systems. It is a general method, i.e., the program once written, may be used for analyzing any system having

the same boundary conditions, and the transient state conditions obtained by using this method are close to the actual situation. The only restriction in this method is that the flow must be one dimensional; the wave speed is constant during the transient state and the time increment chosen to satisfy the stability conditions.

The two quasi-linear, hyperbolic, partial differential equation (9) & (10) are transformed by the method of characteristics in to four ordinary differential equations which are solved numerically using Newton Raphson method.[2]

5- Power Failure to Pump

When the power to a pump motor is suddenly cut off a rapid deceleration in the speed of the motor and pump will take place immediately and cause a rapid change in flow condition. As a result of this change a low pressure wave will be transmitted in the discharge pipe and a wave of high pressure will transmitted in the suction pipe. After a short time the flow in the discharge pipe will be reduced to zero and reverses through the pump. If it is not provided with a non return valve, causing reverse rotation to the rotating elements will takeplace. As the speed of the pump increases in the reverse direction, it causes greater resistance to the reversal of the

flow, which causes high pressure to develop upstream of the pump and low pressure downstream of the pump. These pressures accompanying the transient state which follows the power failure in centrifugal pump system are the most extreme that the system must withstand.

The pump operation at pumping station, before and after the power fails may be divided into three zones as follows:[5]

- 1- Normal pumping zone, where the pump is operating at normal conditions. In this zone the discharge, head, speed, and torque are considered positive.
- 2- Energy dissipation zone, where the discharge is negative (i.e. reverse flow) and the pump speed and torque are still positive.
- 3- Turbine zone, where the speed, discharge, and torque are negative.

When dealing with the transient states for a system involving pumps, the relation between the pump discharge (Q), speed (N), torque (T), and head (H), under different operating conditions must be taken into consideration. For a given geometrically similar pumps the homologous relations may be presented as:[2]

$$\begin{aligned} \frac{H}{N^2 D^2} &= Constant \\ \frac{N}{QD^3} &= Constant \\ \frac{T}{N^2 D^2} &= Constant \end{aligned} \tag{11}$$

When restricted to particular unit, the diameter of the impeller is considered a constant then

$$\begin{aligned} \frac{H}{N^2} &= Constant \\ \frac{N}{Q} &= Constant \\ \frac{T}{N^2} &= Constant \end{aligned} \tag{12}$$

By defining the non dimensional parameters

$$\alpha = N/N_r, \beta = T/T_r, \nu = Q/Q_r \quad \text{and} \quad h = H/H_r \quad (13)$$

In which the subscript r refers to the rated conditions and the equation (12) can be written as

$$h/\alpha^2 = \text{const.}, \quad \alpha/\nu = \text{const.}, \quad \text{and} \quad \beta/\alpha^2 = \text{const.} \quad (14)$$

In order to avoid having h/α^2 , α/ν , and β/α^2 reach infinity when α , and ν equal to zero, $h/(\alpha^2+\nu^2)$ are normally used instead of h/α^2 , $\beta/(\alpha^2+\nu^2)$ instead of β/α^2 , and $\theta = \tan^{-1}(\alpha/\nu)$ instead of α/ν . If $h/(\alpha^2+\nu^2)$ is plotted as ordinate against $\theta = \tan^{-1}(\alpha/\nu)$ as abscissa, the resulting curve is termed the complete characteristics head curve. Similarly, if $\beta/(\alpha^2+\nu^2)$ is plotted versus $\theta = \tan^{-1}(\alpha/\nu)$ the resulting curve is termed the complete characteristics torque curve. These two curves are used to determine the relation between pumps discharge, speed, torque, and head during different operation conditions[1].

Pumps manufacturers usually supply the characteristics curve of normal operation zone and very few of them supply the complete characteristics curve. If these curves are not available for a pump, then the curves for a pump of the same type with approximately the same specific speed may be used. In case study presented in this work (Al-

Mazak closed irrigation system) the complete characteristic curves of the plant pumps whose specific speed is 5.1 were not supplied by the manufacturer. The curves used were those of a pump specific speed 4.94 stating that they are sufficiently close to those of specific speed of 5.1 that their use is acceptable.

To use pump characteristic curves in a mathematical model, points on the curve are stored at intervals of $\Delta\theta$ from 0° to 360° . Each segment of the curve between two points may be approximated by a straight line. If a sufficient number of points are stored, then the error introduced by the segmented straight lines is negligible. Figures (2), (3), (4), and (5) show the characteristic curves for the pumps used in Al-Mazak closed irrigation system. The data used to plot figures 2 to 5 were taken from the data sheet supplied by pumps manufacturing company [8].

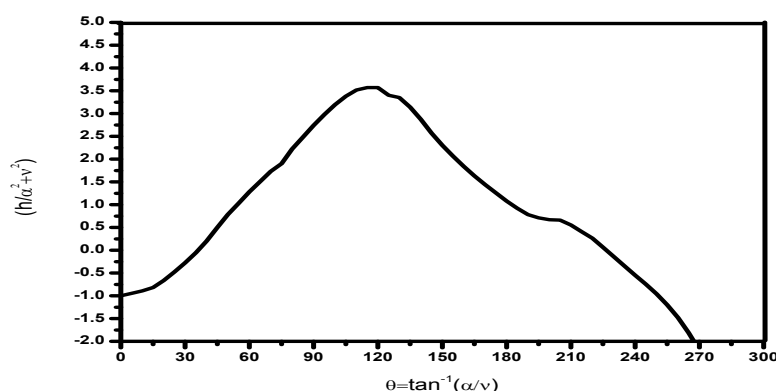


Figure (2): The characteristic curve for head in pumping station # 1

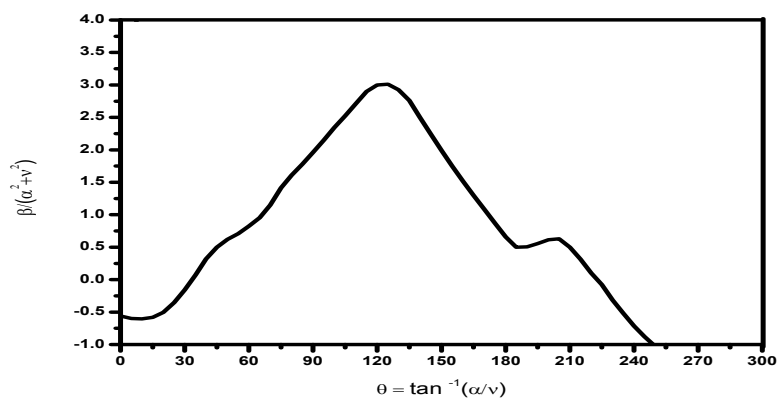


Figure (3): The characteristic curve for torque in pumping station # 1

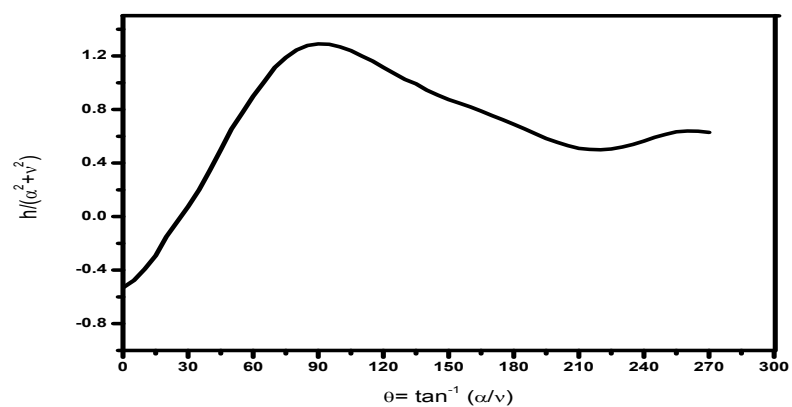


Figure (4): The characteristic curve for head in pumping station # 2 & 3

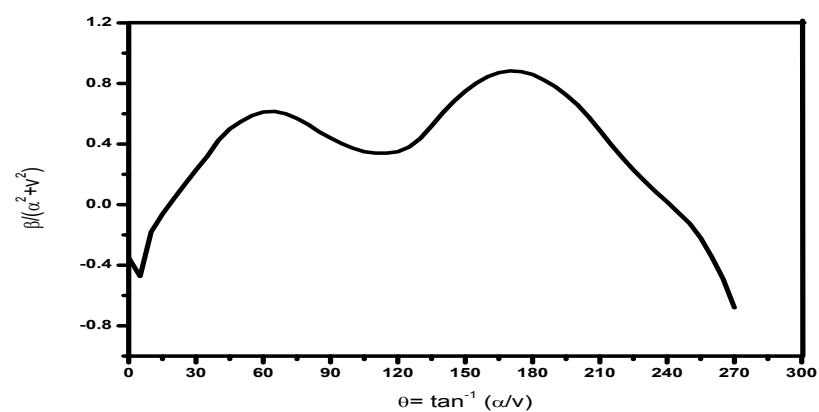


Figure (5): The characteristic curve for torque in pumping station # 2 & 3

6- Pump speed change

Speed change of the rotating elements of a pump following power interruption or pump start, result from unbalanced torque applied which is equal to the product of the mass moment of inertia of the rotating elements and the angular acceleration[6,7]

$$T = -I \frac{2\pi}{60} \frac{dN}{dt} \tag{15}$$

Where $I =$ Combined moment of Inertia = $W R^2 / g$

$W =$ Weight of rotating parts.

$R =$ Radius of Gyration of rotating parts

$$\frac{2\pi}{60} \frac{dN}{dt} = \text{angular acceleration}$$

Equation (15) may be written in a dimensionless form as

$$\beta = -I \frac{2\pi N_R}{60 T_R} \frac{d\alpha}{dt} \tag{16}$$

Using an average value of β during each time step, the finite difference form of the above equation becomes

$$\frac{\alpha_p - \alpha}{t_p - t} = - \frac{60 T_R}{2\pi I N_R} \frac{\beta + \beta_p}{2} \tag{17}$$

For programming usage, the equation of the torque curve may be approximated and stored in the same way as shown in section 4 .

7- The equation for surge tanks

Derivation of the equation representing the surge tank boundary condition, with the flow considered positive into the tank, the following equation may be written as

$$Z_p = H_p - h_{orf}$$

$$Z_p = H_p - C_{orf} Q_{ps} |Q_{ps}|$$

Where

$Z_p =$ water level in the surge tank

$h_{orf} = C_{orf} Q_{ps} |Q_{ps}| =$ head loss through the orifice

$C_{orf} =$ orifice head loss coefficient

$Q_{ps} =$ flow into the surge tank

8- Application of the model

8.1 System parameters

System parameters are those variable that may change with distance and remain constant with time. They

include pipe diameter, fluid density, friction factor, and the speed of a pressure wave in the system.

The choice of pipeline friction factor was discussed early in this work. In transient analysis of a system two extreme cases are critical. For pump failure, a new pipeline with lower friction factors is the critical case while the aged pipeline with higher friction factor represents the critical case for pump start-up. Pipe roughness height, k , is generally taken as 1.5 mm for the aged steel pipe. The roughness height for the new pipe depends on the material, manufacturing, and method of connecting pipe segments. Precise information are not available on these and it seemed prudent to investigate the friction factor for a range of k values from 0.06 mm to 0.15 mm for the new pipes. Miner losses were also taken in the consideration and the equivalent friction factors are 0.014 and 0.021 for new and aged pipes, respectively. In (Al-Mazak closed irrigation system) pump station No. 1 is 0.018, and for pump stations No. 2 & 3 are 0.022.

The speed of pressure wave in the pipe is a function of fluid density, and bulk modulus of elasticity, pipe diameter and wall thickness, pipes Young's modulus, and type of supporting. Using typical value of the bulk modulus and Young's modulus the wave speed is about 960 m/s[2]. The value of wave

speed and time increment, Δt , determine the number of reaches into which a pipeline is divided for computational purposes. It is therefore customary to adjust the wave speed by up to +/- 15% in order that an integer number of reach is obtained. In this case it was only necessary to adjust the speed down to 900 m/s. this allowed using 8 reaches, each 250 m long, and a time interval of 0.25 seconds in pipeline for pumping station No. 1 and 5 reaches each 195 m long, and time interval of 0.15 second in pipeline for pumping stations No. 2 & 3.

8.2 Pump characteristics curves

Transient analysis of pumping station requires characteristics curves covering pump operation in four quadrants representing $\theta = \tan^{-1} (\alpha/v)$ values from 0 to 360°. Manufacturers usually supply the curves of normal operation zone, $\theta=0$ to 90°, and it is customary to choose from few complete characteristic curves that are published in the engineering literature. Chaudhry [1] has published the complete characteristic curves of four pumps whose specific speeds are 0.46, 1.61, 2.78, and 4.94. the specific speed can be calculated using the following equation

$$N_s = \frac{N_R \sqrt{Q_R}}{(g H_R)^{0.75}} \tag{18}$$

The pumps of (Al-Mazak closed irrigation system) have $H_R=35$ m, $Q_R=0.163$ m³/s, $N_R=1450$ rpm= 151.848 rad/s. The specific speed as defined by Chaudhry [1] is 5.1 which is very close to $N_s=$

4.94 whose complete characteristics curves were used for this study. The other data used in program are listed in Table (2)[8]

Table (2) Data for pumping stations[8]

Item	Description	Unit	PS#1	PS#2	PS#3
1	Head losses at suction line and fittings	m	0.65	0.69	0.69
2	Head losses at discharge line and fittings	m	1.9	2.1	2.1
3	Friction loss in pipeline	m	6	7.5	7.5
4	Design static head	m	35	35	35
5	Friction factor for new pipes		0.013-0.014	0.016-0.017	0.016-0.017
6	Friction factor for aged pipes		0.021	0.024	0.024
7	Pipe diameter	mm	900	900	900
8	Pipe wall thickness	mm	11.91	11.91	11.91

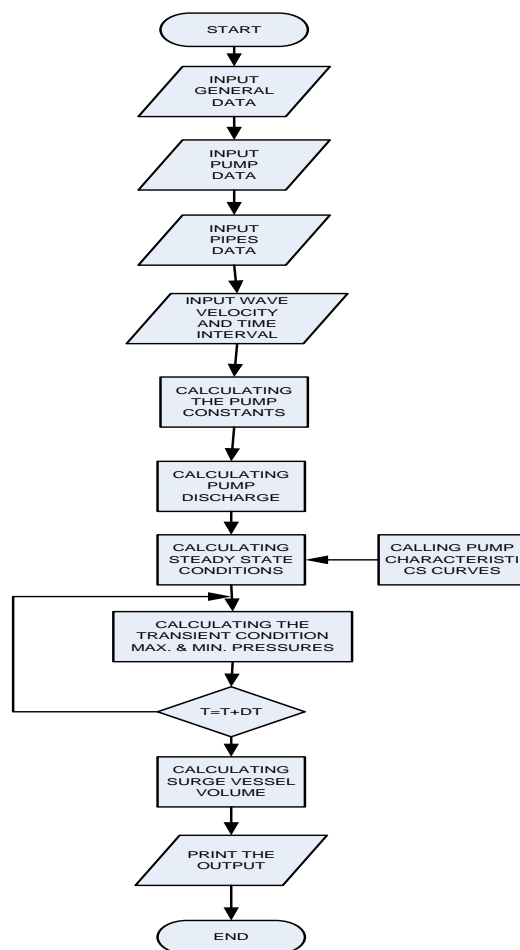


Figure (6): Program Used in Analysis Flow Chart

9- Results and Discussion

9.1 Results for Pumping Station

#1

The pumping station #1 consist of 5 pumps (4 working and 1 stand-by) of total rated capacity of 0.352 m³/s, the head losses due to valves and pipe fittings is 1.9 m, and head loss due to friction is 6 m, the friction factors for new pipe and aged pipe are 0.014 & 0.02 respectively. In power failure to pump the maximum pressure was found 20.2 bar, while the

minimum pressure was found 0.65 bar. To avoid this increasing in pressure a controlling device must be use such as surge tank or pressure vessel. Figure (7) shows the pressure oscillation with time due to power failure without controlling device provided, while Figure (8) shows the pressure with controlling device (pressure vessel) with time. Figure (9) shows the discharge flow rate based on time with controlling device.

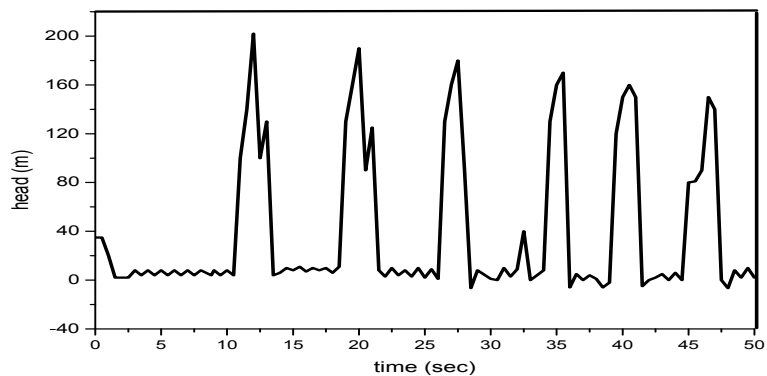


Figure (7): The pressure in pipeline with time due to power failure without pressure vessel for pumping station #1

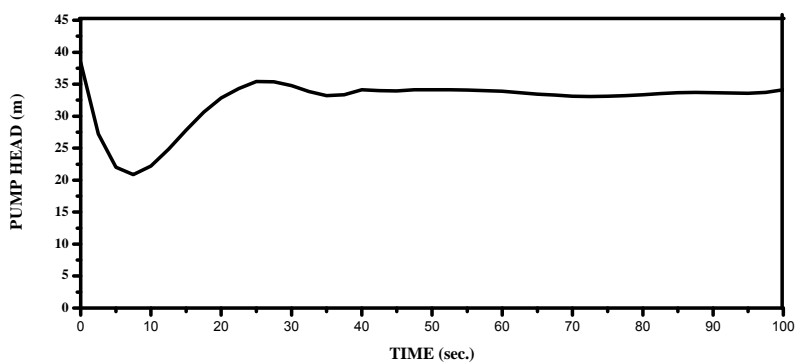


Figure (8): The pressure in pipeline with time due to power failure with pressure vessel for pumping station #1

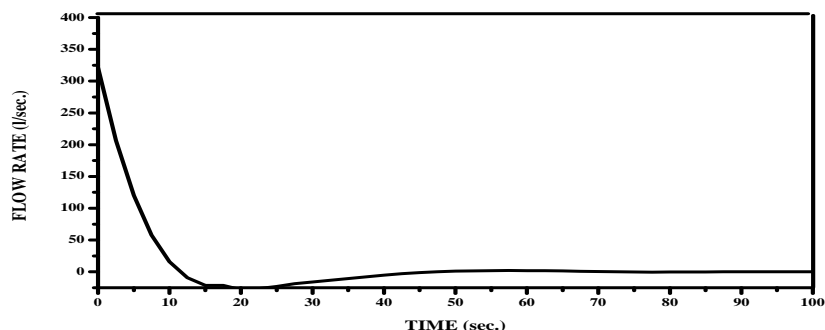


Figure (9): Discharge flow rate with time with pressure vessel connected to pipeline for pumping station #1

9.2 Results for Pumping Stations # 2 & 3

The pumping station #2 & 3 consist of 5 pumps (4 working and 1 stand-by) of total rated capacity of 0.652 m³/s, the head losses due to valves and pipe fittings is 2.1 m, and head loss due to friction is 7.5 m, the friction factors for new pipe and aged pipe are 0.014 & 0.02 respectively. In power failure to pump the maximum pressure was found 20.2 bar, while the minimum

pressure was found 0.65 bar. To avoid this increasing in pressure a controlling device must be used such as surge tank or pressure vessel Figure (10) shows the pressure oscillation with time due to power failure without controlling device provided, while Figure (11) shows the pressure with controlling device (pressure vessel) with time. Figure (12) shows the discharge flow rate with time based on controlling device.

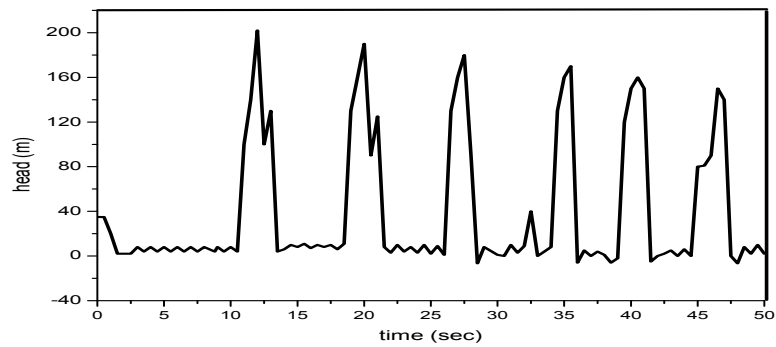


Figure (10): The pressure in pipeline with time due to power Failure without pressure vessel for pumping station #2 &3

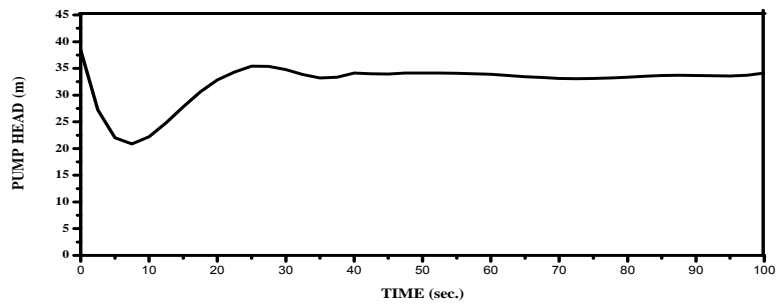


Figure (11): The pressure in pipeline with time due to power failure with pressure vessel for pumping station #2 &3

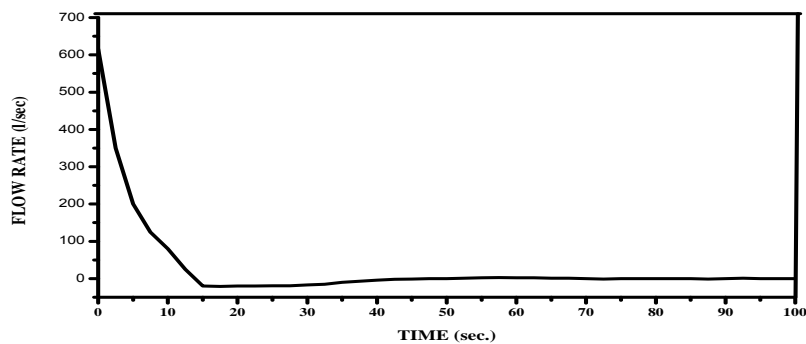


Figure (12): Discharge flow rate with time with pressure

vessel connected to pipeline for pumping station #2 & 3

9.3 Conclusions

A surge tank or a pressure vessel must therefore be provided in order to control transient in the pipeline. High head pump installations generally required a pressure vessel rather than surge tank. Many runs were made simulating pressure vessel of various cross section area and height, for pumping station # 1 the pressure vessel of 3 m diameter and 5 m height is acceptable for controlling the transient state, while for pumping stations 2 & 3, the pressure vessel found to be 4m in diameter, 6 m height was sufficient to controlling the transient stat

Nomenclature

a	water hammer wave velocity	m/s
A	cross sectional area of pipe	m ²
D	pipe diameter	m
EL	elevation	
<i>f</i>	friction factor	
k	pipe roughness	m
g	gravitational acceleration	m/s ²
H	head	m
H _R	rated head	m
I	moment of inertia of rotating elements	kg.m ²
N	rotational speed	rpm
N _r	rated speed	rpm
Q	flow rate	m ³ /s
PS	pump station	
Q _r	rated flow rate	m ³ /s
T	torque	N.m
T _r	rated torque	N.m
z	pump centerline elevation	m
<i>v</i>	dimensionless parameter of flow rate (Q/Q _r)	
h	dimensionless parameter of head (H/H _r)	
<i>α</i>	dimensionless parameter of speed (N/N _r)	
<i>β</i>	dimensionless parameter of torque (T/T _r)	
θ	zone of pump operation	

References

- 1- Chaudhry, H. M. (1987). Applied Hydraulic Transients. Van Nostr and Reinhold, New York, U.S.A.
- 2- Wylie, B. E., and Streeter, V. L. (2010). Fluid Transients. FEB Books, Ann Arbor, Michigan, U.S.A.
- 3- Anton Bergant, et.al "Water Hammer Analysis of Pumping System for Control of Water in Underground Mines", International Mine Water Association, 2012, pp 9-21
- 4- Larsen, Torben "Water Hammer in Pumped Sewer Mains", Aalborg University Publications, 2012, Denmark
- 5- Petry B., Baumann A., Tomasson G. G. & Stefansson B., "Control of hydraulic transients in the power waterways of the Kárahnjúkar HEP in Iceland: Design challenges and solutions", Proceedings, Hydro 2006, Porto Carras, Greece, September (2006).
- 6- Tullis, J. Paul, Hydraulics of Pipelines, 1984 Draft Copy, Utah State University, pp. 249-322
- 7- Kroon, Joseph R., et. al., "Water Hammer: Causes and Effects", AWWA Journal, November, 1984, pp. 39-45.
- 8- Sire Company Manufacturing Catalogue (2014)

Emergency Notification System for the Detection of Falling, Car Accident and Heart Rate Failure Using Smart phone and Smart watch.

Hamid M. Ali* and Ali M. Muslim*

***Computer Engineering Dept., Baghdad University, Iraq**

habdul_hussain@yahoo.com.

*** *M.Sc. Student, Computer Engineering Dept., Baghdad University, Iraq.**

alimajeed.mail@gmail.com.

Abstract:

There are a lot of people facing a problem of unexpected death or health damage due to the lack of medical care at the right time, especially elderly people, patient with disabilities and people that are living alone who are required to be continuously under surveillance for the purpose of safety and emergency response. As the smartphone becomes an integrated part of human daily life which has the ability of complex computation, internet connection and also contains large number of hardware sensors, encourage implementation of the proposed system based on smartphone to be utilized in the public healthcare. Most of the works done in this field imposed the restriction of fixing the smartphone in certain position on human body to easy infer the emergence case from the data of the smartphone sensors. To overcome this restriction, the proposed system incorporated a smartwatch, together with smartphone freely carried by the user, for better performance results. The use of smartwatch assisted in providing distinct separable signal variation from the smartwatch accelerometer and gyroscope sensors to recognize emergency case such as falling, car accident and heart rate failure. Immediately after cases that are mentioned previously the proposed systems ends details information such as videos, location, heart rate etc. to the emergency center and emergency contact to provide help at the right time. The system was practically tested in real simulated environment and achieved quite very good performance results.

Keyword: Emergency Notification, Healthcare, Falling, Car Accident Detection Smartphone, Smartwatch

انشاء نظام ارسال اشعارات طوارئ عند حالات الاغماء او حادث سيارة او فشل في معدل دقات القلب باستخدام الهاتف الذكي وساعة ذكية

<p>²علي مجيد مسلم</p> <p>طالب ماجستير قسم هندسة الحاسوب- كلية الهندسة -جامعة بغداد-العراق</p>	<p>¹حامد محمد علي</p> <p>قسم هندسة الحاسوب -كلية الهندسة-جامعة بغداد-العراق</p>
--	--

الكثير من الأشخاص يتعرضون الى حالات موت مفاجئة نتيجة عدم حصولهم على رعاية صحية في الوقت المناسب خصوصاً كبار السن والعجزة والأشخاص الذين يعيشون بمفردهم سواء بشكل دائم او جزئي والذين هم بحاجة الى رعاية صحية أكثر من غيرهم. أصبح الهاتف الذكي جزء من حياة الكثير من الأشخاص خصوصاً مع تطور قدرته على معالجة البيانات وارسال البيانات واحتوائه على حساسات كثيرة كل هذه العوامل ساعدت على بناء نظام رعاية صحية يعتمد على الهاتف الذكي. الكثير من الانظمة المشابهة تعتمد على تثبيت الهاتف الذكي في مكان معين من جسم الانسان للحصول على بيانات واضحة لتشخيص حالات الطوارئ وهذا الشرط يسبب صعوبة وعدم راحة للمستخدم خصوصاً مع ازدياد استخدام الهاتف الذكي الذي يتطلب تحريك الهاتف من مكانة المثبت. النظام المقترح يستخدم بالإضافة الى الهاتف الذكي ساعة ذكية مثبتة على كاحل المستخدم وبدون أي قيود على مكان او حركة الهاتف والذي يمكن النظام من الحصول على بيانات واضحة للتشخيص حالات الطوارئ مثل الاغماء او حدوث حادث سيارة او فشل في معدل دقات القلب. تم فحص النظام المقترح في بيئة مشابهة لحالات الطوارئ المذكورة سابقاً وحقق النظام نسبة نجاح عالية جداً.

الكلمات المفتاحية: اشعارات طوارئ، رعاية صحية، حالات الاغماء او حادث سيارة، الهاتف الذكي.

Introduction

Recently, smartphone becomes an integrated part of human daily life which becomes more and more sophisticated with growing the computation power, network capability and sensing powers. Smartphone contains large number of hardware sensors that encourage implementation healthcare system such as accelerometer, gyroscope, compasses, barometer, temperature, humidity, light sensor and GPS receiver. All the features that are mentioned above make the smartphone to become a rich environment for many systems like healthcare system that called Mobile Health (mHealth) system. Mobile Health system is the intersection between Electronic Health (eHealth) and smartphone technology[1]. For car accident detection most of the smartphone based car accident detection systems depend on the high speed of the vehicle (extracted from

the smartphone GPS receiver) and the G-Force value (extracted from smartphone accelerometer sensor) to detect car accident. On the other hand, the system will be failed when an accidents occur at low speed of the vehicle. The main obstacle that encounters the low speed accident is how to discriminate between whether the user is inside the vehicle or outside the vehicle especially when the car is traveling in a speed fairly to be walking or running speed. Hence, in addition to the high speed car accident the proposed system has the ability to detect low speed car accident by using both smartphone and smartwatch sensors. For falling incident most of the smartphone based falling detection is depending on a fixed smartphone on the user body. This condition is cumbersome and annoys the user from having always keeping the smartphone in one position. Using both smartphone and smartwatch give the proposed system

ability to detect falling incident without any restricted on the smartphone position or orientation. In the proposed system both smartphone and smartwatch sensors are become sours row data to detect falling, car accident and heart rate failure. The proposed system increases self-dependency and providing better

quality of live for people that are living alone for a full time or part time especially elderly people, patient with disabilities who are required to be continuously under watching for the purpose of safety and emergency response at the right time. figure 1 present overall proposed system structure

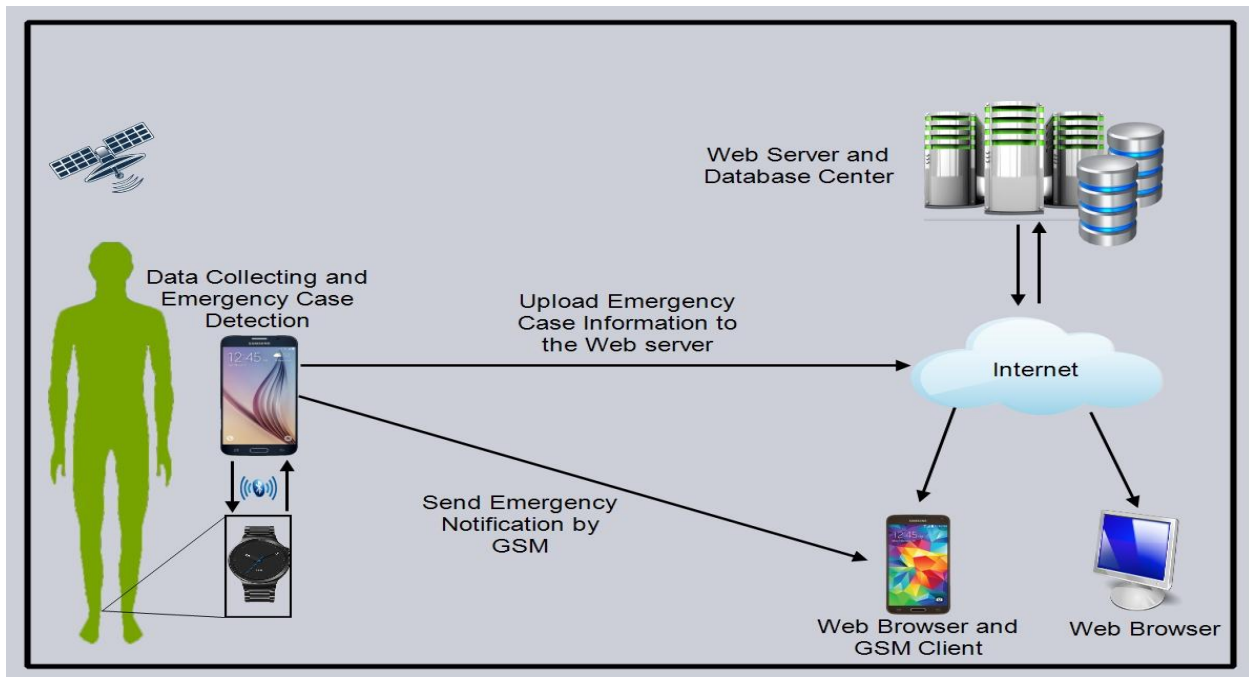


Figure 1 Overall proposed system structure

Proposed System Design

The proposed system, called Emergency Notification System for

Falling, Car Accident and Heart Rate Failure Using Smartphone and Smartwatch, consists of two phases; the detection phase, explained in the

next section II-A, is used to identify the occurrence of falling, car accident and heart rate failure, and notification phase, explained later in the section II-B, is used to inform an emergency center for fast response and recovery.

A-Detection phase

After studying and analyzing most up-to-date related works that are depending on the smartphone inertial sensors to accomplish such systems. Actually, there are so many factors and restrictions that prevent the above mentioned approaches from achieving perfect accurate results. These factors and restrictions are explained later when the proposed system mechanism is discussed in details. The main contribution of this work is the incorporation of android smartwatch as a part of the system components which in turn is used in conjunction with smartphone for better accurate result. As a consequence, the proposed system integrated the use of smartwatch fixed on user ankle

together with smartphone carried, by the user, in any position and orientation. The main technical reason behind using the smartwatch is to place the smartwatch sensors (accelerometer and gyroscope coordinates) in a position that become precisely sensitive to human body movements.

Having justified the use of android watch in the proposed system, Figure 2 shows the overall system design mechanism and its interoperated components that are working simultaneously to achieve the proposed system specifications. The detection phase of the proposed system consists of the following main steps:

- 1- Data Collection: This component is responsible for reading raw data from the smartwatch and smartphone sensors.
- 2- Windowing: This component is responsible for portioning the raw

data into segments called windows suitable for feature extraction.

3- Feature Extraction: This is responsible for examining each window; produced from step 2 above, scale and arrange the data

inside each window that are used to detect emergency case.

4- Classification: This is responsible for checking the data facts produced from step 3 above, and then determine if the emergency case occur or not.

Each step and its functionality are described in detail in the next sections.

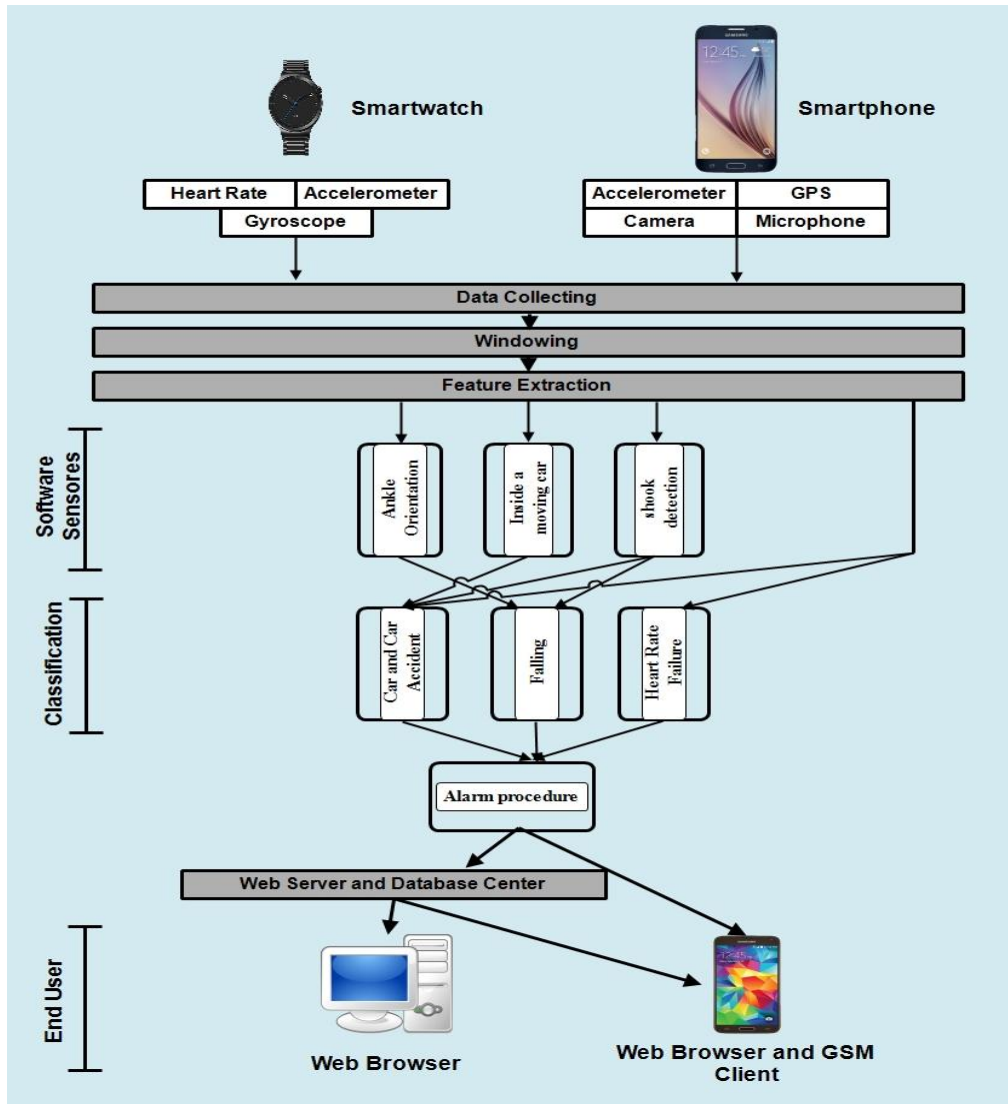


Figure 2 Overall system design mechanism

A1-Data collecting

The smartphone and the smartwatch collect data from their sensors at the same rate (every 20ms), but with different update time for each sensor reading. It should be noted that

in android platform there are many types of sensor event listeners that are responsible to update sensor readings like normal every 200ms, user interface every 60ms, game every 20ms and fastest about every 10ms,

the latter depends on the sensor hardware specifications. The type of the sensors and the sampling rate for each sensor, chosen for this work, are listed in table 1. Also, it is very important to know that the sensor sampling rates and position of every smartwatch sensor are chosen carefully after conducting many

experimental tests with different situations to obtain the best clear features that are suitable for all emergency cases to achieve minimum processing load and separable/generalized features. Figure 3 show the three axes coordinate for smartwatch sensors

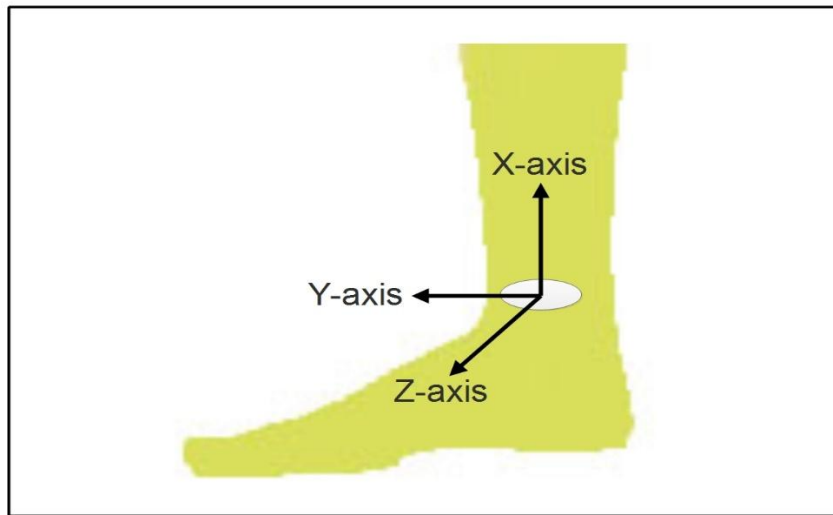


Figure 3 Three axes coordinate for smartwatch sensors

Table 1 Android and android wear platform sensors

No	Type of sensor	location	Type of sensor event listener	Sensor update time
1	Accelerometer	smartwatch	sensor delay game	20ms
2	Gyroscope	smartwatch	sensor delay game	20ms

3	Heart rate	smartwatch	sensor status accuracy high	200ms
4	Accelerometer	smartphone	sensor delay game	20ms

A2- Windowing

The windowing process is used to split the continuous collected data, of each sensor, into small time segments called windows for the purpose of feature extraction. In this work, a window size of 3 seconds is adopted to be adequate for feature extraction. The windowing process is executed continuously in real time simultaneously with other parts of the system such as feature extraction and classification.

A3- Feature extracting

Each sensor window size exemplifies a 150 vectors of raw data; some sensors have 3-axes coordinates. The purpose of feature extraction process is to inspect and measure the

properties of the window raw data pattern relative to the required emergency case detection. In other word, to find the best approximate distribution of the raw data to emergency case it belongs. For example, mean, maximum value, and minimum value are valuable candidates for feature extraction process

A4- Classification

Classification is the process of discriminating each featured window and detects each emergency case. Classification process consists of three parts: Car Accident detection, Heart Rate Failure Detection and Falling Detection.

A4.1- Software Sensors

Before discussing and analyzing the rest of the emergency case

detection, it is found necessary to explain the software sensors, illustrated previously in figure 2, that are used in the forthcoming emergency case detection. It is important to know that there are two types of sensors; software and hardware sensors in android platforms. In this work, three software sensors have been built for the purpose of extracting features that are used in the emergency case detection. The three software sensors are called Ankle Orientation, Shock Detection, and Inside a Moving Car. The purpose and the functions of each software sensor are explained as follows:

A4.1.1- Ankle Orientation

The purpose of the Ankle Orientation sensor is to measure the ankle orientation of the human body. This sensor, on each 3 seconds window size, takes the three axes of the smartwatch accelerometer sensor and calculates the mean of each x, y, and z axes coordinates. Then it

arranges, the three means, according to which axis coordinate is mostly vertical to the earth to obtain user ankle orientation. This sensor is used to detect falling incident.

A4.1.2- Shock Detection

The purpose of Shock Detection sensor is to detect and determine if the user has been exposed to a shock such as falling, car accident, or any other sort of collisions. This sensor, for each sampling of a window size, reads the three axes x, y, and z coordinates of the smartwatch and smartphone accelerometer sensors and check if the absolute reading of each the three axes x, y and z of each accelerometer sensor is greater than 4 G-force [2], then it indicates that the user has exposed to a shock which is used by car accident detection to indicate car accident. On the other hand, it also provides another type of shock detection concerning the fall incident. In falling detection, equation 1[3] is used to calculate the G-force, where

G_x , G_y , G_z are the values of the accelerometer three axes X, Y and Z, then the value of the G-force is checked to indicate a fall incident. The threshold of 2.5 G-force[3] is used to indicate that the user has exposed to a shock incident which is used by falling detection classifier.

$$G - force = \frac{\sqrt{G_x^2 + G_y^2 + G_z^2}}{9.8} \quad (1)$$

A4.1.3- Inside a Moving Car

The purpose of Inside a Moving Car software sensor is to discover the speed on which the user is moving which in turn assist to find out whether the user is inside a car or not. The speed, which is obtained from the smartphone GPS receiver, is not enough indicators to detect whether the user is currently moving or not. As in certain circumstances, the GPS data is prone to error that is produced when the user is moving between locations that contain obstacles preventing the GPS receiver from

properly connecting and obtaining correct data. To recover from such error, a software sensor is created to determine that the user is currently inside a moving car by ignoring incorrect GPS readings. This recovery is accomplished by incorporating the GPS receiver parameters: GPS speed and GPS accuracy which are already available in underlying GPS receiver API. Accordingly, this software sensor determines whether the user speed is fairly to be inside a moving car according to the following procedure:

- 1- The GPS accuracy parameter of the proposed system is set to be less than 7m and also is made acquiring GPS data every 7m passed by the user. Hence, the movement is detected when the GPS accuracy (less than 7m) and 7m (passed by the user) are achieved. This 7m distance is found reasonable and suitable for detection whether that the user inside the car or not.
- 2- The GPS speed parameter is set to be more than or equal to 3 m/s. The reason behind that is as long as the window size is 3 seconds, then there will be at least one GPS reading inside the current window size giving that the GPS acquisition reading is made when the

user has passed 7m, as mentioned in step 1 above.

The above procedure steps are applied because the GPS reading errors occur when the GPS accuracy parameter is altered due to the change in the number of the satellites that are received by the smartphone GPS receiver.

A4.2- Car Accident Detection

The first step in the car accident detection is to find out whether the user is inside a car or not. For example, while the user inside a car and the car exposed to an accident then it is necessary to detect car accident and notify about such event. Hence, this section is divided in two parts; the first part explains the procedure of recognizing the user inside or outside the car, the second part explains the car accident detection.

1- Inside the Car Detection

When the user is in static state (that was detected by using smartwatch gyroscope sensor) and her/his location is changing continuously then it indicates that the user is inside a car. The smartphone GPS receiver is used to find the change in user location by continuously extracting GPS data to measure the car speed (as well as the smartphone) by using the software sensor (inside a moving car) that was explained in

details in the previous section. Due to the computation cost of frequently acquisition of the GPS data, the proposed system is made to acquire GPS data every seven meter passed by the car. This distance could be traveled in different period of time which depends on the car speed that is traveling in crowded traffic or not. It is found that this distance is reasonable for continuously recognition whether if the used inside the car or not. If during this distance the car is stopped and the user is still in static state, then the previous distances will be taken into account to assure that the user is still in the car. Otherwise, if the user gets out of the car and perform any activity (moving) then the smartwatch gyroscope sensor will discover any user movement.

2- Car Accident Detection

While the user is inside the car, the system continuously reads the accelerometer data for both the smartphone and the smartwatch. Then for each window size the software sensor (shock detection) is checked for any smartphone and smartwatch shock occurrence. When a sign of accident is detected by the smartphone and smartwatch, then the system activates the alarm procedure as explained later in notification phase in section B.

A4.3-FallingDetection

The other important emergency case is the detection of user falling incident. While the user meanwhile practicing any daily human activity the falling incident could occur that necessitate the detection of such falling incident and notify for emergency response. The procedure that is used in detecting such incident is listed below:

- 1- The accelerometers of the smartphone and smartwatch are used in such incident. For each window size, the software sensor (shock detection) checks for a shock incident in both smartphone and smartwatch accelerometer sensors, if shock is detected then the following step 2 is activated.
- 2- In the two subsequent windows if the orientation (the x-axis of the smartwatch accelerometer) of the ankle is not vertical (that is read from the software sensor, ankle orientation) then it is concluded that the falling incident has occurred.

Immediately, after detecting a falling incident, the system activates the notification procedure as explained later in section II-B.

A4.4-Heart Rate Failure Detection

A real time detection for the heart rate failure is too important in the healthcare services. Because there are many diseases are linked directly to the heart rate. This procedure, on each 3 seconds window size, checks the mean of the heart rate of the smartwatch sensor. In case the heart rate is found in abnormal condition then an alarm will be set and a notification message is sent to emergency center for the following case:

- a. Increasing in the heart rate (greater than 100 beats a minute for static activities) [4] while the user was static for the last minute.
- b. Decreasing in the heart (lower than 40 beats a minute) [4].

B- Notification Phase

In addition to the recognition of the mentioned emergency case, the system is constructed to provide extra information related to the emergency case which are explained below:

- **Alarm Procedure**

When one of the emergency events is detected during each window size then the alarm set procedure is activated to perform the following actions:

1- Playing an alarm sound and displays a conformation message, on user smartphone, asking the user to confirm the message whether she/he is well or not.

2- The system waits 30 seconds to receive confirmation message from the user and during this period the smartphone will be automatically recording a video by using both front and back camera for a 14 sec for each camera. If the user does not confirm, the message or answer negatively then the alarm procedure will send an emergency notification to the emergency center together with the type of the emergency case, videos and location.

3- Sending GSM notification message, and also make an automatically GSM phone call from the victim phone to the emergency contact for listening to the victim voice to predict the type of help she/he needs and take a first impression about the victim case.

Results and Performance

The three services of emergency notifications heart rate failure, falling, and car accidents are tested and produced quite excellent results. as explained below:

Falling: As it is hard to test real falling incidence, hence this test is conducted by imitating the action of the falling incidence which is accomplished by dropping the smartphone on the ground and then the subject falling to the ground. The reason from that is to generate a G-force of greater

than 2.5m/s^2 for the purpose of falling detection. The result obtained from this test was correct as indicated by the confirmation message displayed on the user smartphone as it was shown in figure 4. After negative answer or no confirmation from the user, the web server inspected and found the video recording of falling incidence was transferred and stored at the web server together with emergency location used to display minimum path between monitoring center and emergency location as it was shown in figure 5. Also the user smartphone sends message via GSM network to the emergency contact and makes an automatic emergency call.

Car accident detection: As it is impossible to conduct this test practically, instead, the smartphone was forcefully hit inside the car and the user foot also shocked hard to produce 4 or greater than 4 G-force at both the smartwatch and smartphone accelerometer sensors as car accident indicator. The result obtained from this test was correct, in a similar manner to the falling test procedure; all the related information is stored at the web server in the same manner as in falling detection as in figure 5.

Heart rate failure: it is too difficult to test the proposed system in a real patient with a

heartbeat less than 40 beat per minute or greater than 100 beat per minute during static activities. The detection of the heart rate failure is foregone conclusion because the accuracy of detection of this case depends on the smartwatch heart rate hardware sensor.

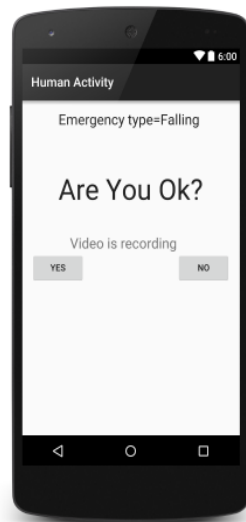


Figure 4. Emergency conformation message interface for the smartphone application

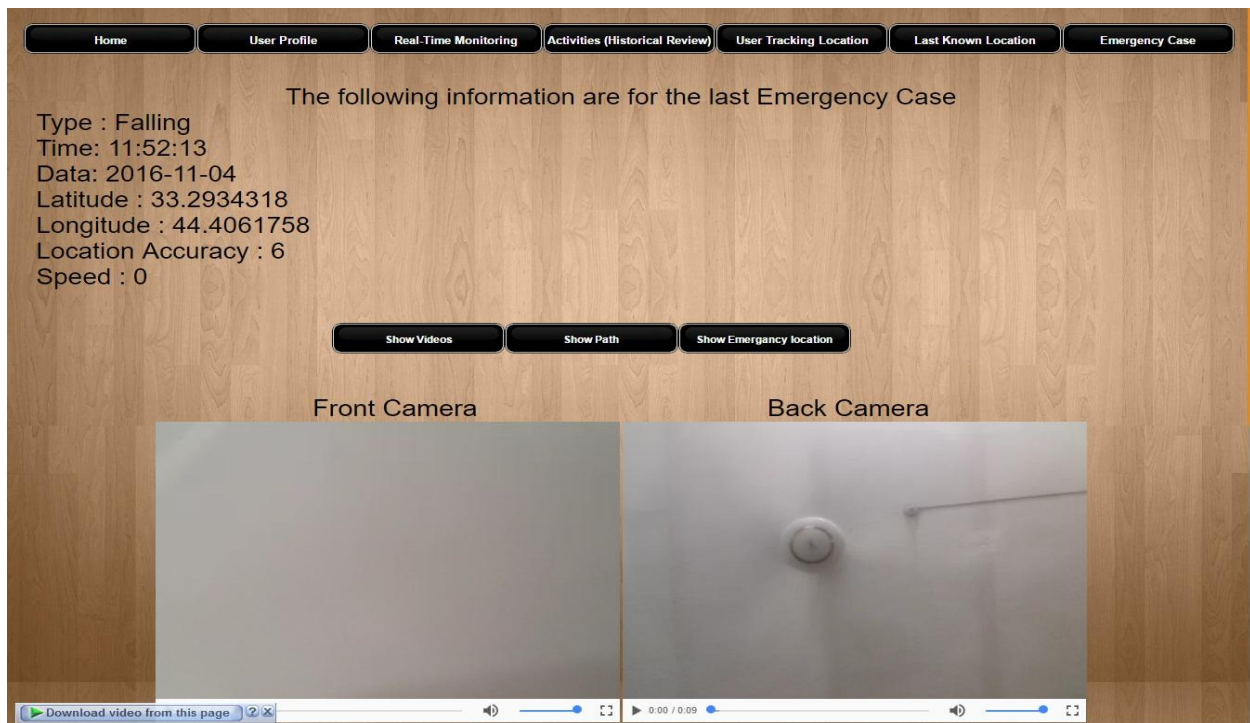


Figure 5-A Emergency notification page

[Home](#)
[User Profile](#)
[Real-Time Monitoring](#)
[Activities \(Historical Review\)](#)
[User Tracking Location](#)
[Last Known Location](#)


Emergency Case

The following information are for the last Emergency Case

Type : Falling
 Time: 11:52:13
 Date: 2016-11-04
 Latitude : 33.2934318
 Longitude : 44.4061758
 Location Accuracy : 6
 Speed : 0

[Show Videos](#)
[Show Path](#)
[Show Emergency location](#)

Your Current Location



Emergency Case Location

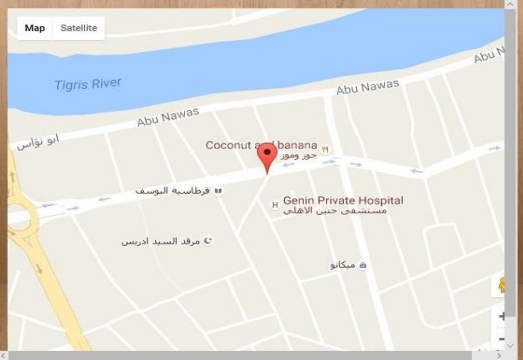


Figure 6-B Emergency notification page

Home User Profile Real-Time Monitoring Activities (Historical Review) User Tracking Location Last Known Location

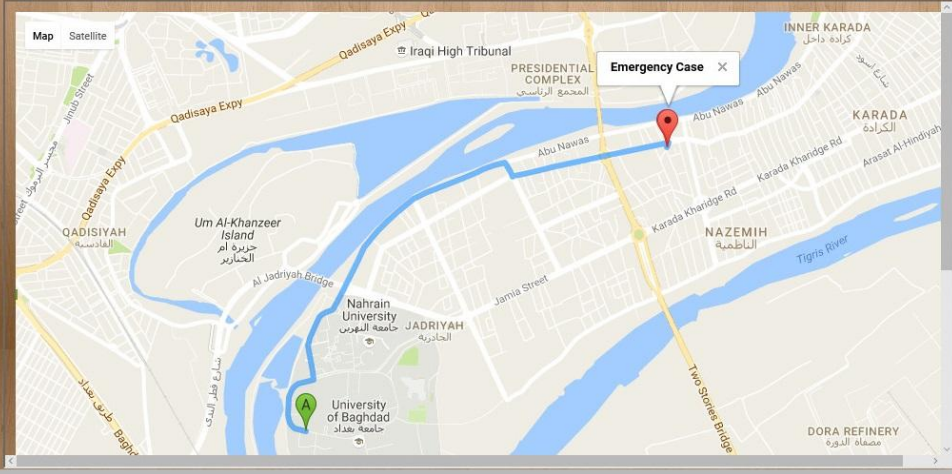
Emergency Case

The following information are for the last Emergency Case

Type : Falling
Time: 11:52:13
Data: 2016-11-04
Latitude : 33.2934318
Longitude : 44.4061758
Location Accuracy : 6
Speed : 0

Show Videos Show Path Show Emergency location

Path Between Your Location and Emergency Case Location



The map displays a route from a starting point (marked with a green 'A') to an 'Emergency Case' location (marked with a red pin). The route is highlighted in blue and yellow. Key locations on the map include the Tigris River, Karada, Nazemih, and the University of Baghdad. Major roads like Qadisiya Expy and Karada Khandge Rd are also visible.

Figure 7-C Emergency notification page

Conclusion

The smartphone based falling and car accident detection system is not an easy task to handle. It is really surrounded with many obstacles that prevent the researchers from achieving high accurate detection system. One of the main obstacles; is determining that the occupant is inside or outside the vehicle while the vehicle is travelling at a low speed and restriction of fixed smartphone on the human body to detect falling instance. The proposed system minimizes the impact of this obstacles which is proved in the practical results conducted in this work. During the study and development of emergency notification system, several points observed and noticed

- 1- Integrating the smartwatch (steady fixed on the human ankle) with smartphone is due to the main reason of obtaining generalized and separable features to detect emergency cases with high accuracy.
- 2- Every smartphone based emergency notification system is exposed to false alarm. In the proposed system, helpful supporting features were added to the system to increase the accuracy of detection process and reduce the probability of false positives. These features are briefly listed below:
 - a. The proposed system presents a confirmation message for emergency notification which gives the user the opportunity to confirm the emergency case. Thus in case false alarm occurs the user can cancel the alarm then the notification is aborted.
 - b. The proposed system allows the smartphone to automatically capture videos from both front and back smartphone camera and send it to the emergency center to help them for better inspection and analysis of the emergency situation.
 - c. When the user doesn't confirm that he/she is okay then the system will make an emergency call from the user phone to the emergency contact. Also emergency information and videos are sent to the emergency center for better diagnostics of the emergency situation.

References

- [1] S. Adibi, "Introduction," in *Mobile Health A Technology Road Map*, Springer International Publishing Switzerland, 2015, p. 1.
- [2] W. Jules, T. Chris, T. Hamilton, D. Brian and C. S. Douglas, "WreckWatch: Automatic Traffic Accident Detection and Notification with Smartphones," *Journal of Mobile Networks and Applications* manuscript, Hingham, MA, USA, 2011.
- [3] E. T. Horta, I. C. Lopes and J. J. Rodrigues, "Ubiquitous mHealth Approach for Biofeedback Monitoring with Falls Detection Techniques and Falls Prevention Methodologies," in *Mobile Health A Technology Road Map*, Springer International Publishing Switzerland, 2015, p. 43.
- [4] "Site Healthy lifestyle," [Online]. Available: <http://www.mayoclinic.org/healthy-lifestyle/fitness/expert-answers/heart-rate/faq-20057979>. [Accessed 24 10 2016].

Analytical Study using Association Rules and Mean of Confidence to Analyze The Poverty Factors in Baghdad Capital of Iraq

Ali Sami*, Dr. Ali Mohammed Sahan*, Ghazi Johnny*

*IT Dept., Technical College of Management, Middle Technical University, Baghdad, Iraq

Abstract:

Poverty is a negative phenomenon that seriously threatened the progress and growth of communities. Studying poverty using scientific research leads to identify the most important influential factors of this phenomenon. In this paper, the poverty in Iraq has been studied through a sample of families in Baghdad city which is the largest and most important city in Iraq. The relational databases as well as the factors related with poverty phenomenon including gender age, the number of family members, educational level, skilled, corruption, disability and disease, wars and disasters have been considered. The association rules and mean of confidence have been used to analyze the main factors for the spread of poverty phenomenon in order to provide clear diagnosis of the most influential factors in the proliferation of this phenomenon, which leads improve appropriate solutions to reduce the impact of these factors.

Keywords:– Association rules, mean of confidence, poverty factors, relational databases.

دراسة تحليلية باستخدام القواعد الارتباطية ومتوسط الموثوقية لتحليل عوامل الفقر في بغداد عاصمة العراق

المستخلص

الفقر هو ظاهرة سلبية تهدد بجدية تقدم ونمو المجتمعات، ان دراسة الفقر باستخدام البحث العلمي يؤدي الى تحديد اهم العوامل المؤثرة في هذه الظاهرة. في هذا البحث تم دراسة الفقر في العراق من خلال دراسة عينة من العوائل في مدينة بغداد كونها اكبر واهم مدن العراق. قواعد البيانات العلائقية بالإضافة الى العوامل المرتبطة بظاهرة الفقر تتضمن الجنس، العمر، عدد أفراد العائلة، المستوى التعليمي، اصحاب المهارات، الفساد، الاعاقة والمرض، الحروب والكوارث. قواعد الارتباط ومتوسط الموثوقية استخدمت في تحليل العوامل الرئيسية لتفشي من اجل توفير تشخيص واضح أكثر العوامل تأثيرا في تفشي هذه الظاهرة مما يقود الى وضع حلول مناسبة لتقليل تأثير هذه العوامل.

الكلمات المفتاحية: العوامل المرتبطة، معدا الثقة، عوامل الفقر، البيانات العلائقية.

1. Introduction

Poverty is a serious, complicated, social, economic, political, historical phenomenon that families and individuals face in different societies, no matter how rich or developed these societies are. So, societies of these countries work hard in order to limit this phenomenon and its effects on family and society level. Contemporary human development has contributed in a way or another in complicating this phenomenon especially in out growth societies whose most people suffer from lack of basic needs (food, residence, health ,education and goods that are needed at home; fridge, oven...etc.) besides other poverty data like; feeling insecure, being afraid of future and lack of self-development opportunities ,which is the destiny of the majority of people in underdeveloped countries ,in which poverty is no longer a new thing .The new thing is realizing this situation and working through every possible mean to reduce or finish it . Because poverty in underdeveloped countries doesn't prove that there are no factors or potential forces which lead to the development and reducing poverty. It is the lack of way and means through which all these factors and forces can become capable of creating tangible growth and development in reality. Poverty in the Arab World is an extremely complicated, economic and social phenomenon as a result of interacting different factors, which don't

belong to a certain geographical area, but it is part of rural and urban societies as well. Within the same society, poverty is more common in the countryside more than in a city and among the illiterate more than the literate. Despite a lot of similar things in the Arab World, there are also some exceptions. Oil-producing countries with low population suffer less poverty than non-producing oil countries which depend basically on agriculture. Sudan has the highest poverty level %46.55 then comes Yemen %45.2, Palestine %38, Lebanon %28 and Iraq %19.9 which means that 6 million Iraqi out of 33 million are living below the line of poorness in a country whose annual budget goes beyond 100 billion dollars among an obvious class disparity in incomes as a result of increasing administrative and financial corruption after the year 2003 within the absence of social injustice. Bagdad, the capital of Iraq, in which we intend to examine poverty, its population is 7.665 million represents %21 of the total population in Iraq with % 50.7 male and % 49.3 female. Poverty in Baghdad outruns %13 of its population due to bad security conditions over the last ten years, in addition to the increasing numbers of widows, orphans, people with no family provider and large numbers of unemployed graduates [1,2,3, 4, 5 ,6].Data Mining is an automated exploratory process of useful data among enormous data sources. Data mining techniques are spread to scour hugedatabase in order to find out useful patterns, which could be unknown without it.

Data Mining is a supplementary part of (KDD) knowledge discovery in data base that is the whole process, through which raw data is transformed into useful information [7, 8,9].

2. Association Rules Mining:

Association rule mining, one of the very powerful and well-researched methods of data mining, was first introduced in [Agrawal et al. 1993]. The main goal of it's to find the

important and exciting correlations, recurrent model, associations or informal Structures among group of items in the transaction databases or other data repositories. The official interpretation of Apriori Algorithm that is applied to detect the association rules, the support of a group of item I, sup(I), is represented as the number of agreement in the database holding I. min_sup (minimal support) is a threshold defined by the user. A group of item is frequent if its support isn't less than the min_sup. A group of item with k items in named a k- group of item.

Let D be a collection of transactions and I = {i1, i2, ...,im}, A group of item is a subgroup of I. Given X and Y are group of sets, an association rule is of the form

$$X \Rightarrow Y, \text{ where } X \subset I, Y \subset I, \text{ and } X \cap Y = \Phi,$$

where the $\text{sup}(X \cup Y) > \text{min_sup}$, and the confidence of $X \Rightarrow Y$ is not below a predefined threshold, min_conf, the confidence of $X \Rightarrow Y$ is.

$$\frac{\text{sup}(X \cup Y)}{\text{sup}(X)}$$

After finding out all frequent group of sets, the algorithm of generating association rules uses the subgroups of a frequent group of set as antecedents to create the rules.

The form $X \Rightarrow Y$ with confidence 60% where X = Mobile phone and Y= Mobile applications, for example,most of the customers who buy a Mobile phone also bought the Mobile applications .

And the form of $X \Rightarrow Y$ is not equal to the form $Y \Rightarrow X$ as a result of

unless X=Y which is called perfect rule.

This must be taken into consideration when analyzing the results of association rules [7,8,9].

Also, we used the Mean of the items confidence (MOC) which can be defined as follows:

$$\text{MOC (A)} = \{\text{conf (A} \rightarrow \text{B)} + \text{conf (A} \rightarrow \text{C)} + \text{conf (A} \rightarrow \text{D)}\} / 3.$$

The formula gives the mean of the occurrence of item A among the items B, C and D which means the influence of item A on the others [10, 11].

3. Study sample:

Data has been collected incorporation with Ministry of Planning and the Central Statistical Organization; a random sample $\frac{\text{Sup}(X \cup Y)}{\text{Sup}(X)}$ NOT EQUAL $\frac{\text{Sup}(Y \cup X)}{\text{Sup}(Y)}$

The following factors are signified in order to be analyzed using Association Rule Mining.

1- A represents Gender; female 1, male 0.

Because the rates are almost equal and, families provided with partnerless-woman are poorer.

2-B represents Age ≥ 20 years; people, who are 20 or older face more difficulties and suffering due to bad conditions the country has been through.

3- C represents Family members ≥ 4 ; the more members a family has, the poorer it is.

4- D represents Educational level; represents a lack of job opportunities for the literate.

5-E represents Posses skills; represents a lack of job opportunities for Posses skill.

6- F represents existence of Corruption; corruption and injustice relating to job opportunities

7- G represents Disability and disease; it refers to the effects on individuals as a result of wars the country has been through.

8-H represents War and disaster; so many families have been impoverished directly or indirectly because of wars and disasters the country has been through.

4. Experimental analysis: After analyzing collected data, a lot of relations that show the cause of poverty in the capital Bagdad. More important relations were chosen with high confidence. Table 1 presented a part of these relations and show clearly the spread of poverty phenomenon in a country which is considered one of the richest countries in the world.

Table (1) some of the relations extracted from given data

Code	Symble	Equ	Relat	Conf
9)	D.H./H.	64/ 82	H→D	78%
9)	D.H./D.	64/ 80	D→H	80%
10)	C.H./H.	61/ 82	H→C	74%
10)	C.H./C.	61/ 76	C→H	80%
11)	B.H./H.	80/ 82	H→B	98%
11)	B.H./B.	80/ 96	B→H	83%
12)	B.F./F.	81/ 83	F→B	98%
12)	B.F./B.	81/ 96	B→F	84%
13)	E.H./H.	33/ 82	H→E	40%
13)	E.H./E.	33/ 44	E→H	75%
14)	F.G./G.	18/ 21	G→F	86%
14)	F.G./F.	18/ 83	F→G	22%
15)	E.G./G.	5/ 21	G→E	24%
15)	E.G./E.	5/ 44	E→G	11%

No Row = 3290

4.1 Association rules results:

Regarding Gender 50%, Age ≥ 20 years 96%, Family members ≥ 4

76%, Educational level 80%, Possess kills 44%, Corruption 83%, Disability and disease 21%, War and disaster 82%.

Figure 1 shows that the highest percentage is for people who are ≥ 20 years and suffering from corruption, wars, and disasters.

1- people with disability or disease are 20 years old or above.

2- All women who have families with 4 members or more, and become poor because of wars are 20 years old or above.

3- All women in a member-families ≥ 4 and suffer from corruption are $20 \geq$ years old.

4- 80% of the literate become poor because of wars and disasters.

5- 80% of member-families ≥ 4 become poor because of wars and disasters.

- 6- 98% of people suffering because of wars and disasters, are 20 years old or above.
- 7- 98% of individuals suffering from corruption are 20 years old or above.
- 8- 86% of the disabled suffer from corruption.
- 9- 88% of highly-educated people suffer from corruption.

- 10- 77% of craft or skill-workers suffer from corruption.
- 11- 84% of women suffer from corruption.
- 12- 84% of skill workers are providers of member-families >= 4.
- 13- 86% of educated people, who become poor because of wars, suffer from corruption.

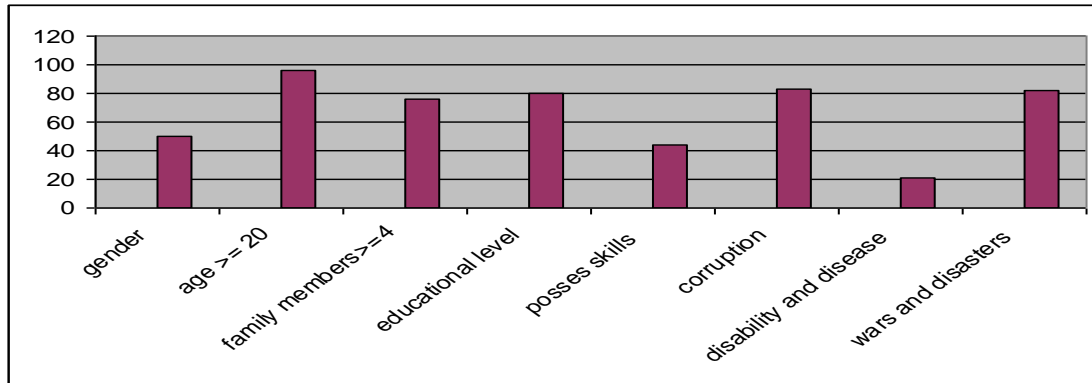


Figure (1) factors percentage from the givendata

4.2. Mean of confidence and the effects of factors:

1. The occurrence of gender is female with other factors.

4 56%, Educational level 78%, Posses skills 38%, Corruption 84 %, Disability and disease 20%, War and disaster 86%. Figure 2 shows that the most effective factors that occur with gender; female, being widows are 20>= years, corruption, wars, and disasters.

Regarding Age >= 20years 96%, Family members >=

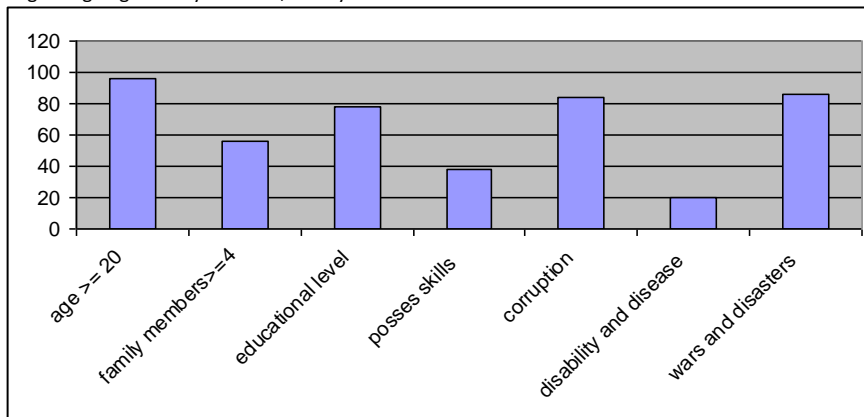


figure (2) shows the Occurrence of gender with the other factors

2. The occurrence of age >= 20 years with other factors.

Regarding Gender 50%, Family members >= 4

77%, Educational level 79%, Posses skills 44%, Corruption 84 %, Disability and disease 22%, War

and disaster 83%. Figure 3 shows that the most effective factors that occur with age are corruption, warctivs, and disasters.

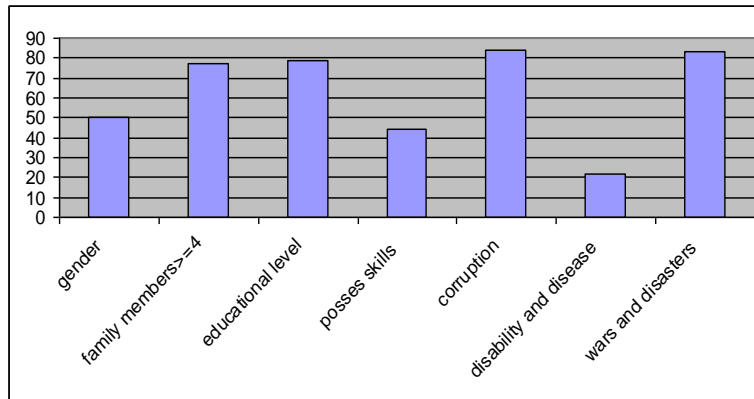


Figure (3) shows the Occurrence of age >= 20 years with the other factors

3. The occurrence of family members >= 4 with the other factors.
 Regarding Gender 37%, Age >= 20years 97%,
 Educational level 84%, Posses skills 49%,
 Corruption 83 %, Disability and disease 26%, War

and disaster 80%. Figure 4 shows that the most effective factors, that occur with the family of members are age, educational level, and corruption.

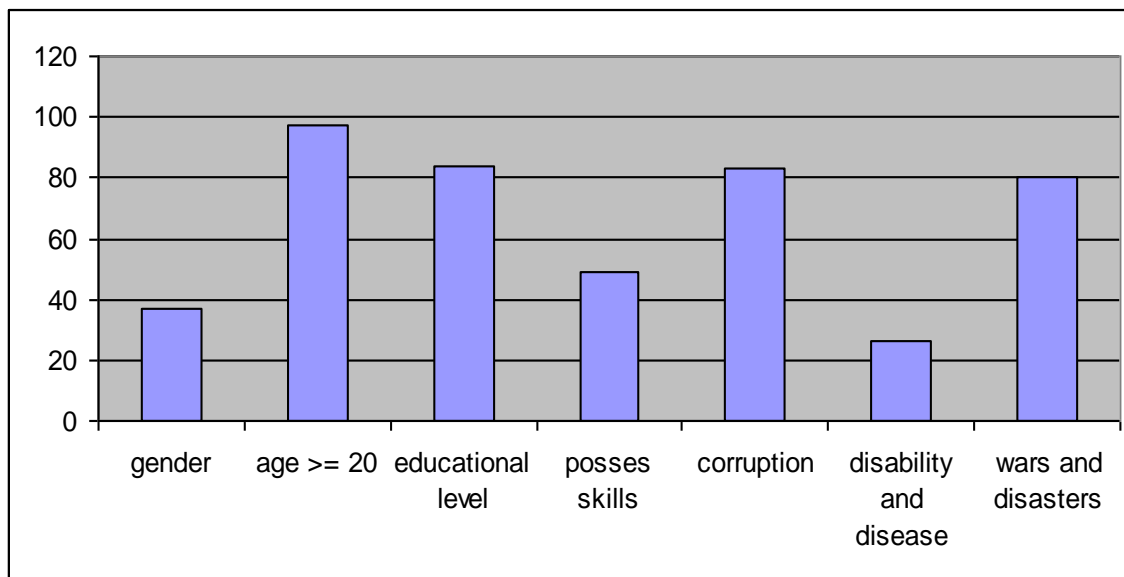


Figure (4) shows the Occurrence of family members >= 4with the other factors

4. The occurrenceof Educational levels with the other factors.
 Regarding Gender 49%, Age >= 20years 95%, Family members >= 4

80%, Posses skills 48%, Corruption 80 %, Disability and disease 19%, War and disaster 80%. Figure 5 shows that the most effective factors that occur with educational level are age, and equally the number of family members, corruption, wars, and disasters.

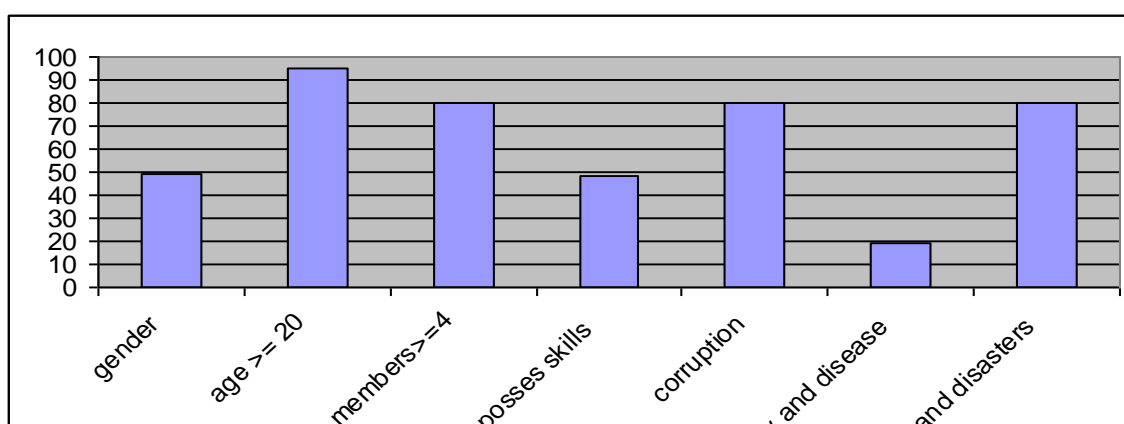


Figure (5) shows the Occurrence of Educational level with the other factors

5. The occurrence of posses skills with the other factors.
 Regarding Gender 43%, Age >= 20 years 95%,
 Family members >= 4

84%, Educational level 86%, Corruption 77 %,
 Disability and disease 11%, War and disaster 75%.
 Figure 6 shows that the most effective factors that occur with Posses skills are age, educational level and the family members.

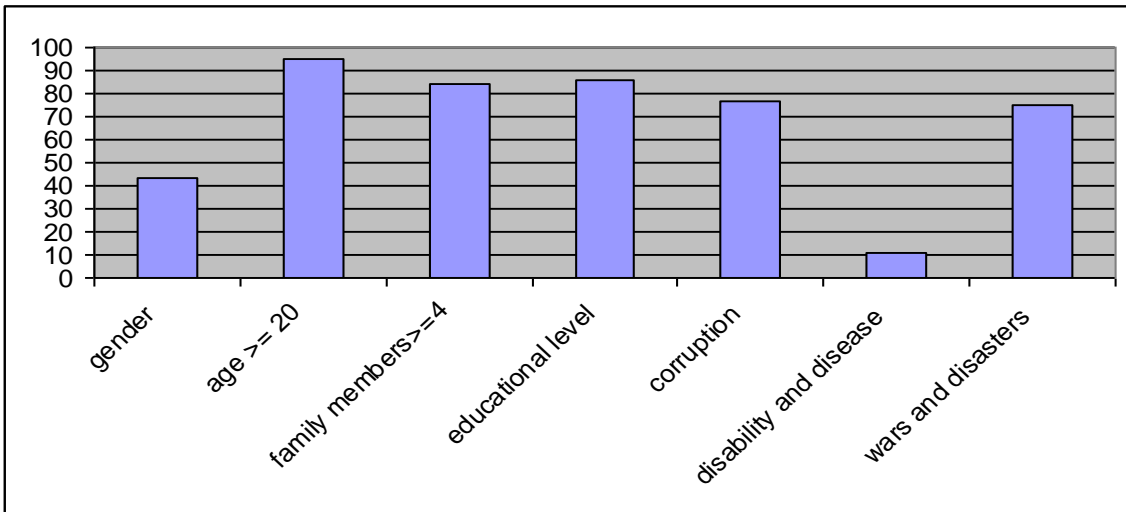


Figure (6) shows the Occurrence of posses skills with the other factors

6. The occurrence of corruption with the other factors.
 Regarding Gender 51%, Age >= 20 years 98%,
 Family members >= 4

76%, Educational level 77%, Posses skills 41%,
 Disability and disease 22%, War and disaster 87%.
 Figure 7 shows that the most effective factors that occur with corruption are age, educational level, wars, and disasters.

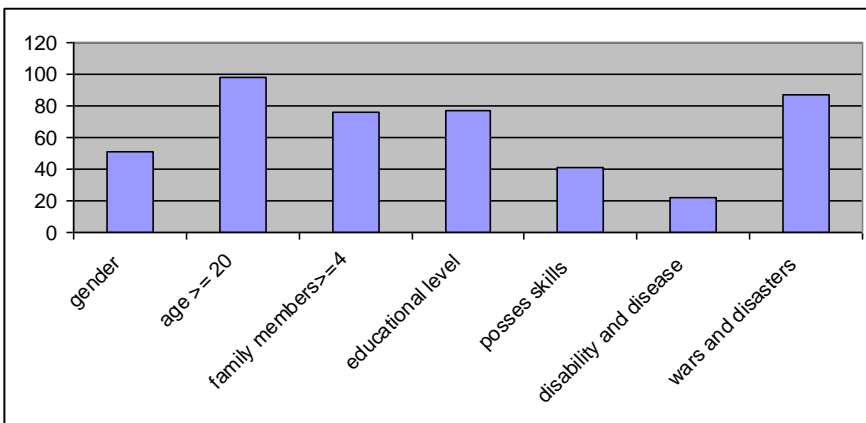
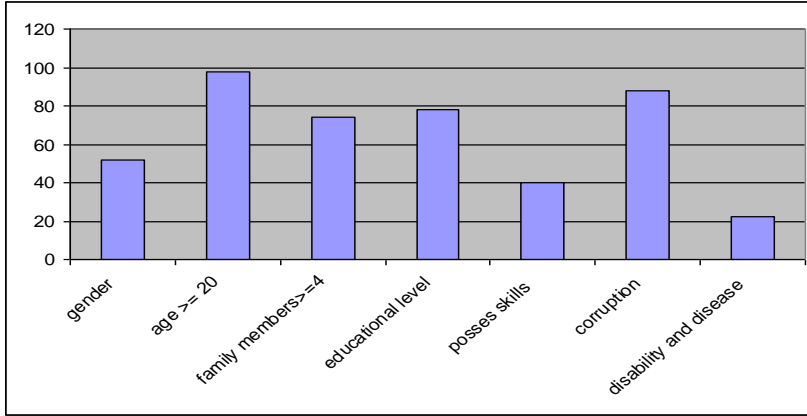


Figure (7) shows the Occurrence of corruption with the other factors

95%, Educational level 71%, Posses skills 24%, Corruption 86 %, War and disaster 86%. Figure (8) shows that the most effective factors that occur with disability and disease are age, family members and equally corruption, wars, and disasters.

7. The occurrence of Disability and disease with the other factors.
 Regarding Gender 48%, Age >= 20years 100%, Family members >= 4



8. The occurrence of War and disaster with the other factors.
 Regarding Gender 50%, Age >= 20years 96%, Family members >= 4

76%, Educational level 80%, Posses skills 44%, Corruption 83 %, Disability and disease 21%. Figure 9 shows that the most effective factors that occur with war and disaster are age, corruption.

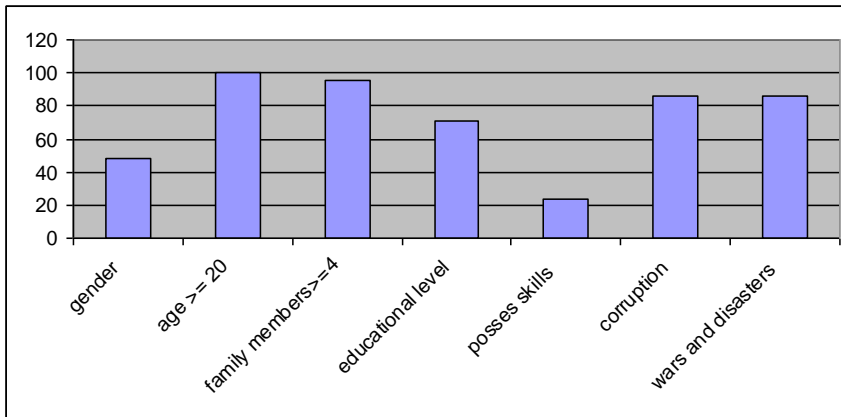


Figure (9) shows the Occurrence of the War and disasters with another factor

9. Mean of confidence (occurrence of the other factors with each single factor),

Regarding Gender 65%, Age >= 20years 63%, Family members >= 4

65%, Educational level 64%, Posses skills 67%, Corruption 65 %, Disability and disease 73%, War and disaster 65%. Figure 10 shows that the average of means of occurrence for each factor on the other factors focuses mainly on disability - disease factor and Posses skill factor.

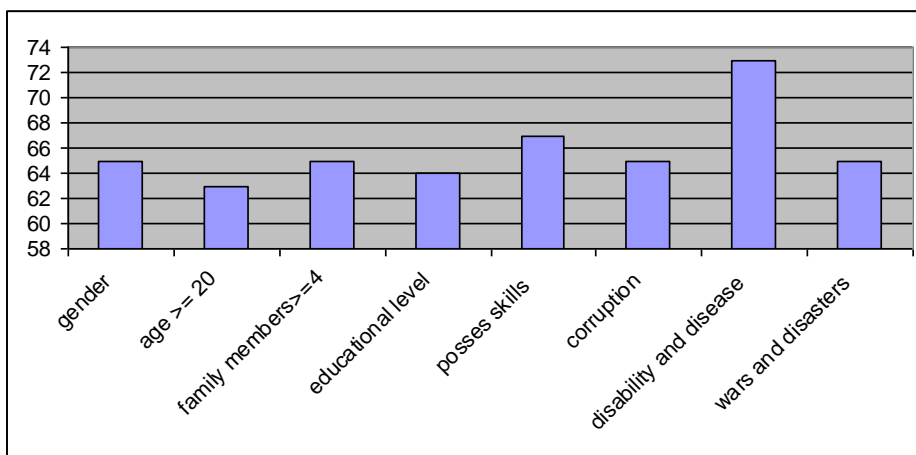


Figure (10) shows the Mean of confidence

5. Conclusions and Recommendations:

5.1 Conclusions:

- 1- The percentage of women, who are providers for poor families, are very close to a male percentage, because most of these women are widows, who lost their husbands in wars.
- 2- All people, who are at their 20s now, are orphans who lost their fathers in wars especially the Gulf War in 1991 and American Invasion in 2003. People, who are above the 20s, have participated in, suffered from the wars or widows.
- 3- Families that have 4 or more members: this is natural in the third world countries; people there don't follow birth control policy.
- 4- Educational level

The 70s have witnessed a great concern of education with all its sections elementary, general, professional and in military schools. Because being employed by the government was worthy; Iraqi dinar equaled 3.33 dollar at that time.

Though many generations of the educated and Posses skill have emerged, most of which died during the wars. People who managed to survive, suffered from the consequences of wars, and for them being employed by the government is no longer worthy ;1 dollar=3000 Iraqi dinar. The collapse of national currency has affected all aspects of life.

- 5- As a consequence of wars, economic collapse and lack of opportunities, a corrupted class emerged, they have practiced every type of corruption in order to keep their positions in the government. This was so obvious after invading Bagdad; the country's infrastructure was destroyed, unplanned construction started. Many people made advantage of these circumstances; they caused poverty and unemployment for so many families because of their being corrupted besides destroying the private sector massively. Shutting down many important factories helped spreading poverty and unemployment.
- 6- One of the consequences of wars is the emergence of a lot of disabled and sick people due to neglecting public health issues in the country.
- 7- Wars are the main reason behind destroying any country. Disasters are also caused by wars; destroying Iraq and making its people poor is a consequence of the wars Iraq has been through.

All the country's incomes are spent to lengthen the war, the thing that weakens every aspect of life in this country. This is the dictatorship when it rules it causes destruction and when it's gone there would be destruction and misery as well.

5.2 Recommendations:

- 1-A country of integral institutions, non-insulating decision making, well choosing for competences owners within a system that neglects all inherited means, which caused spread of corruption, all these are the means needed to build a country free of corruption.
- 2-Establishing a new institution for widows to check people who are under the line of poverty and to provide job opportunities.
- 3-Establishing an institution for orphans who lost their fathers as a consequence of the wars the country has been through.
- 4-Rehabilitating every governmental companies that have been shut down, and rerun all the factories especially military industry companies, and make them civil companies.
- 5-Encouraging human investment through training and improving individuals to make them more efficient and productive, so they could get more wages or incomes.
- 6-Fighting against illiteracy and spreading cultural consciousness in the society.

- 7-Developing administrative work in health, education, family and social services fields.
- 8-Developing countryside and showing interest in agriculture which has been neglected for decades, encouraging rural industries using middle technological means to provide as job opportunities as possible.
- 9-Fighting finical and administrative corruption.
- 10-Take advantage of the civilized world experiences such as Japanese, Chinese and Indian experience. Homelands are built by loyal people, but people who are corrupted with sick, individual dreams destroy homelands.

References:

- [1] B.M. HUSSEIN, Measuring the poverty in the Economic and Social Commission for Western Asia, a series of anti-poverty studies / United Nations / New York/1996.
- [2] H. M. ALRUFAL, the problem of poverty in the Islamic world / causes and solutions, ALNUKASH House for printing, publishing and distribution/Lebanon 2006.
- [3] S. AZIZ. ALATBI, Statistic in Geography, AKRAM Press, Baghdad 2012.
- [4] S. ALTAEER, Poverty and corruption in the Arabian world/DAR ALSAQI/London 2009.
- [5] A. A. ALBALDAWI, Statistical methods for Economic Sciences and Business Administration with the use of SPSS program/First Edition /WAEL Publishing house/Jordan /Oman2009.
- [6] A. ALFARIS, Poverty and the distribution of income in the Arabian land / Center for Arab Unity Studies/Bruit 2001.
- [7] Y.S. Koh and N. Rountree, Rare Association Rule Mining and Knowledge Discovery: Technologies for Infrequent and Critical Event Detection, Information Science Reference (an imprint of IGI Global), New York - 2010.
- [8] A. gkoulals and V. S. Vergykios, Association Rule Hiding for Data Mining, Springer Science, Business Media, LLC, New York, USA ,2010.
- [9] Zhang C. and S. Zhanger , Association Rule Mining Models and Algorithms, Springer-Verlag Berlin Heidelberg ,2002.
- [10] R. Agrawal and R. Srikant, "Fast algorithms for mining association rules", In Proc. of Int. Conf. on Very Large Data Bases (VLDB'94), Santiago, Chile, September 1994, pp. 487-499.
- [11] G. Johnny and H.S. ABBAS "Analytical Study using Association Rules and Mean of Confidence to Assess the Acceptance of (Industrial Schools/Computer) students at computer systems Dept\ Institute of Administration Rusafa" 2nd conference, Technical College of Management – Baghdad 28-29 /11/2012.

Estimation of Daily Evaporation from Calculated Evapotranspiration in Iraq

1-Dr. Hussain Zaydan Ali

Expert / Remote Sensing, Ministry of Science and Technology-Baghdad-Iraq

hussainzayali53@yahoo.com

2- Saad H. Faraj,

Iraqi Meteorological Organization and Seismology-Iraq

swattar2001@yahoo.com

Abstract:

The knowledge of the evapotranspiration (ET) of natural ecosystems and plant populations is of fundamental importance in several branches of science, research and practical uses. Calculation of total daily Evaporation related to calculate the loss of water by daily evapotranspiration from FAO Penman-Monteith equation. Twenty two climatological stations are used in this work for the period 2004-2013 in Iraq. Estimating conversion constant in order to calculate Evaporation value and comparing it with measured value from Iraqi meteorological organization and seismology. The results show high correlation coefficient. We formulated method is proposed to for calculate the amount of evaporation for missing data of climatological Iraqi stations from calculated evapotranspiration value. GIS maps reflect distribution of evaporation, evapotranspiration and Kp in Iraq.

Key words: evapotranspiration, ecosystems, daily Evaporation, Iraq.

الخلاصة:

تكتسب معرفة البخر والنبات من النظم الإيكولوجية الطبيعية ومجموعة النباتات و لها أهمية أساسية في العديد من فروع العلوم والبحوث والاستخدامات العملية. حساب إجمالي التبخر اليومي المرتبط بحساب فقدان الماء عن طريق التبخر اليومي للتبخر من معادلة بنمان-مونتيث (منظمة الغذاء و الزراعة). وتستخدم في هذا العمل اثنتان وعشرون محطة مناخية للفترة 2004-2013 في العراق. تقدير ثابت التحويل من أجل حساب قيمة التبخر ومقارنتها بالقيمة المقاسة من منظمة الأرصاد الجوية العراقية وعلم الزلازل. أظهرت النتائج معامل ارتباط عال. وضعنا طريقة مقترحة لحساب كمية التبخر لبيانات مفقودة من المحطات العراقية المناخية من قيمة التبخر المحسوبة. وتعكس خرائط نظم المعلومات الجغرافية توزيع التبخر والتبخر والنتج في العراق.

الكلمات المفتاحية: التبخر، النظم البيئية، التبخر اليومي، العراق.

1. Introduction:

Evaporation in a soil-plant-atmosphere system occurs from each of the system component. Evaporation from the soil is affected by soil water content, type and tillage [1]. Evaporation occurs when liquid water is converted into water vapor. The rate is controlled by the availability of energy at the water surface, and the ease with which water vapor can mix into the atmosphere [2]. Evapotranspiration (ET) is the loss of water from vegetation surface through the combined processes of plant transpiration and soil evaporation. Both environment and biological factor affect ET. Important environmental factor include climate parameter. Biological factor affecting ET include type of vegetation, foliage geometry and foliage density [3]. The problem of measuring evaporation from open water surfaces, and transpiration from different types of vegetation, has been a central problem in hydrology for many years. In terms of the hydrological cycle and the water balance, evaporation and transpiration make up the second largest component. Many weather stations include measurements of the evaporation from a Class-A pan [4], as the basis for calculating the water loss from lakes or from crops [5, 6]. But most places are without such

measurements, and, even where there is a pan, the measurements may be vitiated by poor maintenance, leading to errors due to leaks, the growth of algae in the water, an incorrect water level, weed-growth nearby, water scarcity, and so on. Also, it is hard to measure evaporation accurately during rainfall [8], perhaps because of splashing of water in or out of the pan. In view of these difficulties, it would be useful and cheaper to have some means of estimating pan evaporation with reasonable accuracy, from FAO Penman-Monteith method which demonstrate how the crop reference evapotranspiration which determined from meteorological data, such as temperatures, relative humidity, wind speed, sunshine duration. Pan coefficient (K_p) is away to calculate pan evaporation (mm/day)(E_{pan}), or reference evapotranspiration (mm/day)(E_{To}) in indirectly method, there are different method used to predict pan coefficient value depending on climate data, type of pan, ground cover in climate station, it's surrounding, the sitting of the pan and pan environment[9]. Many different equations for calculating pan coefficient was stated by Doorenbos and Pruitt's Table (Doorenbos & Pruitt, 1977)[9], Cuenca (1989)[10],

Snyder (1992)[11], Pereira et al. (1995)[12], Raghuwanshi & Wallender (1998)[13], and FAO/56 (Allen et al.,(1998)[8]. The selection of the best technique to use for a

particular computation is largely a function of the data available, type or size of water body, and the required accuracy of the estimated evaporation.

2. Methodology:

2.1

Penman-Monteith equation:

In 1948, Penman [14] combined the energy balance with the mass transfer method and derived an

equation to compute the evaporation from an open water surface from standard climatological records. The Penman-Monteith form of the combination equation is:

$$ET = \frac{\Delta(R_n - G) + \rho_a c_p \frac{(e_s - e_a)}{r_a}}{\Delta + \gamma(1 + \frac{r_s}{r_a})} \quad (1)$$

where R_n is the net radiation, G is the soil heat flux, $(e_s - e_a)$ represents the vapor pressure deficit of the air, ρ_a is the mean air density at constant pressure, c_p is the specific heat of the air, Δ represents the slope of the saturation vapor pressure temperature relationship, γ is the psychrometric

constant, r_s and r_a are the (bulk) surface and aerodynamic resistances.

2.2 Aerodynamic resistance (r_a):

The transfer of heat and water vapor from the evaporating surface into the air above the canopy is determined by the aerodynamic resistance:

$$(2) \quad r_a = \frac{\ln\left[\frac{z_m - d}{z_{om}}\right] \ln\left[\frac{z_h - d}{z_{oh}}\right]}{K^2 u_z}$$

Where

r_a aerodynamic resistance [$s\ m^{-1}$],
 z_m height of wind measurements [m],
 z_h height of humidity measurements

[m],
 d zero plane displacement height [m],
 z_{om} roughness length governing momentum transfer [m],
 z_{oh} roughness length governing transfer of heat and vapor [m],
 k von Karman's constant, 0.41,
 u_z wind speed at height z [m s⁻¹].

$$r_s = \frac{r_1}{LAI_{active}} \quad (3)$$

Where

$$ET_o = \frac{0.408\Delta(R_n - G) + \gamma \frac{900}{T+273} u_2 (e_s - e_a)}{\Delta + \gamma(1 + 0.34u_2)} \quad (4)$$

Where

ET_o reference evapotranspiration [mm day⁻¹],
 R_n net radiation at the crop surface [MJ m⁻² day⁻¹],
 G soil heat flux density [MJ m⁻² day⁻¹],
 T mean daily air temperature at 2 m height [°C],
 u_2 wind speed at 2 m height [m s⁻¹],
 e_s saturation vapor pressure [kPa],
 e_a actual vapor pressure [kPa],
 $e_s - e_a$ saturation vapor pressure deficit [kPa],
 Δ slope vapor pressure curve [kPa °C⁻¹],
 γ psychrometric constant [kPa °C⁻¹].

r_s (bulk) surface resistance [s m⁻¹],
 r_1 bulk stomatal resistance of the well-illuminated leaf [s m⁻¹],
 LAI_{active} active (sunlit) leaf area index [m² (leaf area) m⁻² (soil surface)].

From combination of the original Penman-Monteith equation (Equation 1) and the equations of the aerodynamic (Equation 2) and surface resistance (Equation 3), given the FAO Penman-Monteith method to estimate ET_o , it is indicated below in equation(4):

The reference evapotranspiration, ET_o , provides a standard to which evapotranspiration at different periods of the year or in other regions can be compared; evapotranspiration of other crops can be related. The equation uses standard climatological records of solar radiation (sunshine), air temperature, humidity and wind speed. To ensure the integrity of computations, the weather measurements should be made at 2 m (or converted to that height) above an extensive surface of green grass, shading the ground and not short of water.

CROPWAT 8.0 for Windows is a computer programme for the calculation of crop water requirements and irrigation requirements from existing or new climatic and crop data.

Furthermore, the program allows the development of irrigation schedules for different management conditions and the calculation of scheme water supply for varying crop patterns.

2.4 Pan evaporation:

The evaporation rate from pans filled with water is easily obtained. In the absence of rain, the amount of water evaporated during a period (mm/day) corresponds with the decrease in water depth in that period. Pans provide a measurement of the integrated effect of radiation, wind, temperature and humidity on the evaporation from an open water surface. Although the pan responds in a similar fashion to the same climatic factors affecting crop transpiration, several factors produce significant differences in loss of water from a water surface and from a cropped surface. Reflection of solar

2.3 ET_o computed by CROPWAT:

radiation from water in the shallow pan might be different from the assumed 23% for the grass reference surface. Storage of heat within the pan can be appreciable and may cause significant evaporation during the night while most crops transpire only during the daytime. There are also differences in turbulence, temperature and humidity of the air immediately above the respective surfaces. Heat transfer through the sides of the pan occurs and affects the energy balance.

The pan evaporation is related to the reference evapotranspiration by an empirically

derived pan coefficient:

$$ET_o = K_p E_{pan} \quad (5)$$

Where

ET_o reference evapotranspiration [mm/day],

K_p pan coefficient,

E_{pan} pan evaporation [mm/day].

Pan coefficient (K_p): 2.6

Pan types and environment:

In selecting the appropriate pan coefficient, not only the pan type, but also the ground cover in the station, its surroundings as well as the general wind and humidity conditions, should be checked. The sitting of the pan and the pan environment also influence the results. This is particularly so where the pan is placed in fallow rather than

cropped fields. Two cases are commonly considered: Case A where the pan is sited on a short green (grass) cover and surrounded by fallow soil; and Case B where the pan is sited on fallow soil and surrounded by a green crop, we will use equation (6) to calculate pan coefficient for case A which is stated as:

$$K_p = 0.108 - 0.0286 u_2 + 0.0422 \ln(FET) + 0.1434 \ln(RH_{mean}) - 0.000631 [\ln(FET)]^2 \ln(RH_{mean}) \quad (6)$$

K_p pan coefficient

u_2 average daily wind speed at 2 m height ($m s^{-1}$)

RH_{mean} average daily relative humidity [%] = $(RH_{max} + RH_{min})/2$

FET fetch, or distance of the identified surface type (grass or short green agricultural crop for case A, dry crop or bare soil for case B upwind of the pan).

Evaporation is one of important element using in proper irrigation management although evapotranspiration, calculating of monthly average daily of evaporation through calculating the loss of water by monthly average daily evapotranspiration from FAO Penman–Monteith equation (Equation 4). We applied this equation for 22 different climate station in Iraq using

3. Result and discussion:

climate elements (max. temp., min temp., RH %, sunshine duration, wind speed). During the period 2004-2013, the lowest value was calculated in January for Mosel station 0.68 mm/day while highest value was calculated in June for Basrah station was 14.565 mm/day.

Figures (1), (2) and (3) Represent monthly distribution of evapotranspiration in Iraq.

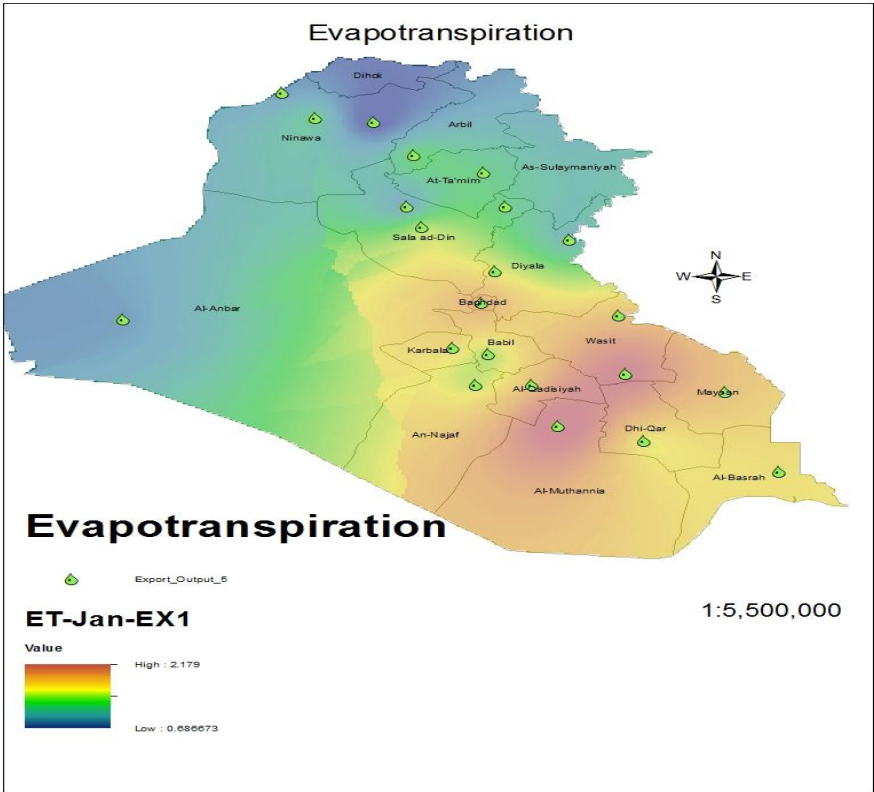


Figure (1): Evapotranspiration map for Iraq in January.

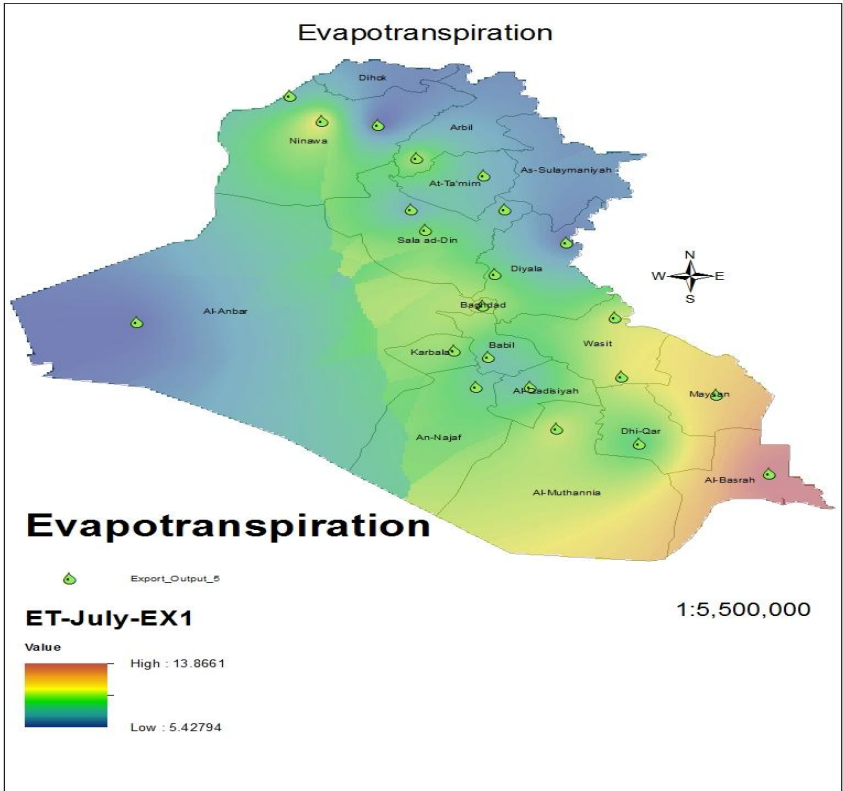


Figure (2): Evapotranspiration map for Iraq in July.

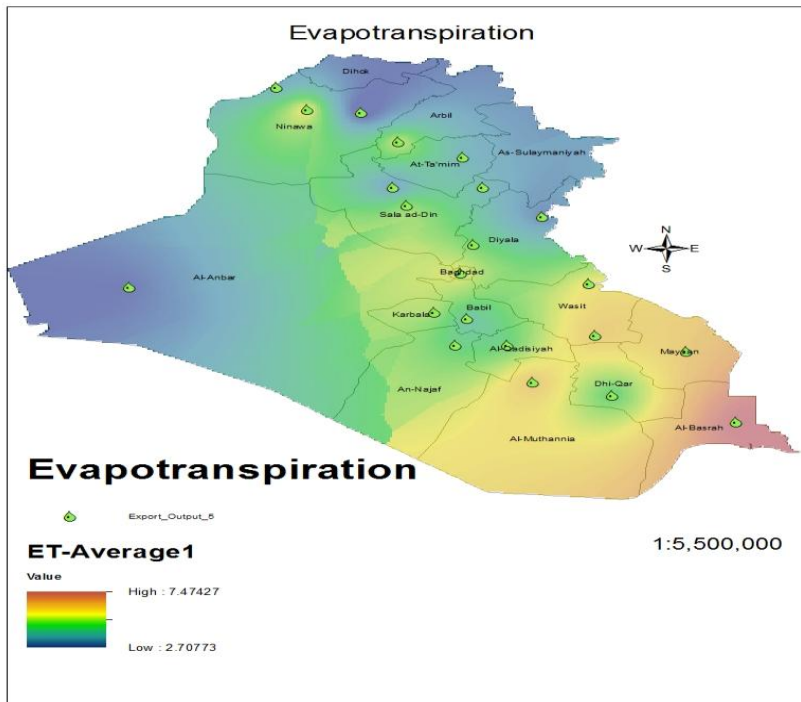


Figure (3): Average Evapotranspiration map for Iraq.

Mean monthly total evaporation measured for 15 climate stations for the period (2004 – 2013) in Iraqi meteorological organization and seismology which are less than 22 stations used in calculating evapotranspiration due to shortage in measuring evaporation data. Lowest mean monthly total evaporation was

recorded in January in Mosel climate station was 34.9 mm while highest value recorded in Al Hai climate station in July was 651.4 mm. Fig (4) represent mean monthly total evaporation for Iraq which illustrate increasing in a mount of evaporation as we directed south.

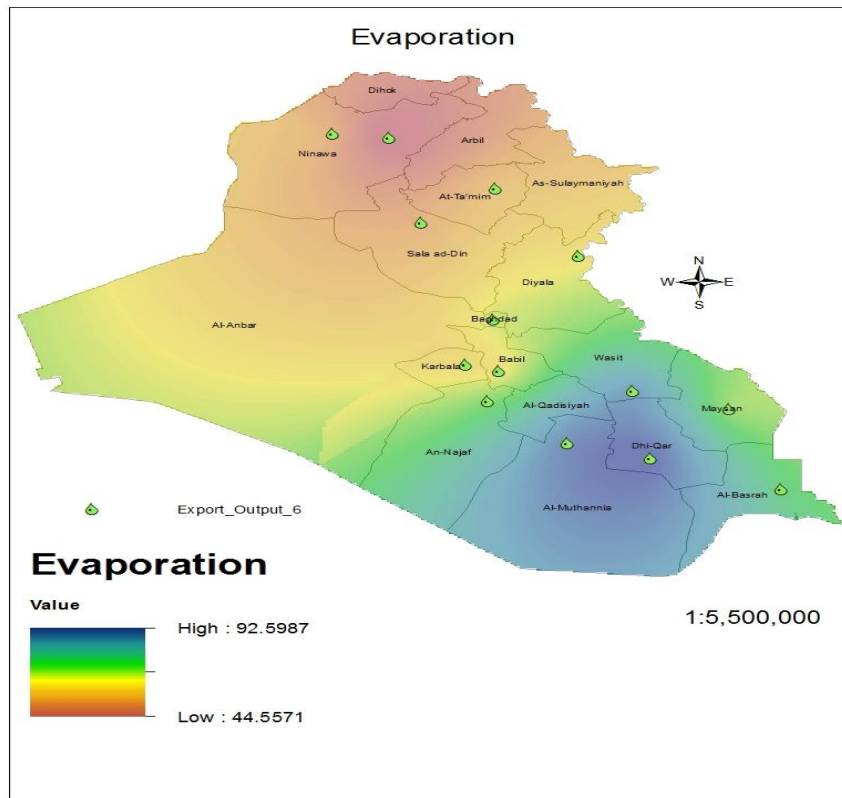


Figure (4): Average Evaporation map for Iraq.

From equation (5) we calculate pan coefficient (conversion constant) for 11 climate stations. Table (1) represent seasonal conversion constant K_p for some station in Iraq and the mean

value equal to 0.67 in winter cooler time in the year and 0.59 in summer or warm period. These values were close to the recorded value 0.7 and 0.6 respectively for other cities [3].

Table (1): K_p for Iraqi stations.

Conversion Constant				
	Winter	Spring	Summer	Autumn
Mousel	0.59	0.57	0.43	0.5
Kirkuk	0.61	0.7	0.54	0.47
Beji	0.56	0.53	0.54	0.52

Khanaqen	0.4	0.4	0.32	0.34
Baghdad	0.76	0.67	0.6	0.68
Karbala	0.81	0.75	0.69	0.74
Hilla	0.8	0.78	0.74	0.76
Hai	0.65	0.58	0.51	0.55
Najaf	0.6	0.57	0.53	0.53
Amara	0.83	0.81	0.77	0.79
Basrah	0.78	0.86	0.82	0.85
Average	0.67	0.66	0.59	0.61

Figure (5) illustrate the relation between ETo calculated from Penman-Montieth equation and evaporation measured by Iraqi meteorological organization and seismology for

Basrah climate station (2004-2013). We found that the relation was linear as indicated by the relation:

$$Y=0.918+0.239x$$

with

$$R^2=0.9615$$

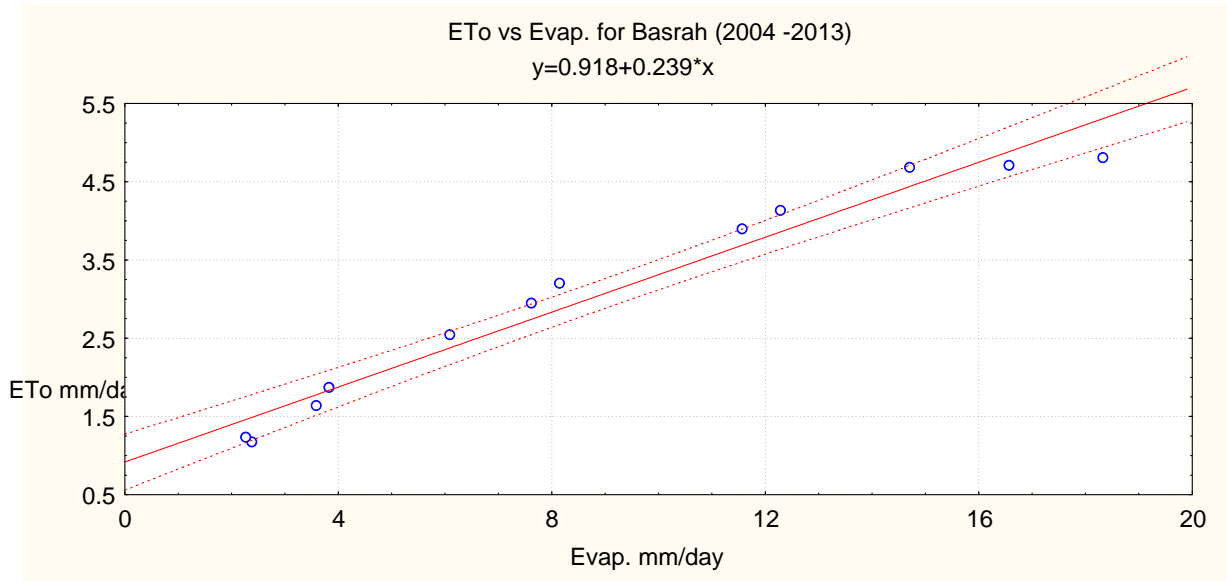


Figure (5): Relation between ETO and Evaporation (Basrah).

Figure (6) illustrate relation between ETo calculated from Penman–Monteith equation and evaporation

Measured by IMO for Baghdad climate station.
 We find $R^2=0.9955$.

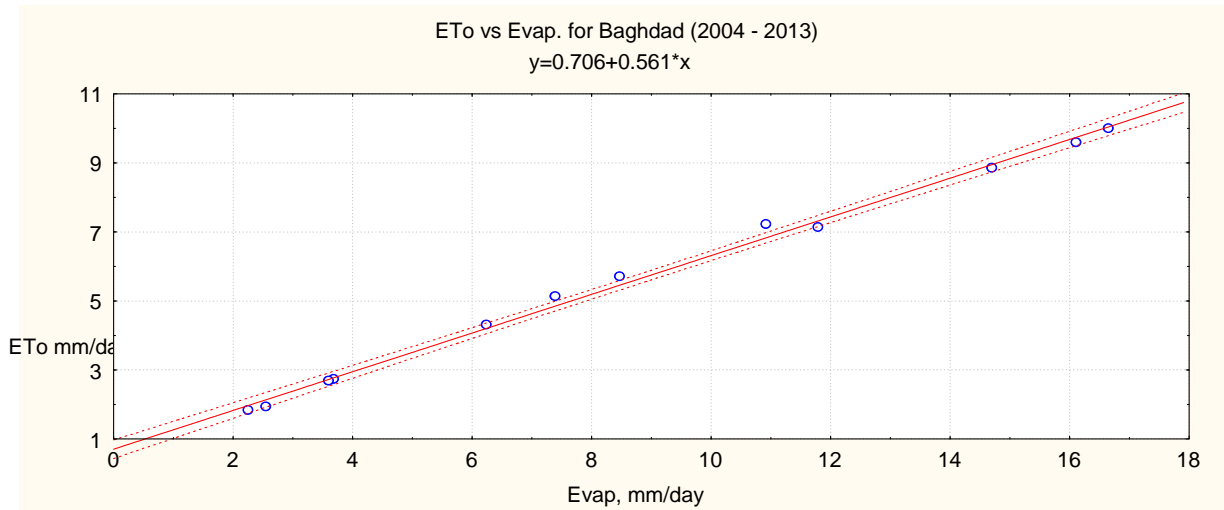


Figure (6): Relation between ETO and Evaporation (Baghdad).

Figure (7) represent a degree of a comparison between evaporation

calculated by applying equation (5) and evaporation measured for Baghdad

climate station for 2013.

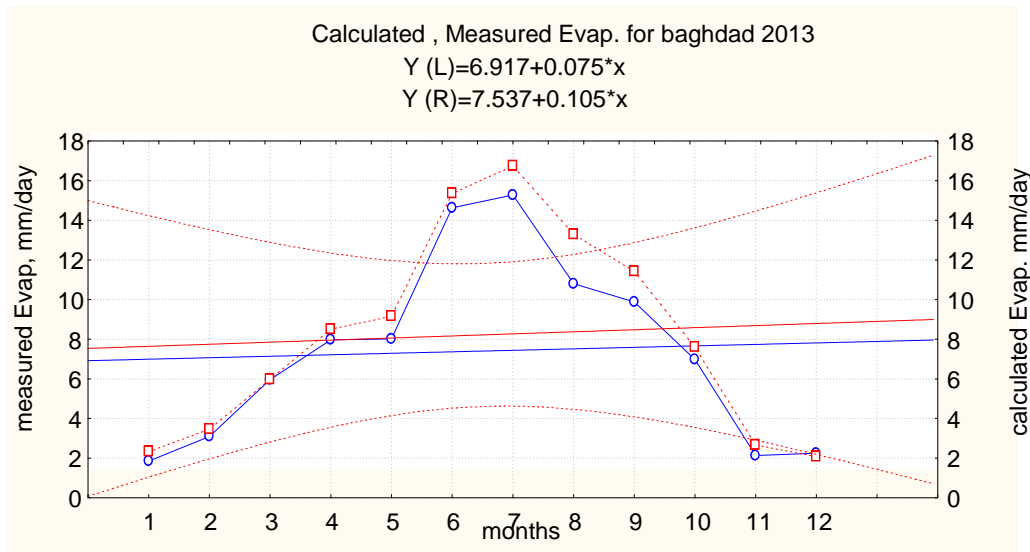


Figure (7): Comparison between measured and calculated evaporation.

Conclusion:

We notice from the distribution map for evapotranspiration and evaporation climate elements that its values were less than the values of its records in Nassirya, Ammara, Simawa as that's related to Basrah city were it is surrounded by water area be a source of water vapor in the atmosphere increasing humidity decreasing evapotranspiration and evaporation process. Evaporation affected by relative humidity and wind speed surrounding station like Nassirya having higher speed of air than Basrah also prevailing wind in Basrah was SE for some month which mean that the blowing air on Basrah city comes from Arab Gulf saturated by water vapor decrease evaporation and evapotranspiration. Evaporation is very important element in irrigation process , the amount of water evaporated during time affected by more than one parameters complicated the measurement accuracy, our procedure aimed to calculate amount of evaporation from calculating evapotranspiration and pan coefficient using cropwat v 8.0, from Figure(7) we found a similarity between calculated and measured evaporation giving high reliability to adopt this method to find missing data for evaporation element for different places in Iraq.

References:

- [1] C.M. Burt, A.J. Mutziger, R.G. Allen, T.A. Howell, (2005), Evaporation Research: Review and Interpretation, journal of irrigation and drainage engineering, ASCE, (2005)131:1(37). [2] Estimated of open water Evaporation, A Review of Methods R&D Technical Report W6-043/TR <http://ag.arizona.edu/azmet/et1.htm>.
- [3] Azmete Vapotranspiration Estimates: A Tool for Improving Water Management of Turf Grass. Paul w. Brown.
- [4] Brutsaert, W.1982. Evaporation into the Atmosphere. (Reidel, Amsterdam) 299pp.
- [5] Doorenbos, J. and Pruitt, W.O. 1977. Guidelines for Predicting Crop Water Requirements Irrigation and Drainage Paper 24. (Food & Agriculture Organization, United Nations, Rome) 144pp.
- [6] Hanson, C.L. and Rauzi, F. 1977. "Class A pan evaporation as affected by shelter, and a daily prediction equation". Agricultural Meteorology. 18: 27-35.
- [7] Bloemen, G.W. 1978. "A high-accuracy recording pan-evaporimeter and some of its possibilities." Journal of Hydrology 39: 159-173.
- [8] Allen, R.G., Pereira, L. S., Raes, D., and Smith, M., "Crop Evapotranspiration: Guidelines for Computing Crop Water Requirement.: Irrigation and Drainage paper 56, Food and Agriculture Organization of the United Nations, Rome, 1998.
- [9] Doorenbos, J.; Pruitt, W.O. Crop water requirements. Rome: FAO, 1977. 179p. Irrigation and Drainage Paper, 24.
- [10] Cuenca, R.H. Irrigation system design: an engineering approach. New Jersey: Prentice-Hall, Englewood Cliffs. 1989, 133p.
- [11] Snyder, R.L. Equation for evaporation pan to evapotranspiration conversion. Journal of Irrigation and Drainage Engineering of ASCE, New York, v.118, n.6, p.977-980, 1992.
- [12] Pereira, A.R.; Villa Nova, N.A.; Pereira, A.S.; Barbieri, V. A model for the class A pan coefficient. Agricultural and Forest Meteorology, Amsterdam, v.76, p.75-82, 1995.
- [13] Raghuwanshi, N.S.; Wallender, W.W. Converting from pan evaporation to evapotranspiration. Journal of Irrigation and Drainage Engineering of ASCE, New York, v.124, n.5, p.275-277, 1998.
- [14] Penman, H. 1948, " Natural evaporation from open water, bare soil and grass". Proc. Roy. Soc. London, A193, 120-146.

On Solve Fuzzy Boundary Value Problem

Amani E. Kadhm/Assist Lecturer

Department of Automotive, Engineering Technical College Baghdad, Middle Technical University, Baghdad, Iraq.

Abstract

The main objective of this paper is to study the pyramidal fuzzy numbers in fuzzy differential equations and introduce a new approach for solving fuzzy boundary value problems. Also, we give an example, where we compare the fuzziness of "pyramidal" solution to that one, which is derived by the extension principle.

Keywords: Fuzzy sets, Boundary Fuzzy differential equation, Boundary value problems, Pyramidal fuzzy numbers

المعادلات التفاضلية الضبابية

اماني النفات كاظم/مدرس مساعد

قسم السيارات, الكلية التقنية الهندسية بغداد, الجامعة التقنية الوسطى, بغداد, العراق

المستخلص

الهدف الرئيس من هذا البحث هو دراسة الاعداد الضبابية الهرمية في المعادلات التفاضلية الضبابية واستخدام نهج مطور لحل المعادلات التفاضلية الضبابية الحدودية. وايضا اعطاء مثال, حيث قارنا بين الحلول الضبابية الهرمية للمعادلات التفاضلية الضبابية الحدودية لهذه المسألة والتي اشتقت بواسطة مبدأ التوسيع.

الكلمات المفتاحية: مجموعات ضبابي، الحدود المعادلة التفاضلية، مشاكل قيمة الحدود

1-Introduction:

The concept of fuzzy sets was introduced initially by Zadeh in 1965, [1]. Since then, this concept is used extensively in fuzzy systems described by fuzzy processes which look as their natural extension into the time domain.

The term "fuzzy differential equation" was coined in 1978 by A. Kandel, Wj. Byatt, in [2] they were carefully studied, for example, solution of fuzzy differential equations provide a noteworthy example of time dependent fuzzy sets in [3],[4].it was followed up by dubois and prade [5] who used the extension principle in their approach. The study of fuzzy differential equations has been initiated as an independent subject in conjunction with fuzzy valued analysis [6] and [7] and set-valued differential equations [8] Initially, the derivative for fuzzy valued mappings was developed by Puri and Ralescu the theory of fuzzy differential equations seems to have split into two independent branches, where the first one relies upon the notion of Hukuhara derivative [9], and the second we define the class of pyramidal fuzzy numbers and offer a new definition of the solution to fuzzy differential equations.

In the last few years, many works have been done by several authors in theoretical and applied fields see [10, 11, 12]. A variety of exact, approximate and purely numerical methods are available to find the solution of a fuzzy initial value problem. It is an important problem that we know a differential equation has a unique solution. There are many theorems and reasonable conditions for this aim. The shooting method can approximate the unique solution for a linear fuzzy boundary value differential equations see [13, 14].

In this paper, the concept of pyramidal fuzzy numbers have been used to solve differential equations and then extended to solve fuzzy boundary value problems (FBVP)

2-Preliminaries

In this section, several basic concepts of fuzzy system, fuzzy differential equations and function of matrices will be recalled; we start with the obvious definition of fuzzy differential equation.

Definition (2.1) [15]:

A fuzzy set \tilde{A} on the set of real numbers \mathbb{R} is convex if and only if:

$$M_{\tilde{A}}(\lambda x_1 + (1-\lambda) x_2) \geq \text{Min} \{M_{\tilde{A}}(x_1), M_{\tilde{A}}(x_2)\} \dots (2.1)$$

for all $x_1, x_2 \in \mathbb{R}$ and all $\lambda \in [0, 1]$.

Remark (2.2):

A fuzzy number is a function $u: \mathbb{R} \rightarrow [0, 1]$ satisfying the following properties:

- 1-u is normal, i.e. there exists a unique $x_0 \in \mathbb{R}$ with $u(x_0) = 1$.
- 2-u is convex fuzzy set.
- 3- u is upper semi continuous on \mathbb{R} .
- 4-The support of A is compact.

The family of fuzzy numbers which will be denoted by E and for $0 < r < 1$, $[u]^r$ denotes $\{x \in R: u(x) \geq r\}$ which is called the r -level set and $[u]^0$ denotes $\{x \in R: u(x) > 0\}$ which is called the support of the fuzzy number u it should be noted that for any $0 \leq r \leq 1$, $\lambda[u]^r$ is abounded closed interval for $u, r \in E$ and $\lambda \in R$, the sum $u+v$ and the product λu can be defined by :

$$[u + v]^r = [u]^r + [v]^r$$

$$[\lambda u]^r = [\lambda u]^r, r \in [0, 1]$$

Where $[u]^r + [v]^r$ means the addition of two intervals of R and $\lambda[u]^r$ means the product between a scalar and a subset of R .

Arithmetic operation of arbitrary fuzzy numbers $u = (\underline{u}(r), \bar{u}(r))$, $v = (\underline{v}(r), \bar{v}(r))$ and $\lambda \in R$ can be defined as:

$$1-u=v \text{ if and only if } \underline{u}(r) = \underline{v}(r) \text{ and } \bar{u}(r) = \bar{v}(r)$$

$$2-u+ v = (\underline{u}(r) + \underline{v}(r), \bar{u}(r) + \bar{v}(r))$$

$$3-u- v = (\underline{u}(r)-\underline{v}(r), \bar{u}(r)-\bar{v}(r)) \tag{2.2}$$

$$4-\lambda u = \begin{cases} (\lambda \underline{u}(r), \lambda \bar{u}(r)), & \text{if } \lambda \geq 0 \\ (\lambda \bar{u}(r), \lambda \underline{u}(r)), & \text{if } \lambda < 0 \end{cases}$$

Note that the crisp number σ is simply represented by $\underline{u}(r) = \bar{u}(r) = \sigma$ which is obtained by letting $r=1$.

In the following, we recall some definitions concerning fuzzy differential equations:

Definition (2.3) [16]:

Let $P_k(R^n)$ denote the family of all non-empty compact convex subsets of R^n and define the addition and scalar multiplication in $P_k(R^n)$ as usual. Let A and B be two non-empty and bounded subsets of R^n , then the distance between A and B is defined by the following Housdorff metric:

$$d(A,B) = \max\{\sup_{a \in A} \inf_{b \in B} d(a,b), \sup_{b \in B} \inf_{a \in A} d(b,a)\} \tag{2.3}$$

Where $d(a, b)$ denotes the usual distance function in R^n .

Now, we denote $E^n = \{u: R^n \rightarrow [0, 1] \text{ u satisfies (1)-(4) above.}$

Definition (2.4) [17]:

A mapping $f: T \rightarrow E$ for the interval $T \subseteq R$ is called a fuzzy process. Therefore, its r -level set can be written as follows:

$$[f(t)]^r = [f_-(t), f_+(t)]^r, t \in T, r \in [0,1] \tag{2.4}$$

Definition (2.5)[18]:

A function $F_\alpha: E^n \rightarrow P_k(R^n)$ is called Hukuhara differentiable at a point $t_0 \in R^n$ if for $h > 0$ sufficiently small, we have:

$$\begin{aligned} \dot{F}_\alpha(t_0) &= \lim_{h \rightarrow 0^+} \frac{F_\alpha(t_0+h) - F_\alpha(t_0)}{h} \\ &= \lim_{h \rightarrow 0^-} \frac{F_\alpha(t_0) - F_\alpha(t_0-h)}{h} \\ &= \lim_{h \rightarrow 0} \frac{F_\alpha(t_0+h) - F_\alpha(t_0)}{h} \end{aligned} \tag{2.5}$$

where the limits of Hukuhara derivative are taken in the metric space $(P_k(R^n), d)$, and $F_\alpha(t_0+h) - F_\alpha(t_0) = (\bar{a} - \bar{b}, \underline{a} - \underline{b})$.

Definition (2.6)[19]:

A mapping $F: T \rightarrow E^n$ is called differentiable at $t_0 \in T$, if for any $\alpha \in [0, 1]$, the set valued mapping $F_\alpha(t) = [F(t)]^\alpha$ is Hukuhara differentiable at a point t_0 with $D F_\alpha(t_0)$ and the family $\{D F_\alpha(t_0) | \alpha \in [0, 1]\}$ define a fuzzy number $F'(t_0) \in E^n$, which is called the differentiation of F at t_0 .

If $F: T \rightarrow E^n$ is differentiable at $t_0 \in T$, then we say that $F'(t_0)$ is the fuzzy derivative of $F(t_0)$

at the point t_0 .

3. Solutions of Pyramidal Fuzzy Numbers

The pyramidal number is one of the fundamental aspects in differential equations, in general and of fuzzy differential equations in particular. Therefore, several approaches are proposed to study this subject.

Hence, in this section, we will give one of such approaches as a theorem. Also, we will set and present some of the basic ideas for the construction and proof of the pyramidal fuzzification.

Definition (3.1)[20]:

The fuzzy number $x \in E^n$ is called pyramidal if its α -level sets are n-dimensional rectangles for $0 \leq \alpha \leq 1$.

The Pyramidal Method For Solving Fuzzy Differential Equations (3.2):

There exists a fuzzy process $x: [0, T] \rightarrow E^n$, such that

$$[x(t)]^\alpha = x_k^n [g_{1\alpha}^k(t), g_{2\alpha}^k(t)] \tag{3.1}$$

Where X denotes the usual set theoretical Cartesian product

Proof: see [20].

Pyramidal Fuzzification For Solving Linear Fuzzy Systems (3.3):

In this section, if the function $z(t, x_0)$ from the preceding section may be given in a closed form, then a more direct method of fuzzification of the crisp solution may be proposed and used later to solve FBVP'S.

Theorem

Consider an initial value problem for the linear system

$$X(t) = \begin{pmatrix} x_1 \\ x_2 \\ \vdots \\ x_n \end{pmatrix} = e^{At} \text{ Where } A(t) \text{ is an } n \times n \text{ matrix}$$

$$e^{At} = I + At + \frac{A^2}{2!} t^2 + \dots \tag{4.1}$$

Then the fuzzy process $x(t)$ satisfies

$$\left. \begin{aligned} \dot{x}(t) &= A(t)x(t) + a(t) \\ x(t_0) &= x_0 \end{aligned} \right\} \tag{4.2}$$

Where $\dot{x}(t) = \frac{dx(t)}{dt}$, will be solved.

There it can be obtained

$$\tilde{x}(t) = (E_{t_0}^t \tilde{A}) \tilde{x}_0 + \int_{t_0}^t (E_{t_0}^{t-\tau} \tilde{A}) \tilde{a}(\tau) d\tau \tag{4.3}$$

Proof see [20].

4-Solution of Fuzzy Boundary Value Problems

Differential equations which are given with fuzzy conditions given at two or more points of the domain of definition are called FBVP'S. We consider non fuzzy differential equations of order two with boundary fuzzy conditions at the end points a, b.

$$y' = f(x, y, y'), a \leq x \leq b, y(a) = \alpha \text{ and } y(b) = \beta \dots \dots \tag{1}$$

under what conditions a boundary value problem has a solution or has a unique solution.

Existence and uniqueness (4.1) [11,16]

Suppose that f is continuous on the set

$$D = \{(x, y, y'); a \leq x \leq b, -\infty < y < \infty, -\infty < y' < \infty\}$$

and the partial derivatives f_y and $f_{y'}$ are also continuous on D . if

- 1) $f_y(x, y, y') > 0$, for all (x, y, y') in D , and
- 2) there exists a constant M such that

$$|f_{y'}(x, y, y')| \leq M \text{ for all } (x, y, y') \text{ in } D,$$

then the boundary value problem(1) has a unique solution.

Example (4.2)

Consider the following boundary value problem:

$$y'' + e^{-xy} + \sin(y) = 0, 1 \leq x \leq 2, y(1) = y(2) = 0.$$

Determine if the boundary value problem has a unique solution.

Rewrite $y'' = -e^{-xy} - \sin(y)$. So $f(x, y, y') = -e^{-xy} - \sin(y)$

Check conditions:

$f(x, y, y') = -e^{-xy} - \sin(y)$, $f_y(x, y, y') = xe^{-xy}$, and $f_{y'}(x, y, y') = -\cos(y)$ are continuous on $D = \{(x, y, y'); 1 \leq x \leq 2, -\infty < y < \infty, -\infty < y' < \infty\}$

(i) $f_y(x, y, y') = xe^{-xy} > 0$ on D .

(ii) $|f_{y'}(x, y, y')| = |-\cos(y)| \leq 1 = M$.

So, the boundary value problem has a unique solution in D .

Example (4.3)

Consider the linear boundary value problem:

$$y'' = p(x)y' + q(x)y + r(x), a \leq x \leq b, y(a) = \alpha \text{ and } y(b) = \beta.$$

Under what condition(s) a linear BVP has a unique solution?

$f(x, y, y') = p(x)y' + q(x)y + r(x)$, $f_y(x, y, y') = q(x)$, $f_{y'}(x, y, y') = p(x)$ are continuous on D if $p(x), q(x)$ and $r(x)$ are continuous for $a \leq x \leq b$

a. $f_y(x, y, y') = q(x) > 0$ for $a \leq x \leq b$.

b. Since $f_{y'}$ is continuous on a, b , $f_{y'}$ is bounded.

So, if $p(x), q(x)$ and $r(x)$ are continuous for $a \leq x \leq b$, and $q(x) > 0$ for $a \leq x \leq b$, then the boundary value problem has a unique solution.

The existence of a unique solution for fuzzy initial value problems will relate by the shooting method of the existence of a unique solution for fuzzy boundary value problems is studied depending on the initial fuzzy value problem.

5. The Shooting Method for Solving Fuzzy Linear BVP's [13, 14]:

The shooting method for solving fuzzy linear differential equation is based on the replacement of the fuzzy boundary value problem by its two related fuzzy initial value problems, as it is in usual case for solving non-fuzzy boundary value problems.

Now, consider the linear second order fuzzy boundary value problem:

$$y'' = p(x)y' + q(x)y + r(x), a \leq x \leq b \dots\dots\dots(5.1)$$

with fuzzy boundary conditions:

$$y(a) = \tilde{\alpha}, y(b) = \tilde{\beta} \dots\dots\dots(5.2)$$

where $\tilde{\alpha}$ and $\tilde{\beta}$ are to pyramidal fuzzy .the differential equation

(i) $p(x), q(x)$ and $r(x)$ are continuous on $[a, b]$.

(ii) $q(x) > 0$ on $[a, b]$.

Hence, the related two fuzzy initial value problems are given by:

$$u'' = p(x)u' + q(x)u, a \leq x \leq b, u(a) = \tilde{0}, u'(a) = \tilde{1} \dots\dots\dots(5.3)$$

and

$$v'' = p(x)v' + q(x)v + r(x), a \leq x \leq b, v(a) = \tilde{\alpha}, v'(a) = \tilde{0} \dots\dots\dots(5.4)$$

To find the solutions of the fuzzy initial value problems (5.3) and (5.4), respectively, the α -level equations related to these fuzzy differential equations are evaluated, which are:

$$[u'']_{\alpha} = p(x)[u']_{\alpha} + q(x)[u]_{\alpha}, [u(a)]_{\alpha} = \tilde{0}_{\alpha}, [u'(a)]_{\alpha} = \tilde{1}_{\alpha} \dots\dots\dots(5.5)$$

and

$$[v'']_{\alpha} = p(x)[v']_{\alpha} + q(x)[v]_{\alpha} + r(x), [v(a)]_{\alpha} = \tilde{\alpha}_{\alpha}, [v'(a)]_{\alpha} = \tilde{0}_{\alpha} \dots\dots\dots(5.6)$$

We can check that $\underline{y}(x)$ is indeed the solution of the original fuzzy BVP, since:

$$\underline{y}'(x) = \underline{v}'(x) + \frac{\tilde{\beta} - \underline{v}(b)}{\underline{u}(b)} \underline{u}'(x)$$

and

$$\underline{y}''(x) = \underline{v}''(x) + \frac{\tilde{\beta} - \underline{v}(b)}{\underline{u}(b)} \underline{u}''(x)$$

So:

$$\begin{aligned} \underline{y}''(x) &= p(x)\underline{v}'(x) + q(x)\underline{v}(x) + r(x) + \frac{\tilde{\beta} - \underline{v}(b)}{\underline{u}(b)}(p(x)\underline{u}'(x) + q(x)\underline{u}(x)) \\ &= p(x)\left\{\underline{v}'(x) + \frac{\tilde{\beta} - \underline{v}(b)}{\underline{u}(b)} \underline{u}'(x)\right\} + q(x)\left\{\underline{v}(x) + \frac{\tilde{\beta} - \underline{v}(b)}{\underline{u}(b)} \underline{u}(x)\right\} + r(x) \\ &= p(x)\underline{y}'(x) + q(x)\underline{y}(x) + r(x) \end{aligned}$$

Moreover:

$$\begin{aligned} \underline{y}(a) = \underline{x}_1(\theta, t) &= \underline{v}(a) + \frac{\tilde{\beta} - \underline{v}(b)}{\underline{u}(b)} \underline{u}(a), \quad 0 \leq \theta \leq 2\pi \\ &= \tilde{\alpha} + \frac{\tilde{\beta} - \underline{v}(b)}{\underline{u}(b)} \times 0 = \tilde{\alpha} \end{aligned}$$

and

$$\underline{y}(b) = \underline{x}_1(\theta, t) = \underline{v}(b) + \frac{\tilde{\beta} - \underline{v}(b)}{\underline{u}(b)} \underline{u}(b)$$

$$\begin{aligned}
 &= \underline{v}(b) + \frac{\tilde{\beta} - \underline{v}(b)}{\underline{u}(b)} \underline{u}(b) \\
 &= \underline{v}(b) + \tilde{\beta} - \underline{v}(b) = \tilde{\beta}
 \end{aligned}$$

Hence, $\underline{y}(x)$ is the unique solution to the linear BVP, provided, of course, that $\underline{u}(b) \neq 0$.

Similarly, as in upper case, we have:

$$\bar{y}(x) = \overline{x_2(\theta, t)} = \bar{v}(x) + \frac{\tilde{\beta} - \bar{v}(b)}{\bar{u}(b)} \bar{u}(x) \quad , \quad 0 \leq \theta \leq 2\pi$$

Next, an illustrative example for solving FBVP analytically will be considered.

Example (5.1):

To solve the nonlinear fuzzy boundary value problem using the shooting method, where:
 $y'' = 2yy'$, $y(0) = -\tilde{1}$, $y(\frac{\pi}{2}) = -\tilde{1}$, $x \in [0, \frac{\pi}{2}]$

Hence the linearized system evaluated at the point $[\frac{1}{2}, 0]$ is given by:

Let $\tilde{y}'_1 = \tilde{y}'_2$

$$\tilde{y}'_2 = 2\tilde{y}_1\tilde{y}'_2$$

Hence in matrix form:

$$\begin{bmatrix} \tilde{y}'_1 \\ \tilde{y}'_2 \end{bmatrix} = \begin{bmatrix} 0 & 1 \\ 0 & 1 \end{bmatrix} \begin{bmatrix} \tilde{y}_1 \\ \tilde{y}_2 \end{bmatrix}, \quad \tilde{y}_1(0) = -\tilde{1} \quad \tilde{y}_2(\frac{\pi}{2}) = -\tilde{1}$$

$$\tilde{\beta} = -\tilde{1} \quad \tilde{\alpha} = \tilde{1} \quad x \in [0, \frac{\pi}{2}]$$

In order to solve the above fuzzy BVP consider the first non-fuzzy BVP:

$$\begin{bmatrix} \tilde{u}'_1 \\ \tilde{u}'_2 \end{bmatrix} = \begin{bmatrix} 0 & 1 \\ 0 & 1 \end{bmatrix} \begin{bmatrix} \tilde{u}_1 \\ \tilde{u}_2 \end{bmatrix}, \quad \tilde{u}_1(0) = \tilde{0}, \quad \tilde{u}_2(0) = \tilde{1} \quad ,$$

and hence the eigenvalues of A are given by $\lambda_1 = 0$, $\lambda_2 = 1$

Therefore to find the corresponding eigenvectors

Let $Au = \lambda u$

Then

$$\begin{bmatrix} 0 & 1 \\ 0 & 1 \end{bmatrix} \begin{bmatrix} \tilde{u}_1 \\ \tilde{u}_2 \end{bmatrix} = 0 \begin{bmatrix} \tilde{u}_1 \\ \tilde{u}_2 \end{bmatrix}$$

This implies

$$\tilde{u}_2 = 0 \quad \tilde{u}_1 \Rightarrow \tilde{u}_1 = r, \quad r=1$$

$$\tilde{u}_1 = \begin{bmatrix} 1 \\ 0 \end{bmatrix}, \tilde{u}_2 = \begin{bmatrix} 1 \\ 0 \end{bmatrix}$$

Hence

$$p = \begin{bmatrix} 1 & 1 \\ 0 & 0 \end{bmatrix}, e^{At} = p e^{at} p^{-1}$$

$$p^{-1} = \begin{bmatrix} 0 & -1 \\ 0 & 1 \end{bmatrix}$$

Therefore

$$e^{at} = \text{diag}(e^{\alpha t})$$

And so

$$\begin{aligned} \tilde{u}(t) &= \begin{bmatrix} 1 & 1 \\ 0 & 0 \end{bmatrix} \begin{bmatrix} e^{0t} & 0 \\ 0 & e^t \end{bmatrix} \begin{bmatrix} 0 & -1 \\ 0 & 1 \end{bmatrix} \begin{bmatrix} \tilde{u}_{01} \\ \tilde{u}_{02} \end{bmatrix} \\ &= \begin{bmatrix} 1 & e^t \\ 0 & 0 \end{bmatrix} \begin{bmatrix} 0 & -1 \\ 0 & 1 \end{bmatrix} \begin{bmatrix} \tilde{u}_{01} \\ \tilde{u}_{02} \end{bmatrix} \\ &= \begin{bmatrix} 0 & -1 + e^t \\ 0 & 0 \end{bmatrix} \begin{bmatrix} \tilde{u}_{01} \\ \tilde{u}_{02} \end{bmatrix} \end{aligned}$$

Hence

$$\tilde{u}_1(t) = 0 \tilde{u}_{01} \quad \tilde{u}_1(t) = -1 + e^t \tilde{u}_{02}$$

$$\tilde{u}_2(t) = 0 \tilde{u}_{01} \quad \tilde{u}_2(t) = 0 \tilde{u}_{02}$$

$$\tilde{u}_{01} = -\sqrt{1-\alpha} \quad \tilde{u}_{01} = \sqrt{1-\alpha} \quad , \alpha=1$$

$$\tilde{u}_{02} = 1 - \sqrt{1-\alpha} \quad \tilde{u}_{02} = 1 + \sqrt{1-\alpha}$$

Now, consider the second nonfuzzy BVP:

$$\begin{bmatrix} \tilde{v}'_1 \\ \tilde{v}'_2 \end{bmatrix} = \begin{bmatrix} 0 & 1 \\ 0 & 1 \end{bmatrix} \begin{bmatrix} \tilde{v}_1 \\ \tilde{v}_2 \end{bmatrix}, \quad \tilde{v}_1(0) = \tilde{1}, \tilde{v}_2(0) = \tilde{0}$$

and hence the eigenvalues of A are given by $\lambda_1 = 0, \lambda_2 = 1$

Therefore to find the corresponding eigenvectors

$$\text{Let } Av = \lambda v$$

Then

$$\begin{bmatrix} 0 & 1 \\ 0 & 1 \end{bmatrix} \begin{bmatrix} \tilde{v}_1 \\ \tilde{v}_2 \end{bmatrix} = 1 \begin{bmatrix} \tilde{v}_1 \\ \tilde{v}_2 \end{bmatrix}$$

this implies

$$\tilde{v}_2 = \tilde{v}_1 \Rightarrow \tilde{v}_1 = r, r=1$$

$$\tilde{v}_1 = \begin{bmatrix} 1 \\ 1 \end{bmatrix}, \quad \tilde{v}_2 = \begin{bmatrix} 1 \\ 1 \end{bmatrix}$$

Hence

$$p = \begin{bmatrix} 1 & 1 \\ 1 & 1 \end{bmatrix}, \quad e^{At} = p e^{at} p^{-1}, \text{ where}$$

$$p^{-1} = \begin{bmatrix} 1 & -1 \\ -1 & 1 \end{bmatrix}$$

Therefore

$$e^{at} = \text{diag}(e^{at})$$

and so

$$\begin{aligned} \tilde{v}(t) &= \begin{bmatrix} 1 & 1 \\ 1 & 1 \end{bmatrix} \begin{bmatrix} e^t & 0 \\ 0 & e^t \end{bmatrix} \begin{bmatrix} 1 & -1 \\ -1 & 1 \end{bmatrix} \begin{bmatrix} \tilde{v}_{01} \\ \tilde{v}_{02} \end{bmatrix} \\ &= \begin{bmatrix} e^t & e^t \\ e^t & e^t \end{bmatrix} \begin{bmatrix} 1 & -1 \\ -1 & 1 \end{bmatrix} \begin{bmatrix} \tilde{v}_{01} \\ \tilde{v}_{02} \end{bmatrix} \\ &= \begin{bmatrix} 0 & 0 \\ 0 & 0 \end{bmatrix} \begin{bmatrix} \tilde{v}_{01} \\ \tilde{v}_{02} \end{bmatrix} \end{aligned}$$

Hence:

$$\tilde{v}_1(t) = -\cos t \tilde{v}_{01} \quad \tilde{v}_1(t) = -\sin t \tilde{v}_{02}$$

$$\tilde{v}_2(t) = \sin t \tilde{v}_{01} \quad \tilde{v}_2(t) = -\cos t \tilde{v}_{02}$$

$$\tilde{v}_{01} = 1 - \sqrt{1 - \alpha} \quad \tilde{v}_{01} = 1 + \sqrt{1 - \alpha} \quad , \quad \alpha = 1$$

$$\tilde{v}_{02} = -\sqrt{1 - \alpha} \quad \tilde{v}_{02} = \sqrt{1 - \alpha}$$

$$\text{Now } \underline{\lambda} = \frac{\bar{\beta} - \tilde{v}_1(t)}{\tilde{u}_1(t)} = \frac{-1 - 0\tilde{v}_{01}}{0\tilde{u}_{01}}$$

$$\bar{\lambda} = \frac{\bar{\beta} - \tilde{v}_1(t)}{\tilde{u}_1(t)} = \frac{-1 - 0\tilde{v}_{02}}{-1 + e^t \tilde{u}_{02}}$$

Since the general solution of fuzzy boundary value problem using the shooting method is given by:

$$\underline{y}(t) = \underline{v}(t) + \lambda \underline{u}(t), \quad \bar{y}(t) = \bar{v}(t) + \lambda \bar{u}(t)$$

The results could be compared with the crisp solution at $\alpha=1$, and for $t = \frac{\pi}{2}$, to given

$$\underline{y}\left(\frac{\pi}{2}\right) = \underline{v}\left(\frac{\pi}{2}\right) + \lambda \underline{u}\left(\frac{\pi}{2}\right) = -1.$$

$$\bar{y}\left(\frac{\pi}{2}\right) = \bar{v}\left(\frac{\pi}{2}\right) + \lambda \bar{u}\left(\frac{\pi}{2}\right) = -1.$$

Where the crisp solution at $t = \frac{\pi}{2}$ is given by:

$$y\left(\frac{\pi}{2}\right) = -1.$$

Also, we can make a comparison between the crisp solution and fuzzy solution with $\alpha=1$ as in the following Fig. (1)

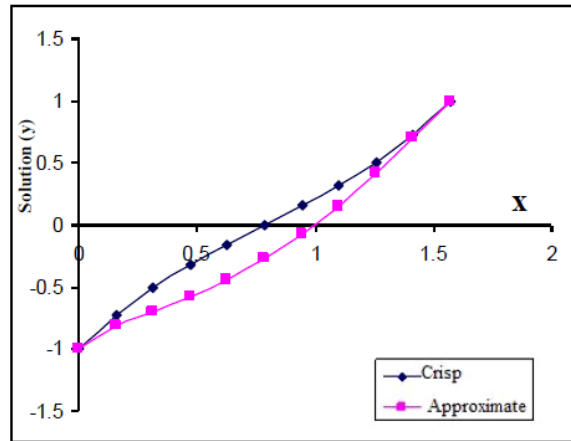


Fig. (1) : A comparison between crisp and fuzzy solution with , $\alpha=1$

Example (5.2):

Consider the second order fuzzy differential equation of boundary value problem:

$$y' = -y, y(0) = \tilde{1}, y(1) = -\tilde{1}, x \in [0, 1]$$

Let $\tilde{y}'_1 = \tilde{y}_2$

$$\tilde{y}'_2 = -\tilde{y}_1$$

Hence in matrix form:

$$\begin{bmatrix} \tilde{y}'_1 \\ \tilde{y}'_2 \end{bmatrix} = \begin{bmatrix} 0 & 1 \\ -1 & 0 \end{bmatrix} \begin{bmatrix} \tilde{y}_1 \\ \tilde{y}_2 \end{bmatrix}, \quad \tilde{y}_1(0) = \tilde{1} \quad \tilde{y}_2(1) = -\tilde{1}$$

$$\tilde{\beta} = -\tilde{1} \quad \tilde{\alpha} = \tilde{1} \quad x \in [0, 1]$$

In order to solve the above fuzzy BVP consider the first non-fuzzy BVP:

$$\begin{bmatrix} \tilde{u}'_1 \\ \tilde{u}'_2 \end{bmatrix} = \begin{bmatrix} 0 & 1 \\ -1 & 0 \end{bmatrix} \begin{bmatrix} \tilde{u}_1 \\ \tilde{u}_2 \end{bmatrix}, \quad \tilde{u}_1(0) = \tilde{0}, \tilde{u}_2(0) = \tilde{1}$$

and hence the eigenvalues of A are given by $\lambda_1 = i, \lambda_2 = -i$

Therefore to find the corresponding eigenvectors

Let $Au = \lambda u$

Then

$$\begin{bmatrix} 0 & 1 \\ -1 & 0 \end{bmatrix} \begin{bmatrix} \tilde{u}_1 \\ \tilde{u}_2 \end{bmatrix} = i \begin{bmatrix} \tilde{u}_1 \\ \tilde{u}_2 \end{bmatrix}$$

This implies

$$\tilde{u}_2 = i\tilde{u}_1 \Rightarrow \tilde{u}_1 = r, r=1$$

$$\tilde{u} = \begin{bmatrix} 1 \\ i \end{bmatrix} = \begin{bmatrix} 1 \\ 0 \end{bmatrix} + i \begin{bmatrix} 0 \\ 1 \end{bmatrix}$$

Hence

$$p = \begin{bmatrix} 0 & 1 \\ 1 & 0 \end{bmatrix}, e^{At} = p e^{jt} p^{-1}$$

$$p^{-1} = \begin{bmatrix} 0 & -1 \\ -1 & 0 \end{bmatrix}$$

Therefore

$$e^{jt} = e^{\alpha t} \begin{bmatrix} \cos bjt & -\sin bjt \\ \sin bjt & \cos bjt \end{bmatrix}$$

And so

$$\begin{aligned} \tilde{u}(t) &= \begin{bmatrix} 0 & 1 \\ 1 & 0 \end{bmatrix} \begin{bmatrix} \cos t & -\sin t \\ \sin t & \cos t \end{bmatrix} \begin{bmatrix} 0 & -1 \\ -1 & 0 \end{bmatrix} \begin{bmatrix} \tilde{u}_{01} \\ \tilde{u}_{02} \end{bmatrix} \\ &= \begin{bmatrix} \sin t & \cos t \\ \cos t & -\sin t \end{bmatrix} \begin{bmatrix} 0 & -1 \\ -1 & 0 \end{bmatrix} \begin{bmatrix} \tilde{u}_{01} \\ \tilde{u}_{02} \end{bmatrix} \\ &= \begin{bmatrix} -\cos t & -\sin t \\ \sin t & -\cos t \end{bmatrix} \begin{bmatrix} \tilde{u}_{01} \\ \tilde{u}_{02} \end{bmatrix} \end{aligned}$$

Hence

$$\begin{aligned} \tilde{u}_1(t) &= -\cos t \tilde{u}_{01} & \tilde{u}_1(t) &= -\sin t \tilde{u}_{02} \\ \tilde{u}_2(t) &= \sin t \tilde{u}_{01} & \tilde{u}_2(t) &= -\cos t \tilde{u}_{02} \\ \tilde{u}_{01} &= -\sqrt{1-\alpha} & \tilde{u}_{01} &= \sqrt{1-\alpha}, \alpha=1 \\ \tilde{u}_{02} &= 1-\sqrt{1-\alpha} & \tilde{u}_{02} &= 1+\sqrt{1-\alpha} \end{aligned}$$

Now, consider the second nonfuzzy BVP:

$$\begin{bmatrix} \tilde{v}_1' \\ \tilde{v}_2' \end{bmatrix} = \begin{bmatrix} 0 & 1 \\ -1 & 0 \end{bmatrix} \begin{bmatrix} \tilde{v}_1 \\ \tilde{v}_2 \end{bmatrix}, \quad \tilde{v}_1(0) = \tilde{1}, \tilde{v}_2(0) = \tilde{0}$$

and hence the eigenvalues of A are given by $\lambda_1 = i, \lambda_2 = -i$

Therefore to find the corresponding eigenvectors

Let $Av = \lambda v$

Then

$$\begin{bmatrix} 0 & 1 \\ -1 & 0 \end{bmatrix} \begin{bmatrix} \tilde{v}_1 \\ \tilde{v}_2 \end{bmatrix} = i \begin{bmatrix} \tilde{v}_1 \\ \tilde{v}_2 \end{bmatrix}$$

this implies

$$\tilde{v}_2 = i\tilde{v}_1 \Rightarrow \tilde{v}_1 = r, r=1$$

$$\tilde{v} = \begin{bmatrix} 1 \\ i \end{bmatrix} = \begin{bmatrix} 1 \\ 0 \end{bmatrix} + i \begin{bmatrix} 0 \\ 1 \end{bmatrix}$$

Hence

$$p = \begin{bmatrix} 0 & 1 \\ 1 & 0 \end{bmatrix}, e^{At} = p e^{jt} p^{-1}, \text{ where}$$

$$p^{-1} = \begin{bmatrix} 0 & -1 \\ -1 & 0 \end{bmatrix}$$

Therefore

$$e^{jt} = e^{at} \begin{bmatrix} \cos bjt & -\sin bjt \\ \sin bjt & \cos bjt \end{bmatrix}$$

and so

$$\begin{aligned} \tilde{v}(t) &= \begin{bmatrix} 0 & 1 \\ 1 & 0 \end{bmatrix} \begin{bmatrix} \cos t & -\sin t \\ \sin t & \cos t \end{bmatrix} \begin{bmatrix} 0 & -1 \\ -1 & 0 \end{bmatrix} \begin{bmatrix} \tilde{v}_{01} \\ \tilde{v}_{02} \end{bmatrix} \\ &= \begin{bmatrix} \sin t & \cos t \\ \cos t & -\sin t \end{bmatrix} \begin{bmatrix} 0 & -1 \\ -1 & 0 \end{bmatrix} \begin{bmatrix} \tilde{v}_{01} \\ \tilde{v}_{02} \end{bmatrix} \\ &= \begin{bmatrix} -\cos t & -\sin t \\ \sin t & -\cos t \end{bmatrix} \begin{bmatrix} \tilde{v}_{01} \\ \tilde{v}_{02} \end{bmatrix} \end{aligned}$$

Hence:

$$\tilde{v}_1(t) = -\cos t \tilde{v}_{01} \quad \tilde{v}_1(t) = -\sin t \tilde{v}_{02}$$

$$\tilde{v}_2(t) = \sin t \tilde{v}_{01} \quad \tilde{v}_2(t) = -\cos t \tilde{v}_{02}$$

$$\tilde{v}_{01} = 1 - \sqrt{1 - \alpha} \quad \tilde{v}_{01} = 1 + \sqrt{1 - \alpha} \quad , \quad \alpha = 1$$

$$\tilde{v}_{02} = -\sqrt{1 - \alpha} \quad \tilde{v}_{02} = \sqrt{1 - \alpha}$$

$$\text{Now } \underline{\lambda} = \frac{\bar{\beta} - \tilde{v}_1(t)}{\tilde{u}_1(t)} = \frac{-1 + \cos t \tilde{v}_{01}}{-\cos t \tilde{u}_{01}}$$

$$\bar{\lambda} = \frac{\bar{\beta} - \tilde{v}_1(t)}{\tilde{u}_1(t)} = \frac{-1 + \sin t \tilde{v}_{02}}{-\sin t \tilde{u}_{02}}$$

the results could be checked by comparing them with the crisp solution at $\alpha=1$, and for $t = 1$, we have

$$\underline{y}(t) = \underline{v}(t) + \underline{\lambda} \underline{u}(t) = -0.9992.$$

$$\bar{y}(t) = \bar{v}(t) + \bar{\lambda} \bar{u}(t) = -0.9992.$$

Where the crisp solution at $t = 1$ is given by $y(1) = -1$

Also, we can make a comparison between the crisp solution and fuzzy solution with $\alpha=1$ as it is illustrative in Fig. (2)

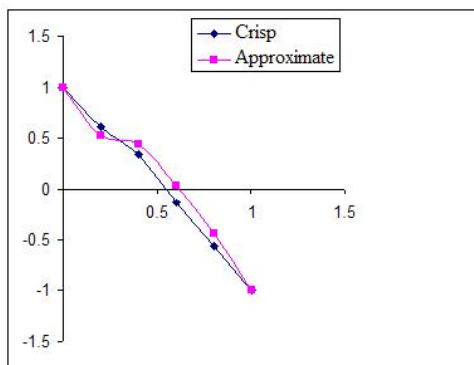


Fig. (2): A comparison between the crisp solution and fuzzy solution at $\alpha=1$.

As a boundary value for the FBVP of θ we take a fuzzy number $x_0 \in E^n$, such that

$$[x_0]^\alpha = \{(x_1^0, x_2^0) \in \mathbb{R}^2 \mid (x_1^0 - x_1^{00}) + (x_2^0 - x_2^{00})^2 \leq r_0^2 (1 - \alpha)^2\}$$

$$x_1^{00} \in \mathbb{R}, x_2^{00} \in \mathbb{R}, r_0 > 0.$$

Using Nguyen's theorem [20], we see that the α level sets of the fuzzy solution $u(t)$ will be convex compact sets in \mathbb{R}^2 , their boundaries having the following parametric representation:

$$x^2 + y^2 = r^2 [1 - M_{x_0}(x, y)]^2, \quad r > 0$$

$$(x_1^0 - x_1^{00})^2 + (x_2^0 - x_2^{00})^2 \leq r_0^2 (1 - \alpha)^2$$

$$x_1^0 - x_1^{00} = r(\alpha) \cos \theta$$

$$x_2^0 - x_2^{00} = r(\alpha) \sin \theta$$

$$x_1^0 = r(\alpha) \cos \theta + x_1^{00}$$

$$x_2^0 = r(\alpha) \sin \theta + x_2^{00}$$

And hence the general solution of the FBVP using the shooting method is given by:

$$\underline{x}_1(\theta, t) = \underline{v}_1(t) + \underline{\lambda} \underline{u}_1(t), \quad \overline{x}_2(\theta, t) = \overline{v}_1(t) + \overline{\lambda} \overline{u}_1(t)$$

$$\underline{x}_1(\theta, t) = -\cos t (r(\alpha) \cos \theta + x_1^{00}) - \sin t (r(\alpha) \sin \theta + x_2^{00})$$

$$\overline{x}_2(\theta, t) = \sin t (r(\alpha) \cos \theta + x_1^{00}) - \cos t (r(\alpha) \sin \theta + x_2^{00})$$

$$[x_0]^\alpha = \{(x_1^0, x_2^0) \in \mathbb{R}^2 \mid r^2(\alpha) \cos^2 \theta + r^2(\alpha) \sin^2 \theta \leq r^2(\alpha) (\cos^2 \theta + \sin^2 \theta) \leq r^2(\alpha) \leq r_0^2 (1 - \alpha)^2\}$$

$$r(\alpha) = r_0(1 - \alpha), \quad 0 \leq \alpha \leq 1, \quad 0 \leq \theta \leq 2\pi$$

Now, consider the fuzzy boundary values

$x_1^0 = -1, x_2^0 = 1, x_1^{00} = x_2^{00} = 0, r_0=2$ and $\alpha \in [0, 1]$.for $t = 0,0.1,0.2,\dots,1$ the approximate solution for $\alpha=0, 0.2, 0.4, 0.6, 0.8$ are obtained in tables 1 to 5.

Table 1: the approximate solution $x_1(\theta, t)$ and $x_2(\theta, t)$

$\alpha = 0.2$										
T	$\theta_{=0}$		$\theta_{=90}$		$\theta_{=180}$		$\theta_{=270}$		$\theta_{=360}$	
	x_1	x_2	x_1	x_2	x_1	x_2	x_1	x_2	x_1	x_2
0	1.6	0	-1.6	0	-1.6	0	1.6	0	1.6	0
0.1	1.598	0.003	-1.598	0.003	-1.598	0.003	1.598	0.003	1.598	0.003
0.2	1.598	0.005	-1.598	0.005	-1.598	0.005	1.598	0.005	1.598	0.005
0.3	1.598	0.008	-1.598	0.008	-1.598	0.008	1.598	0.008	1.598	0.008
0.4	1.598	0.011	-1.598	0.011	-1.598	0.011	1.598	0.011	1.598	0.011
0.5	1.598	0.014	-1.598	0.014	-1.598	0.014	1.598	0.014	1.598	0.014
0.6	1.598	0.016	-1.598	0.016	-1.598	0.016	1.598	0.016	1.598	0.016
0.7	1.598	0.019	-1.598	0.019	-1.598	0.019	1.598	0.019	1.598	0.019
0.8	1.598	0.022	-1.598	0.022	-1.598	0.022	1.598	0.022	1.598	0.022
0.9	1.598	0.026	-1.598	0.026	-1.598	0.026	1.598	0.026	1.598	0.026
1	1.598	0.027	-1.598	0.027	-1.598	0.027	1.598	0.027	1.598	0.027

Table 2: the approximate solution $x_1(\theta, t)$ and $x_2(\theta, t)$

$\alpha = 0.4$										
T	$\theta_{=0}$		$\theta_{=90}$		$\theta_{=180}$		$\theta_{=270}$		$\theta_{=360}$	
	x_1	x_2	x_1	x_2	x_1	x_2	x_1	x_2	x_1	x_2
0	1.2	0	1.2	0	1.2	0	1.2	0	1.2	0
0.1	1.199	0.002	1.199	0.002	1.199	0.002	1.199	0.002	1.199	0.002
0.2	1.199	0.004	1.199	0.004	1.199	0.004	1.199	0.004	1.199	0.004
0.3	1.199	0.006	1.199	0.006	1.199	0.006	1.199	0.006	1.199	0.006
0.4	1.199	0.008	1.199	0.008	1.199	0.008	1.199	0.008	1.199	0.008
0.5	1.199	0.010	1.199	0.010	1.199	0.010	1.199	0.010	1.199	0.010
0.6	1.199	0.012	1.199	0.012	1.199	0.012	1.199	0.012	1.199	0.012
0.7	1.199	0.014	1.199	0.014	1.199	0.014	1.199	0.014	1.199	0.014
0.8	1.199	0.017	1.199	0.017	1.199	0.017	1.199	0.017	1.199	0.017
0.9	1.199	0.019	1.199	0.019	1.199	0.019	1.199	0.019	1.199	0.019
1	1.199	0.020	1.199	0.020	1.199	0.020	1.199	0.020	1.199	0.020

Table 3: the approximate solution $x_1(\theta, t)$ and $x_2(\theta, t)$

$\alpha = 0.6$										
T	$\theta=0^\circ$		$\theta=90^\circ$		$\theta=180^\circ$		$\theta=270^\circ$		$\theta=360^\circ$	
	x_1	x_2	x_1	x_2	x_1	x_2	x_1	x_2	x_1	x_2
0	0.8	0	0.8-	0	0.8-	0	0.8	0	0.8	0
0.1	0.799	0.002	0.799-	0.002	0.799-	0.002	0.799	0.002	0.799	0.002
0.2	0.799	0.002	0.799-	0.002	0.799-	0.002	0.799	0.002	0.799	0.002
0.3	0.799	0.004	0.799-	0.004	0.799-	0.004	0.799	0.004	0.799	0.004
0.4	0.799	0.007	0.799-	0.007	0.799-	0.007	0.799	0.007	0.799	0.007
0.5	0.799	0.007	0.799-	0.007	0.799-	0.007	0.799	0.007	0.799	0.007
0.6	0.799	0.008	0.799-	0.008	0.799-	0.008	0.799	0.008	0.799	0.008
0.7	0.799	0.001	0.799-	0.001	0.799-	0.001	0.799	0.001	0.799	0.001
0.8	0.799	0.011	0.799-	0.011	0.799-	0.011	0.799	0.011	0.799	0.011
0.9	0.799	0.012	0.799-	0.012	0.799-	0.012	0.799	0.012	0.799	0.012
1	0.799	0.014	0.799-	0.014	0.799-	0.014	0.799	0.014	0.799	0.014

Table 4: the approximate solution $x_1(\theta, t)$ and $x_2(\theta, t)$

$\alpha = 0.8$										
T	$\theta=0^\circ$		$\theta=90^\circ$		$\theta=180^\circ$		$\theta=270^\circ$		$\theta=360^\circ$	
	x_1	x_2	x_1	x_2	x_1	x_2	x_1	x_2	x_1	x_2
0	0.4	0	0.4-	0	0.4-	0	0.4	0	0.4	0
0.1	0.391	0.001	-0.391	0.001	0.391-	0.001	0.391	0.001	0.391	0.001
0.2	0.391	0.001	0.391-	0.001	0.391-	0.001	0.391	0.001	0.391	0.001
0.3	0.391	0.002	0.391-	0.002	0.391-	0.002	0.391	0.002	0.391	0.002
0.4	0.391	0.003	0.391-	0.003	0.391-	0.003	0.391	0.003	0.391	0.003
0.5	0.391	0.004	0.391-	0.004	0.391-	0.004	0.391	0.004	0.391	0.004
0.6	0.391	0.004	0.391-	0.004	0.391-	0.004	0.391	0.004	0.391	0.004
0.7	0.391	0.005	0.391-	0.005	0.391-	0.005	0.391	0.005	0.391	0.005
0.8	0.391	0.006	0.391-	0.006	0.391-	0.006	0.391	0.006	0.391	0.006
0.9	0.391	0.006	0.391-	0.006	0.391-	0.006	0.391	0.006	0.391	0.006
1	0.391	0.007	0.391-	0.007	0.391-	0.007	0.391	0.007	0.391	0.007

Table 5: the approximate solution $x_1(\theta, t)$ and $x_2(\theta, t)$

$\alpha = 0$					
T	$\theta=0^\circ$	$\theta=90^\circ$	$\theta=180^\circ$	$\theta=270^\circ$	$\theta=360^\circ$

	X ₁	X ₂	X ₁	X ₂	X ₁	X ₂	X ₁	X ₂	X ₁	X ₂
0	2	0	2-	0	2-	0	2	0	2	0
0.1	1.998	0.004	1.998-	0.004	1.998-	0.004	1.998	0.004	1.998	0.004
0.2	1.998	0.006	-1.998	0.006	1.998-	0.006	1.998	0.006	1.998	0.006
0.3	1.998	0.01	1.998-	0.01	1.998-	0.01	1.998	0.01	1.998	0.01
0.4	1.998	0.014	1.998-	0.014	1.998-	0.014	1.998	0.014	1.998	0.014
0.5	1.998	0.018	1.998-	0.018	1.998-	0.018	1.998	0.018	1.998	0.018
0.6	1.998	0.02	1.998-	0.02	1.998-	0.02	1.998	0.02	1.998	0.02
0.7	1.998	0.024	1.998-	0.024	1.998-	0.024	1.998	0.024	1.998	0.024
0.8	1.998	0.03	1.998-	0.03	1.998-	0.03	1.998	0.03	1.998	0.03
0.9	1.998	0.032	1.998-	0.032	1.998-	0.032	1.998	0.032	1.998	0.032
1	1.998	0.034	1.998-	0.034	1.998-	0.034	1.998	0.034	1.998	0.034

6 - Conclusion

In this paper, we applied the pyramidal fuzzy numbers to solve fuzzy boundary value problems under generalized shooting method another application of fuzzy boundary value problems. This method can be extended for an nth order fuzzy boundary value problem. In the future, and following the ideas, we plan to consider the equations $y'(t) = -ty(t)$, or $y'(t) = c_1 y^2(t) + c_2$ with c_1, c_2 arbitrary constants.

References

[1]L. Zadeh, Fuzzy sets, Inform. And control 8(1965)338-353.

[2]A. Kandel, W. J. Byatt, Fuzzy differential equations, in proc. Internet. Conf. on Cybernetics and society, Tokyo- Kyoto, jupon, November 3 -7, 1978, pp. 1213- 1216.

[3]A. Kandel, W.J. Byatt, fuzzy processes, fuzzy sets and systems 4(1980)117-152.

[4]B.P. Lientz, on time dependent fuzzy sets, Inform. Sci. 4(1972)367-376.

[5]D. Dubois, H. Prade, Towards fuzzy differential calculus: part3, differentiation, fuzzy Sets and Systems 8(1982)225-233.

[6]P. Diamond, P. Kloeden, Metric Space of Fuzzy Sets:Theory and Application, World Scientific, Singapore, 1994.

[7]C.V. Negoita, D. A. Ralescu, Applications of Fuzzy Sets to System Analysis, Birkhauser, Basel, 1975.

[8]V. Lakshmikantham, T. Gnana Bhaskar, J. Vasundhara Devi, Theory of Set Differential Equations in Metric Spaces, Cambridge Scientific Publishers, Cambridge, 2006.

[9]M.L. Puri, D.A. Ralescu, Differentials of fuzzy function, J. Math. Anal. Appl. 91(1983)552-558.

[10]T. Allahviranloo, E. Ahmad, N. Ahmady, A method for solving N-th order fuzzy differential, International journal of computer mathematics, 2007, Volume86, Issue4, First published 2009, Pages 730-742.

[11]W. Congxin, S.Shiji, Existence theorem to the Cauchy problem of fuzzy differential equations under compactness-type conditions, Inform Sci 108(1998) 123-134.

[12]J. J. Nieto, R. Rodriguez-Lopez Bounded solutions for fuzzy differential and integral equations, Chaos, Solitons and Fractals 27(2006)1376-1386.

[13]L.Jamshid:¹,L.Avazpour² "solution of the fuzzy boundary value differential equations under generalized differentiability by shooting method, Journal of Fuzzy set Valued Analysis,Volume 2012,Year 2012,pp.1-19.

[14] Marwa Mohamed, Ismael" the shooting method for solving fuzzy linear boundary value problems "International Journal of Scientific and Engineering Research, volume5, Issue7, July 2014, pp.930-934.

[15]George, J.Klir and Boynan, "fuzzy sets and" fuzzy logic and Application", printichall , Inc.,1995.

[16]Song, S and Wu, C.:"Existence and uniqueness of solutions to the Cauchy problem of fuzzy Differential Equations", fuzzy sets and system, 110, (2000), pp.55-67.

[17]P.E.Kloeden, Remarks on Peano- like theorems for fuzzy differential equations, fuzzy sets and systems 44(1991)161-163.

[18]O.Kaleva, the Cauchy problem for fuzzy differential equations, fuzzy sets and systems 35(1990)389-396.

[19]Bede, Budgal, S.G.: Generalization of the Differentiability of fuzzy-Number-valued functions with Applications to fuzzy Differential Equations", Fuzzy sets and systems, 2004.

[20]D. Vorobier, S.Seikkala,Towards the theory of fuzzy differential equations, fuzzy sets and systems 125(2002)231-237.

Spectrophotometric Determination of Chloramphenicol in Bulk and Pharmaceutical Preparation

Tariq Y. Mahmoud, Sarmad B. Dikran, Alaa K. Mohammed

Dept. of Chemistry- College of Education for Pure Science (Ibn Al- Haitham)/
University of Baghdad

Abstract

Chloramphenicol is spectrophotometrically determined by the formation of a colored charge transfer exhibiting λ_{\max} at 445 nm after the reaction of the secondary amine with sodium nitroprusside in the presence of NH_2OH in alkaline medium. Classical univariate and chemometric central composite experimental design approaches were used to find the optimum experimental conditions for the parameters affecting the formation of CT-complex. The proposed method is simple and sensitive for the determination of the drug in a concentration range of 1.0-25.0 $\mu\text{g.mL}^{-1}$ with molar absorptivity $8.142 \times 10^3 \text{L.mol}^{-1}.\text{cm}$. and $r = 0.9995$. The validity of the method was confirmed by finding the regression equation, accuracy, precision, and detection limit. Chloramphenicol was successfully determined in its pharmaceutical preparations by the developed procedure with a reasonable of recovery and precision. Statistical validation of the obtained results was made and the method shows acceptable recovery and repeatability.

Key words: chloramphenicol determination, spectrophotometry, central composite experimental design.

دراسة التقدير الطيفي للكلورامفينيكول بشكله النقي وفي المستحضرات الصيدلانية

طارق ياسين محمود , أ.د سرمد بهجت ديكران, أ.د علاء كريم محمد
قسم الكيمياء- كلية التربية للعلوم الصرفة (ابن الهيثم)- جامعة بغداد

الخلاصة

تم تقدير الكلورامفينيكول طيفياً بواسطة تكوين معقد انتقال الشحنة الملون الذي اظهر اعلى امتصاص عند الطول الموجي 445 نانوميتر بعد تفاعل الامين الثانوي مع صوديوم نايتروبروسايد بوجود الهيدروكسيل امين في محيط قاعدي. وقد تم ايجاد الظروف التجريبية الفضلى التي تؤثر على تكوين معقد انتقال الشحنة بالطريقة الكلاسيكية بنمط المتغير الواحد مع بقاء المتغيرات الاخرى ثابتة وطريقة تصميم التجربة. الطريقة المقترحة بسيطة وحساسة لتقدير الدواء على مدى من التراكيز يتراوح بين (1.0-25.0 $\mu\text{g.mL}^{-1}$) وكانت قيمة معامل الامتصاص المولي مساوية الى ($8.142 \times 10^3 \text{L.mol}^{-1}.\text{cm}$) و ($r = 0.9995$). ولقد تمتأكد صلاحية هذه الطريقة من خلال ايجاد معادلة الانحدار والضبط والدقة وحدود الكشف. كما تم تقدير الكلورامفينيكول بنجاح في المستحضرات الصيدلانية بواسطة هذه الطريقة المطورة بدقة وتغطية مقبولة.

الكلمات المفتاحية: تعين الكلورامفينيكول, الطيف الضوئي, تصميم التجربة المركزي.

Introduction

Chloramphenicol (CAP) is a powerful bacterial protein synthesis inhibitor firstly isolated from cultures of *Streptomyces venezuelae*^(1, 2). It is used for salmonella infections (i.e. typhoid and paratyphoid fever and in severe systemic Arizona infections) and

in various bacterial eye infections which occurs particularly in drug abusers. Chemically, the name of the drug is [2,2-Dichloro-N-\[1,3-dihydroxy-1-\(4-nitrophenyl\)-2-propanyl\]acetamide](#) and its chemical formula is and molar mass 323.132 g/mol. The structural formula of CAP is given in Figure 1.

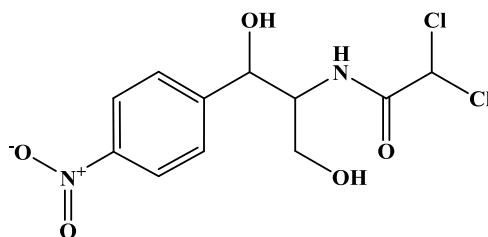


Figure 1: The structural formula of chloramphenicol.

Several analytical methods have been reported for the determination of chloramphenicol CAP in both pure form and as pharmaceutical preparations. Including determination of Simple photometric and colorimetric determinations of chloramphenicol were investigated^[3-5]. Determination of chloramphenicol in tablets by electrogenerated chemiluminescence's coupled to flow injection analysis (FIA)⁽⁶⁾, high performance liquid chromatography (HPLC)⁽⁷⁾, spectrophotometry^(8,9).

This works aims to introduce a new simple and sensitive method for spectrophotometric determination of CPA in its pure form and in pharmaceutical preparations after complexation with sodium nitroprusside. The CT complex is formed in alkaline medium the presence of $\text{NH}_2\text{OH}\cdot\text{HCl}$ ⁽¹⁰⁾. Univariate and chemometric central composite design⁽¹¹⁾ were followed for optimization experimental variables.

Experimental

Instrument

CECLL CE 7200. UK (7000 series) Double beam UV- Visible spectrophotometer with 10 mm quartz cell.

Reagents:

All reagents and chemicals used were of Analar grade. Chloramphenicol powder was obtained from the State Company for Drug Industries and Medical Appliances Samara-Iraq (SDI) in pure form (99.99%).

- Sodium carbonate -1- hydrate solution (6% w/v): six grams of the reagent was dissolved in distilled water and the volume of the solution was made to the mark with the same solvent in a 100 mL-volumetric flask.
- Chromogenic reagent (SNP) solution: 100mL of [0.8% (w/v) sodium nitroprusside and 0.186% (w/v) Hydroxylamine hydrochloride]. Prepared by dissolving 0.8 g of sodium nitroprusside and 0.186 g of hydroxylamine hydrochloride in distilled water. The mixed solution was then diluted to 100 mL in a volumetric flask.

Preparation of standard stock solution (200 $\mu\text{g}\cdot\text{mL}^{-1}$)

0.02 gm of pure chloramphenicol powder was dissolved in 3 mL of 6% Na_2CO_3 solution. The resulted solution was diluted to 100 mL with distilled water. Working standard solutions were

prepared daily by serial dilutions of the stock solution as required with distilled water.

Preparations of sample solutions

1- In Capsule

The contents of 10 capsules were individually weighted out to get the average weight of the capsules. An amount of the powder equivalent to 0.02 gm. of CAP was weighted, then about 5 mL of 6% Na_2CO_3 was added, the mixture was transferred into 100 mL volumetric flask, and the flask contained was swirled. Distilled water was then added to make the volume 100 mL to get $200 \mu\text{g}\cdot\text{mL}^{-1}$ solution of chloramphenicol. The undissolved materials were filtered-out by passing them through a filter paper (Whatman No.41) before using distilled water to prepare more dilute working solution by subsequent dilutions and applying the recommended procedure.

2- In Eye Drop

4 mL of the sample solution was transferred into a 100 mL volumetric flask, 5 mL of 6% Na_2CO_3 was added with continuous swirling. The mixture was left to stand for 5 min. before dilution to the mark with distilled water to get $200 \mu\text{g}\cdot\text{mL}^{-1}$ of chloramphenicol solution. More dilute solutions were freshly prepared as required via dilutions with distilled water, and the recommended procedure was applied for their analysis.

Recommended Procedures

i- Under conditions established via univariate method

Into a series of 10mL-calibrated flasks containing 2.5 mL of chromogenic reagent (SNP) solution, different volumes of the standard ($200 \mu\text{g}/\text{mL}$) solution containing (10-

250) μg of chloramphenicol were transferred. The formed mixtures were shaken for 3 minutes at 25°C followed by the addition of 0.5 mL of 6% Na_2CO_3 to each solution and the flasks were kept aside for 10 minutes in dark. Thereafter, the volumes of the mixtures were made with distilled water to the mark. The absorbance values were measured at 451.0 nm, after mixing and homogenizing the solutions, against the reagent blank.

ii- Under conditions established via chemometric multivariate

aliquots of the standard solution $200 \mu\text{g}/\text{mL}$ containing (5- 260) μg of chloramphenicol were added to a set of 10 mL-calibrated flasks that contain 2.04 mL of chromogenic reagent (SNP) solution were shaken for 3 minutes at 25°C . Then 0.85 mL of 6% Na_2CO_3 was added to each mixture and the solutions were kept for two and half minutes in dark. The total volume in each flask was brought to the mark with distilled water and mixed well before measuring the value of absorbance at 451.0 nm against blank solution.

Results and discussion

Absorption spectra

Absorption spectrum for the reaction of chloramphenicol with SNP in presence of hydroxylamine under alkaline conditions was recorded under the optimum conditions and showed the maximum absorption at 451.0 nm for the red color against the reagent blank Fig [2].

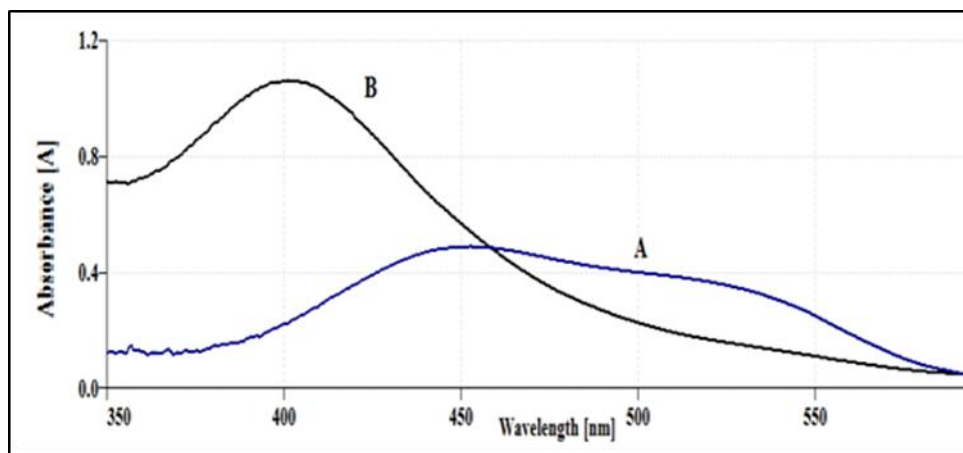


Figure (2): Absorption spectra of $(20.0 \mu\text{g.mL}^{-1})$ chloramphenicol against reagent blank(A), and of reagent blank against D.W. under the optimum conditions.

Optimization of reaction variables

I-Univariate method

Optimum conditions were established by classical univariate one factor a time strategy and following the absorbance of the colored product.

Figures 3, 4 and Table 1 show the results obtained for the study of the effects of volume of chromogenic reagent, volume of Na_2CO_3 solution, reaction time and different diluting solvents on the measured signal .

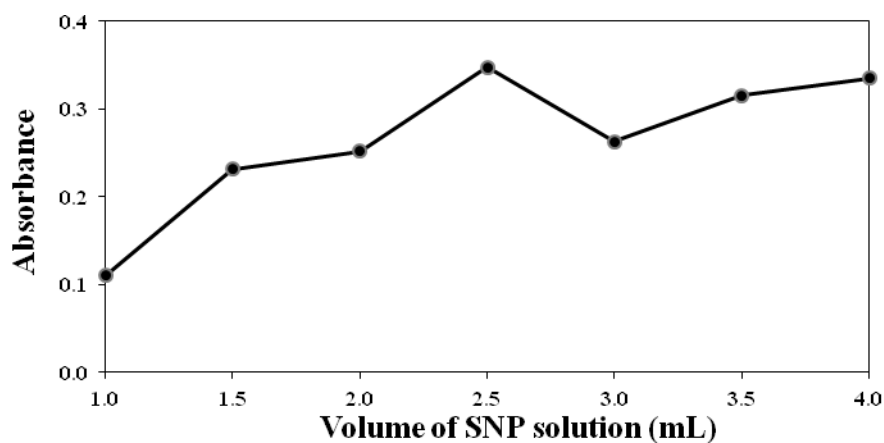


Figure (3): Effect of volume of chromogenic reagent on the color development in the determination of $(20.0 \mu\text{g.mL}^{-1})$ chloramphenicol.

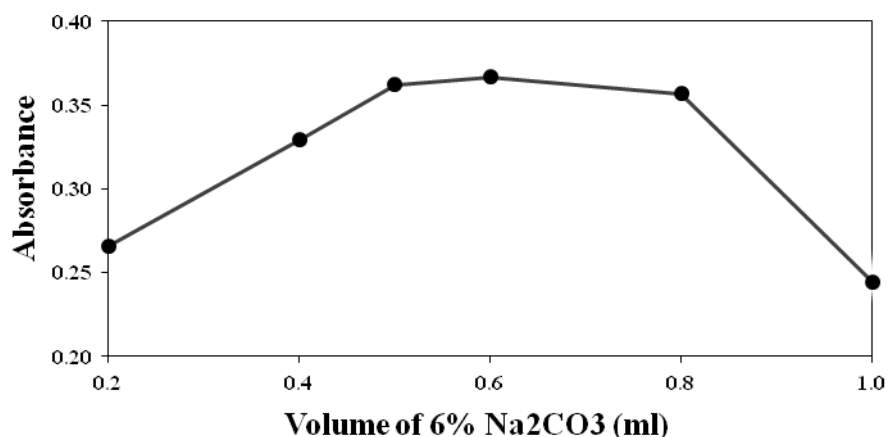


Figure (4): Effect of vol. of 6% Na₂CO₃ solution on the color development in the determination of (20.0 µg.mL⁻¹)chloramphenicol.

Table (1): Effects of reaction time and different diluting solvents on the color development of (20.0 µg.mL⁻¹)chloramphenicol.

<i>Time (min.)</i>	<i>Absorbance</i>	<i>Solvents</i>	<i>Absorbance</i>
0	0.122	Distilled Water	0.437
5	0.325	Methanol	0.525
10	0.367	Ethanol	Turbid
15	0.367	Acetone	Turbid
20	0.276	Acetonitrile	0.364

II- Design of experiment method

A chemometric multivariate optimization approach was used to obtain the optimum values of three of variables having the greatest importance on the reaction yield (viz. the volume of SNP solution, the volume of 6% Na₂CO₃ solution and the reaction time).The

conditions of these variables were optimized via face centered central composite design while other experimental parameters were maintained unchanged at their optimum values that obtained by following the univariate approach. Table [2] shows the uncoded values of each of the studied variable.

Table [2]: The CCD for three independent variables (uncoded) together with their corresponding values of absorbance for (20 µg.mL⁻¹) CAP.

Exp. No.	Vol. of SNP sol. (mL)	Vol. of 6% Na ₂ CO ₃ sol. (mL)	Reaction time (min)	Abs.
1	2.5	0.6	10	0.424
2	4.0	1.0	20	0.400
3	1.0	1.0	0.0	0.432
4	1.0	0.6	10	0.364
5	2.5	0.6	10	0.412
6	1.0	0.2	20	0.346
7	2.5	1.0	10	0.395
8	2.5	0.6	10	0.417
9	2.5	0.6	10	0.426
10	2.5	0.6	10	0.431
11	2.5	0.2	10	0.423
12	2.5	0.6	20	0.339
13	4.0	0.2	20	0.150
14	4.0	0.2	0.0	0.000
15	2.5	0.6	0.0	0.423
16	1.0	0.2	0.0	0.491
17	1.0	1.0	20	0.167
18	4.0	1.0	0.0	0.370
19	4.0	0.6	10	0.368
20	2.5	0.6	10	0.432

Statistical 12 software (Stat. Soft. Inc., release 2013) was used to estimate the values of coefficients for the response surface equation. The results are expressed in Table [3].

Table [3]: ANOVA table for the second order polynomial linear-quadratic model.

Variable	Regression coefficient	Standard error of coefficient	t-value	P
Constant	0.56849	0.01280	0.39722	0.45424
SNP vol.	-0.05095	0.01177	-0.07743	-0.02497
(SNP vol.) ²	-0.027929	0.02245	-0.11283	-0.01281
Na ₂ CO ₃ vol.	-0.13474	0.01177	0.00917	0.06163
(Na ₂ CO ₃ vol.) ²	-0.12386	0.02245	-0.06983	0.03019
Reaction time	-0.00137	0.01177	-0.05763	-0.00517
(Reaction time) ²	-0.00048	0.02245	-0.09783	0.00219
SNP vol.× Na ₂ CO ₃ vol.	0.17875	0.01316	0.07793	0.13657
SNP vol.×Reaction time	0.00492	0.01316	0.04443	0.10307
Na ₂ CO ₃ vol.×Reaction time	-0.00750	0.01316	-0.05932	-0.00068

Optimum values for the studied variables were 2.04 mL for the volume of (SNP) solution, 0.85 mL for the volume of 6% Na₂CO₃ solution and 2.33 minutes for the reaction time. Figure [5] shows the plots of response surface for couples of variables while maintaining the third variable constant.

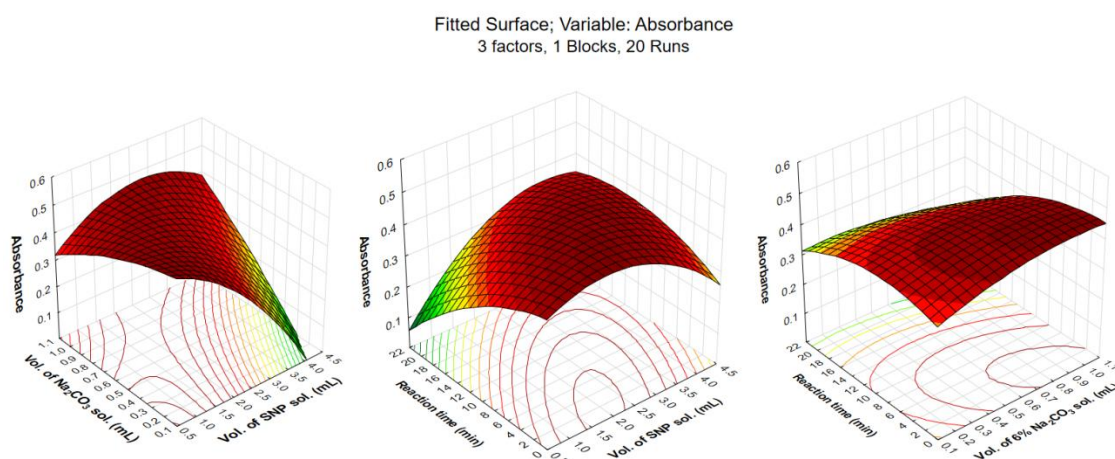
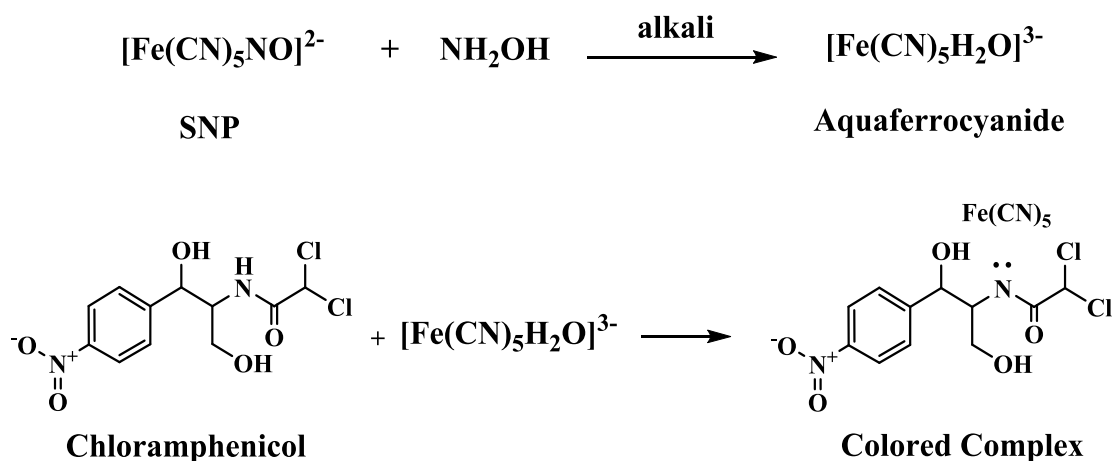


Figure [5]:The plots absorbance response surface for chloramphenicol- SNP complex against of any pair of variables (keeping third variable constant at its optimum value).

The proposed mechanism for the reaction between CAP and SNP is given in scheme (1).



Scheme [1]:The suggested reaction mechanism for charge-transfer reaction between CAP and sodium nitroprusside.

Calibration curves and analytical data

Table [4]:Spectral and statistical data for spectrophotometric determination CAP under conditions obtained via univariate and DOE methods.

<i>Parameter</i>	<i>Univariate condition</i>	<i>multivariate condition</i>
λ_{max} (nm)	451.0	
Color	Red	
Linearity range ($\mu\text{g.mL}^{-1}$)	1.0-25.0	0.5-26.0
Regression equation	$y = 0.0252[\text{CAP } \mu\text{g/ml}] - 0.0066$	$y = 0.0277[\text{CAP}\mu\text{g/ml}] + 0.0699$
Slope ($\text{mL.}\mu\text{g}^{-1}$)	0.0252	0.0277
Correlation coefficient (r)	0.9995	0.9991
Molar absorptivity ($\text{L.mol}^{-1}.\text{cm}^{-1}$)	8.142×10^3	8.949×10^3
Sandell's sensitivity ($\mu\text{g.cm}^{-2}$)	3.968×10^{-2}	3.610×10^{-4}
Detection limit ($\mu\text{g.mL}^{-1}$)	0.350	0.210
Quantification limit ($\mu\text{g.mL}^{-1}$)	1.166	0.7

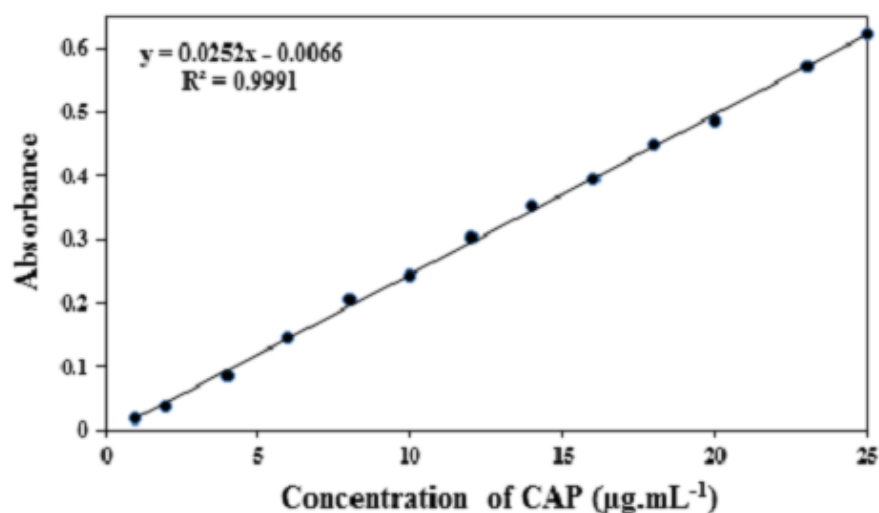


Figure [6]: Calibration curve for the determination of CAP under optimal conditions obtained by univariate optimization.

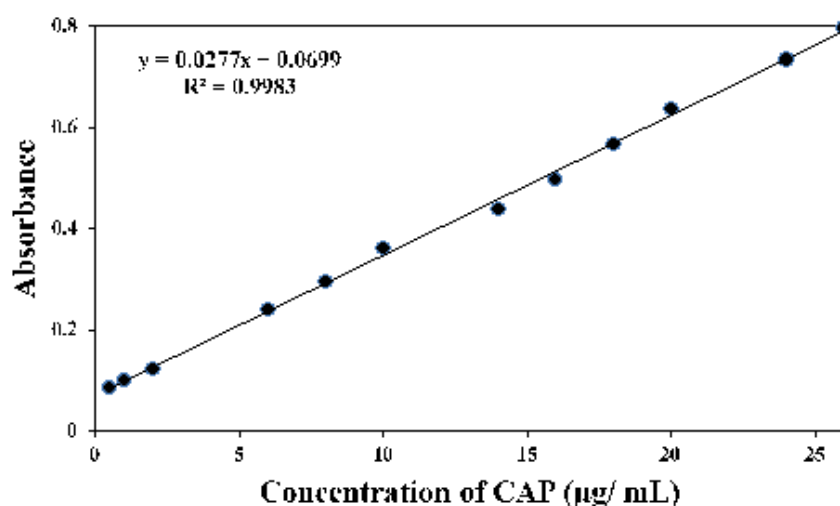


Figure [7]: Calibration curve for the determination of chloramphenicol under optimum condition obtained by DOE.

Accuracy and precision

The accuracy and the precision of the proposed method were established by analyzing five replicates for three concentration levels of the pure drug. The values of relative error and coefficient of variation (C.V %) were determined, Table [5].

Table [5]:The accuracy and precision of the method.

	<i>Conc. of Chloramphenicol</i>		<i>Relative Error</i>	<i>C.V*</i>
	<i>(µg.mL⁻¹)</i>			
	<i>Taken</i>	<i>Found*</i>	<i>%</i>	<i>%</i>

For univariate	4.000	3.99	-0.250	0.355
	12.000	12.07	0.583	0.117
	24.000	23.915	-0.354	0.059
For DOE	4.000	4.021	0.525	0.334
	12.000	12.056	0.466	0.111
	24.000	24.107	0.445	0.055

*Average of five determinations.

2-3-5 Interference study

To assess the analytical potential of the suggested procedure, the effect of the presence of the commonly used excipients (viz; sucrose, glucose,

lactose, and starch) were examined by carrying out the determination of 20.0 $\mu\text{g.mL}^{-1}$ of chloramphenicol in the presence of above compounds. The results presented in Table [6] indicate no interferences were found from any of the excipients studied in determination of chloramphenicol.

Table [6]: The effect of the presence of the excipients(1000 $\mu\text{g.mL}^{-1}$)on the analysis of 20.0 $\mu\text{g.mL}^{-1}$ of chloramphenicol.

Excipients	Concentration	Chloramphenicol Conc. Taken (20.0 $\mu\text{g.mL}^{-1}$)	
		Conc. Found* $\mu\text{g.mL}^{-1}$ (Recovery*%
Sucrose	1000	20.11	100.55
Glucose		19.97	99.85
Lactose		19.71	98.55
Starch		19.88	99.4

*Average of three determinations.

2-3-6 Application on pharmaceutical Sample

The developed method was successfully used for assaying chloramphenicol in pharmaceutical samples. The results showed in Table [7] were satisfactory.

Table [7]: Application of the proposed method under conditions obtained via univariate optimization for chloramphenicol determination in pharmaceutical samples.

<i>Sample</i>	<i>Conc. taken ($\mu\text{g.mL}^{-1}$)</i>	<i>Conc.* found ($\mu\text{g.mL}^{-1}$)</i>	<i>Recovery %</i>	<i>C.V* %</i>
Phenicol (eye drop)	20.00	19.77	98.85	0.072
Chloroper (eye drop)	20.00	19.26	96.33	0.073
Chloramphenicol Capsule	20.00	20.04	100.2	0.070

*Average of three determinations.